Max-Planck-Institut
für Meteorologie

MAX-PLANCK-GESELLSCHAFT

The Water and Heat Cycles in a Coupled Ocean-Atmosphere-Model for the Baltic Sea

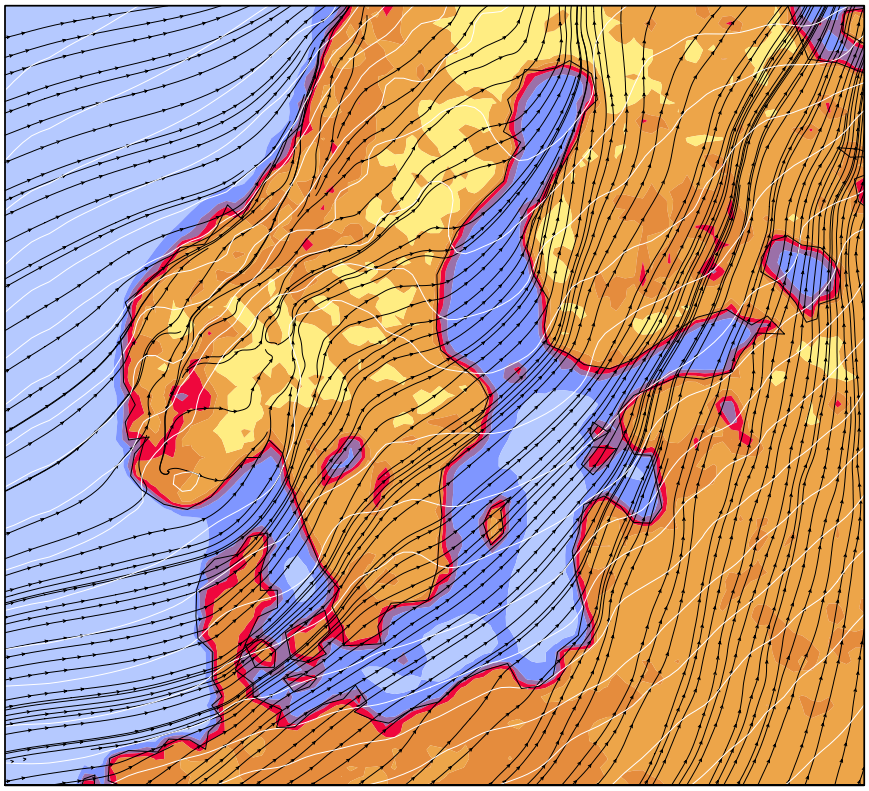

Thomas Raub

Hamburg 2015

Berichte zur Erdsystemforschung
Reports on Earth System Science

169
2015

Hinweis

Die Berichte zur Erdsystemforschung werden vom Max-Planck-Institut für Meteorologie in Hamburg in unregelmäßiger Abfolge herausgegeben.

Sie enthalten wissenschaftliche und technische Beiträge, inklusive Dissertationen.

Die Beiträge geben nicht notwendigerweise die Auffassung des Instituts wieder.

Die "Berichte zur Erdsystemforschung" führen die vorherigen Reihen "Reports" und "Examensarbeiten" weiter.

Notice

The Reports on Earth System Science are published by the Max Planck Institute for Meteorology in Hamburg. They appear in irregular intervals.

They contain scientific and technical contributions, including Ph. D. theses.

The Reports do not necessarily reflect the opinion of the Institute.

The "Reports on Earth System Science" continue the former "Reports" and "Examensarbeiten" of the Max Planck Institute.

Anschrift / Address

Max-Planck-Institut für Meteorologie
Bundesstrasse 53
20146 Hamburg
Deutschland

Tel./Phone: +49 (0)40 4 11 73 - 0
Fax: +49 (0)40 4 11 73 - 298

name.surname@mpimet.mpg.de
www.mpimet.mpg.de

Layout

Bettina Diallo and Norbert P. Noreiks
Communication

Copyright

The Water and Heat Cycles in a Coupled Ocean-Atmosphere-Model for the Baltic Sea

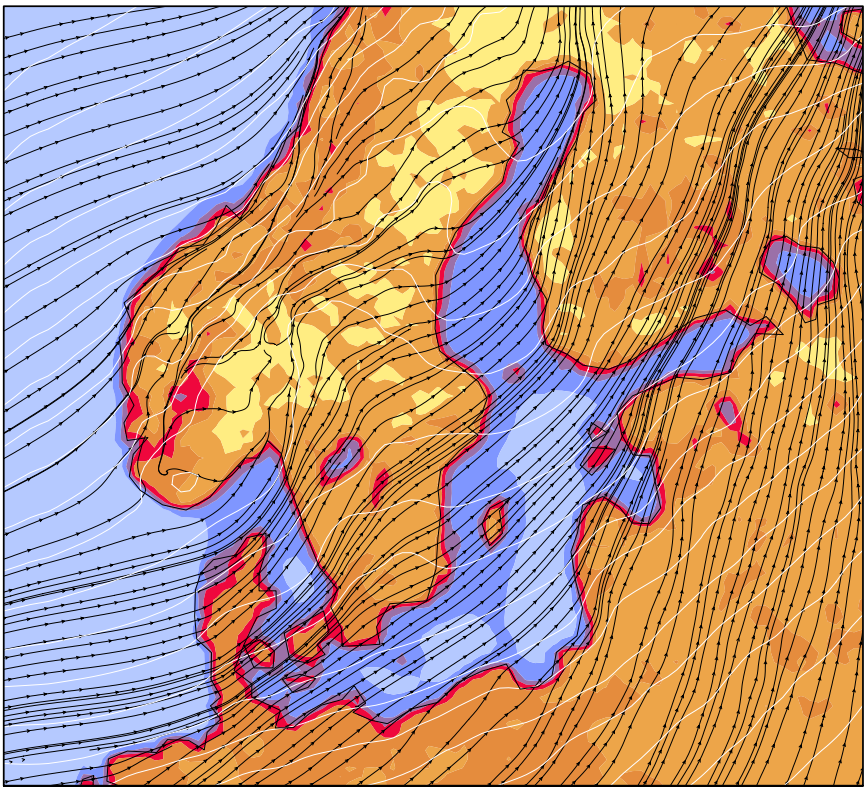

Thomas Raub

Hamburg 2015

Thomas Raub
aus Aschaffenburg

Max-Planck-Institut für Meteorologie
Bundesstrasse 53
20146 Hamburg

Als Dissertation angenommen
vom Fachbereich Geowissenschaften der Universität Hamburg

auf Grund der Gutachten von
Dr. Daniela Jacob
und
Prof. Dr. Guy Brasseur

Hamburg, den 20.10.2014
Professor Dr. Christian Betzler
Leiter des Departments Geowissenschaften

Berichte zur Erdsystemforschung / Max-Planck-Institut für Meteorologie 169
Reports on Earth System Science / Max Planck Institute for Meteorology 2015

ISSN 1614-1199

Abstract

This work investigates the water and energy cycles of the Baltic Sea and its catchment area using a coupled regional atmosphere-ocean model.

The aim of this dissertation is a better understanding of the physical system and the interaction of its components in order to improve possible climate change assessments in this region. The coupled model consists of the regional atmospheric Model REMO and the Baltic Sea ice ocean model BSIOM.

Coupled and uncoupled simulations have been performed using the ERA-Interim reanalysis product from ECMWF as lateral boundary conditions for the period from 1989 to 2008. The simulations have been evaluated using satellite and in-situ measurements.

In general, the coupled and uncoupled atmospheric simulations show quite similar results.The coupled model performs reasonably well in reproducing the heat fluxes at the sea surface of the Baltic Sea. However, some deficits still exist with respect to the water cycle that relates to the salinity dynamics. A clear added value of the coupled model is a nearly closed heat budget within the ocean. Another advantage of the interactive coupling is the representation of certain processes such as coastal upwelling. The analysis has shown that the process of coastal upwelling causes considerable differences in the near-surface wind speed over the affected areas. This result can be explained by an increased stability of the atmospheric boundary layer due to the colder sea surface temperature. As a consequence, the vertical mixing of momentum is reduced and thus modifies the near-surface wind speed. This process shows the importance of the interactive coupling for example for short-term wind forecast, which is relevant for offshore wind-energy plans.

Contents

1 Introduction **1**

1.1 The Baltic Sea . . . 2

1.2 Numerical Models . . . 4

1.3 Research Questions . . . 4

1.4 Outline . . . 4

2 The Coupled Model System **7**

2.1 Models . . . 7

2.1.1 REMO . . . 7

2.1.2 BSIOM . . . 10

2.2 Coupling . . . 12

2.2.1 Exchanged variables . . . 12

2.2.2 Sea ice . . . 13

2.3 Performed Experiments . . . 13

2.4 Observational and Reanalysis Datasets . . . 13

3 Model Evaluation **17**

3.1 Baltic Catchment Area . . . 17

3.2 Baltic Sea surface . . . 26

3.2.1 Atmospheric variables . . . 27

3.2.2 Oceanic variables . . . 33

3.2.3 Sea level . . . 37

3.3 Conclusions . . . 43

4 Water & Energy Budget of the Baltic Sea **45**

4.1 The BALTEX box . . . 45

4.2 Surface Fluxes at the Baltic Sea . . . 46

4.2.1 Heat Fluxes . . . 46

4.3 Exchange North Sea - Baltic Sea . . . 54

4.4 Rivers . . . 55

4.5 Precipitation & Evaporation . . . 56

4.6 Storage changes . . . 56

4.7 Closure of the Water Budget . . . 59

4.8 Closure of the Energy Budget . . . 59

4.9 Conclusions . . . 62

5 Differences between the Coupled and the Stand-Alone Version **63**

5.1 Temporal mean . . . 63

5.2 Effect of Coastal Upwelling . . . 70

5.2.1 Physical mechanism . . . 71

5.2.2 Upwelling Regions . . . 72

5.2.3 Detection Method . . . 72

5.2.4 Spatial upwelling distribution . . . 73

5.2.5 Temporal Mean . . . 74

5.2.6 Temporal Evolution . . . 77

5.3 Conclusions . . . 79

6 Conclusions & Outlook **83**

6.1 Conclusions . . . 83

6.2 Outlook . . . 85

Bibliography **87**

Chapter 1

Introduction

The Earth's climate represents a complex physical system consisting of four major components: the atmosphere, the ocean, the land, and the cryosphere. Due to the interactions among the components and also due to external drivers as the sun or human activities its state is subject to permanent variations/change. In order to understand how the climate evolves, especially with respect to the actual experiment of increasing greenhouse gases, each component and the interactions between them must be understood sufficiently. A lot of research is carried out at the moment using observations and computer simulations to increase the understanding of the climate system. The available computer resources are far from being sufficient to allow to resolve the earth system on all its relevant scales. When simulation the whole globe, many regional details are not represented adequately, as coastal processes for example. To investigate the processes happening at finer scales, studies that investigate only parts of the globe are conducted.

The Baltic Sea region includes all major components of the earth system. Due to its semi-enclosed nature the Baltic Sea represents an ideal testbed to study water and energy budgets and processes/ interactions between these components . Coastal processes play an important role in this regional earth system.

The Baltic Sea and its catchment area are expected to be largely affected by the projected global climate change due to the increase of greenhouse gas emissions (BACC 2008). Besides the strong influence of the global climate change, also regional and local effects determine the strength of the climate change signal, as the storage of heat in the water body of the Baltic Sea. The heat storage is mainly determined by the surface fluxes between the atmosphere and the ocean and exhibits a strong annual cycle and inter-annual variations. The water and energy cycles of the Baltic Sea and its catchment area were one of the major topics in BALTEX (the Baltic Sea Experiment), which was part of the Global Energy and Water Exchanges Project (GEWEX) of the World Climate Research Programme (WCRP). Major advancements of the understanding of the physical system of the Baltic Sea have been achieved during its active phase from 1993 to 2012. However, important questions were left open, for example potential feedbacks in the atmosphere-ocean interactions. The

individual components of the heat fluxes are not yet quantified at high confidence, since the spread among different available datasets are still considerable. This work tries to further improve the understanding and quantification of the air-sea fluxes and investigate the effect of potential feedback mechanisms.

1.1 The Baltic Sea

The Baltic catchment area lies in the transition zone between the maritime climate of western Europe and the strongly continental climate of Siberia, from 48°N to 69°N latitude and from 8°E to 38°E longitude. Its climate is determined by the atmospheric circulation over the North Atlantic in the west and over the Eurasian continent in the east. Therefore, the climate varies from temperate maritime in the south to sub-arctic in the north (Johannessen 1970).

The Baltic Sea plays an important role for the economy of the Baltic region. The most important sectors of its maritime economy are fishing, maritime transport, and coastal tourism. A still relatively small, but fast growing sector is the offshore wind energy. All these sectors more or less depend on the actual state of the Baltic Sea: The development of the fish stocks is very sensitive to several physical and biological variables like temperature, salinity, and the availability of nutrients. Ship transport is highly affected when the Baltic Sea is covered by sea ice. Touristic attractiveness depends on the water temperature and is very sensitive to pollution and algae. There is also a strong inter-dependence/competition among these factors.

The Baltic Sea is one of the largest brackish-water systems of the world with a sea surface area of about 350,000km^2 and a catchment area of about 1,735,000km^2. It is relatively shallow with a mean depth of about 55m and a maximum depth of 459m. With the drainage basin being about four times larger than its sea surface, the Baltic Sea is highly affected by the surrounding land (Stigebrandt 2001). The mean river discharge amounts to about 450$^{km^3}/_{y}$ which is more than 2% of the total volume.

The only connection to the North Sea are the shallow and narrow Danish Straits. Together with the high freshwater flow, this leads to a relatively low basin-averaged salinity of about 7.4 PSU (Janssen et al. 1999). The Baltic Sea is characterized by strong horizontal as well as vertical salinity gradients. The surface salinity decreases from about 10 PSU at Darss Sill to almost freshwater conditions in the Bothnian Bay and the Gulf of Finland. There exists a permanent halocline separating the relatively fresh water of the upper layer from the more saline and thus denser bottom water at about 50 to 80m as illustrated in Figure 1.1 (Leppäranta and Myrberg 2009). Vertical mixing is strongly suppressed within the halocline due to the high stratification. The only mechanism to refresh the oxygen concentrations in the bottom layer is therefore via major inflows of high saline and oxygenated water masses from the North Sea which are dense enough to replace the water in the deep basins of the Baltic Sea (Matthäus and Franck 1992). Their occurrence is

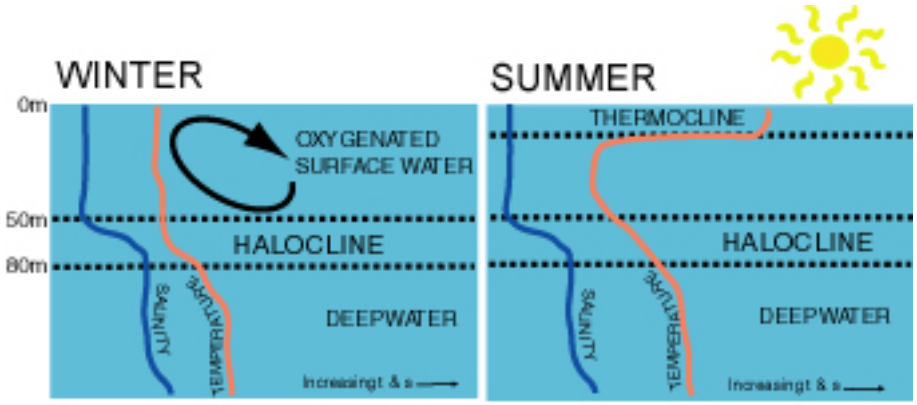

Figure 1.1: Annual variations of the temperature and salinity profiles (from: Hermanni Backer, http://www.itameriportaali.fi/en/tietoa/veden_liikkeet/en_GB/hydrografia/)

very irregular, on average every 10 years. In between, the oxygen gets depleted leading to anoxic conditions with large impact on the ecologic system.

Wallerius (1932) already found that the Baltic Sea is almost in thermo-dynamic balance with the atmosphere. The temperature exhibits a distinct annual cycle. In winter the water above the halocline is well mixed with temperatures only a few degrees above freezing. In spring the sun starts to heat the upper layers. When the temperature of maximum density is reached (about 2.3-3.5°C for the brackish water of the Baltic Sea) a seasonal thermocline (a layer of strong vertical temperature gradients) develops at about $5m$ depth in spring and deepens to about 15-20m during summer through wind and wave-induced mixing. Usually in late summer, the net heat flux at the surface becomes negative, and the cooling water becomes heavier. This leads to convection and thus additional vertical mixing, further deepening the mixed-layer depth (Leppäranta and Myrberg 2009). The thermocline usually vanishes with the first autumn storms (Krauss 1981).

Due to its complex coastline and shallowness, coastal upwelling is one of the most important physical processes in the Baltic Sea (Hela 1976). In summer it can cause a local temperature drop by more than 10°C. It also can considerably contribute to the replenishing the surface layers with nutrients which are necessary for the biological productivity (Kononen and Niemi 1986).

The Baltic Sea is located at Earth's climatological sea ice margin (Leppäranta and Myrberg 2009). Therefore, the Baltic Sea is covered by sea ice every winter, with a large inter-annual variability. The average maximum coverage is about half of the surface area (Vihma and Haapala 2009).

1.2 Numerical Models

This study aims at improving the physical understanding of the Baltic Sea region. Global circulation models (GCMs) with a typical resolution of about 200km cannot sufficiently resolve the Baltic Sea with its average width of about 190km. Here regional climate models (RCMs) come into play. RCMs are used to downscale the results from global models onto a region of interest with a much higher resolution, typically 10 to 50km. The added value of the increased resolution is a much better representation of the topography and the land-sea mask for example. Usually atmosphere-only models are used with prescribed sea surface conditions (temperature and ice cover). The results then strongly depend on the quality of the data used. Especially when coming from coarse GCMs these may not be very realistic. Due to the static nature of the surface conditions, uncoupled models are not able to represent potential feedbacks in the air-sea interactions adequately. They also represent an infinite heat reservoir which is not suitable for heat budget studies.

Within the first phase of the BALTic sea EXperiment (BALTEX) (Raschke et al. 2001), several coupled model systems for the Baltic Sea have been developed (Gustafsson et al. 1998; Hagedorn et al. 2000; Döscher et al. 2002; Schrum et al. 2003). One of them was the BALTex Integrated MOdel System (BALTIMOS), which consists of the regional atmospheric model REMO and the Baltic Sea ice ocean model BSIOM (Hagedorn et al. 2000; Lorenz and Jacob 2009). This model system was used to investigate potential coupling effects (Hagedorn et al. 2000). The model was also able to reproduce the major inflow events in 2002-2003 (Lehmann et al. 2004). It showed major deficits in reproducing the annual energy cycle, however (Bennartz et al. 2009).

1.3 Research Questions

In this thesis the following research questions are tackled:

- How large are the major components in the water and energy cycles of the Baltic Sea?
- How does the interactive coupling of a Baltic Sea ocean model affect the regional climate simulation?
- What is the added value of the coupled model compared to the stand-alone version?

1.4 Outline

This thesis is structured as follows: In Chapter 2 the coupled model system and its components are introduced. The performance of the model is evaluated in Chapter 3 by

comparing its results to observations. The water and energy cycles of the Baltic Sea are investigated in Chapter 4. The differences between the coupled model simulation and the atmosphere-only simulation are investigated in Chapter 5 with a focus on the process of coastal upwelling and its feedback on the atmosphere. Conclusions and an outlook are given in Chapter 6.

Chapter 2

The Coupled Model System

In this chapter the coupled model system is described. The model system is an updated version of BALTIMOS (BALTEX Integrated Model System) which was developed in the frame of BALTEX (Hagedorn 2000; Lorenz and Jacob 2009). It consists of the atmospheric model REMO and the Baltic Sea ice ocean model BSIOM (Lehmann 1995).

First the stand-alone versions are introduced with focus on the air-sea flux parameterizations. It is followed by a description of the coupling strategy of the two models.

2.1 Models

2.1.1 REMO

REMO is a three-dimensional limited-area atmospheric circulation model which solves the discretized primitive equations of atmospheric motion (Jacob and Podzun 1997; Jacob et al. 2001). In this work, the hydrostatic model version is used. The dynamical core is taken from the Europa Modell (Majewski 1991), the former weather forecast model of the German Weather Service. The physical parameterizations are based on those from the general circulation models ECHAM4 and 5 of the Max Planck Institute for Meteorology (Roeckner et al. 1996, 2003). One major modification is the sub-grid-scale tile approach that allows for fractional cover of the surface types land, water, and sea ice (Semmler 2002). This allows for a better representation of the coastal area for example.

The REMO domain is defined on a rotated grid with a resolution of 1/6° (~18km) that covers the catchment area of the Baltic sea, as depicted in Figure 2.1.

For the horizontal discretization, a spherical Arakawa-C grid is used for all prognostic variables except velocity which is defined at the center of the grid boxes. Usually the grid is rotated, which means that the poles are shifted in order to have similar grid-box sizes over the domain.

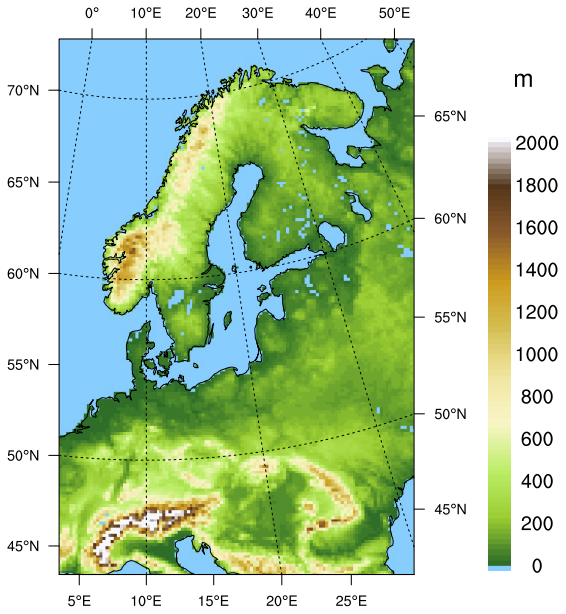

Figure 2.1: REMO domain

For the vertical discretization, hybrid σ-coordinates are used (Simmons and Burridge 1981). They are a combination of terrain following coordinates near the ground and pressure coordinates in the free atmosphere.

Since it is a limited-area model, it needs information of the prognostic variables at its lateral boundaries. These can either come from a general circulations model or from reanalysis data, that are interpolated onto the REMO grid. In this work, the ERA-Interim reanalysis from ECMWF are used.

REMO was used and has been validated in several studies on almost all continents, and especially over Europe and the Baltic catchment area (e.g. Jacob et al. (2001, 2007)).

Parameterization of the Surface Fluxes over water and sea ice

In the following the parameterizations which are most relevant for the the interaction between the atmosphere and the ocean are described. The surface fluxes are parameterized via bulk formulas(Louis 1979) Monin-Obukhov similarity theory (Monin and Obukhov 1954):

$$\boldsymbol{\tau} = \rho_a C_m |V_{10}| \boldsymbol{V}_{10} \tag{2.1}$$

$$Q_{sh} = \rho_a c_p C_h V_{10} \Delta\Theta \tag{2.2}$$

$$Q_{lh} = \rho_a L C_h V_{10} \Delta q \tag{2.3}$$

with ρ_a the air density, $C_{m/h}$ the (turbulent) transfer coefficients for momentum and tracers, $\mathbf{V}_{10}$ the wind velocity in 10m height, $\Delta\Theta$ and Δq the differences in potential temperature and specific humidity between the lowest model level and the surface.

The transfer coefficients are calculated from the coefficients for neutral stratification

$$C_{Nm/h} = \frac{\kappa^2}{\ln\left(\frac{z_L}{z_{0m/h}}+1\right)\ln\left(\frac{z_L}{z_{0m}}+1\right)} \tag{2.4}$$

with a correction function that depends on the Richardson number:

$$C_{m/h} = C_{Nm/h} \cdot f_{m/h}\left(Ri_B, \frac{z_L}{z_{0m/h}}+1\right) \tag{2.5}$$

with the van Kármán constant $\kappa = 0.4$, the height of the lowest model layer z_L, and the roughness lengths for momentum and tracers $z_{0m/h}$.

The dynamic roughness length for momentum over water is calculated with the Charnock formula (Charnock 1955):

$$z_{0m} = \alpha\frac{u_*^2}{g} \tag{2.6}$$

with the Charnock parameter of $\alpha = 0.0123$, and the friction velocity u_* ,and the gravitational acceleration g.

Due to the molecular nature of the tracer transport at the air-sea interface, the roughness length for the tracers heat and humidity is calculated as in Large and Pond (1982):

$$z_{0h} = z_{0m} \cdot \exp\left(2 - 86.276 z_{0m}^{0.375}\right) \tag{2.7}$$

Over sea ice, the roughness length is set to the constant value of $z_{0,ice} = 10^{-3}$m for both momentum and tracers.

Solar radiation

In the model the top of the atmosphere solar radiation is calculated by earth's orbital parameters using a solar constant of $1368\frac{W}{m^2}$. Other variations like the 11-year solar cycle are not considered. Passing through the atmosphere down to the surface, the radiation is partly reflected and absorbed by aerosols, humidity and clouds the latter having the strongest impact. At the surface the radiation is partly absorbed. The reflected fraction is given by the surface albedo.

For water surfaces the albedo is set to a constant value of $\alpha_w = 0.07$. For ice the albedo depends on the surface temperature: for melting conditions (T>0°C) the albedo is set to

0.5. For temperatures lower than -10°C to 0.75 and to a linear combination for temperatures in between. The model does not consider eventual snow cover on sea ice which can have very large impact on the surface albedo (Pirazzini et al. 2006).

2.1.2 BSIOM

The Baltic Sea Ice Ocean Model (BSIOM) is based on the Bryan-Cox-Semtner general circulation model with a free surface (Killworth et al. 1991). It is defined on a staggered Arakawa B grid with a horizontal resolution of about 2.5 km which is considered as eddy permitting. It has 60 vertical levels with a thickness of 3m for the first 100m. The model domain as shown in Figure 2.2 comprises the Baltic Sea including Kattegat and Skagerrak. It includes a simplified North Sea as a closed basin. There, the sea surface salinity is nudged towards a climatology. At its western boundary the sea level is nudged toward values that are calculated via the Baltic Sea Index (BSI) (Lehmann et al. 2002; Novotny et al. 2006).

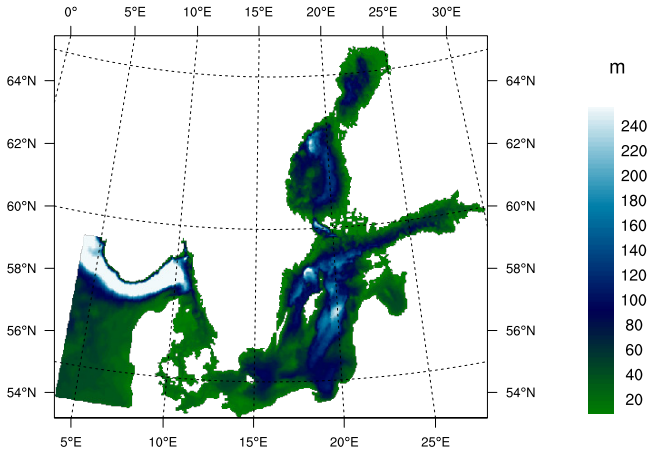

Figure 2.2: BSIOM topography

Wind stress

Wind speed and direction at 10m height are calculated from the geostrophic wind from the Swedish Meteorological and Hydrological Institute's (SMHI) meteorological database (L. Meuller, pers. comm.) taking the distance and direction with respect to the coastline into account (Bumke et al. 1998).

The neutral drag coefficient is calculated empirically after Large and Pond (1981):

$$C_{dn} \cdot 10^3 = \begin{cases} 1.14 & U \leqq 10\frac{m}{s} \\ 0.49 + 0.065U & U > 10\frac{m}{s} \end{cases} \tag{2.8}$$

Turbulence model

The vertical mixing is parameterized using a so called $k - \epsilon-$model, a second-moment turbulence model, where k and ϵ denote the turbulent kinetic energy (TKE) and the dissipation of TKE, respectively (Launder and Spalding 1972; Rodi 1980; Meier 2001).

Solar radiation

The solar radiation is parameterized using the empirical equation from Zillman (1972) with a modification for cloud cover:

$$F_S^{\downarrow} = \frac{S_0 \cos^2 \Theta}{1.085 \cos \Theta + (\cos \Theta + 2.7) e_s 10^{-3} + 0.1}(1 - 0.7cl^2) \tag{2.9}$$

where $S_0 = 1367.0\frac{W}{m^2}$ is the solar constant, Θ the zenith angle, e_s the surface water vapor pressure, and cl the cloud cover.

Thermal radiation

The net thermal radiation is parametrized using the empirical formula from Zapadka et al. (2007):

$$F_{Th} = 0.985 \cdot \sigma \cdot SST^4 - \sigma \cdot T_{2m}^4 \cdot (0.685 + 0.00452 \cdot e_{2m})\,(1 + d_j \cdot cl^2) \tag{2.10}$$

where d_j is a dimensionless constant with a slight annual cycle.

Sea ice

The sea ice is represented by a dynamic–thermodynamic sea ice model (Stössel and Owens 1992; Harder 1996; Lehmann and Hinrichsen 2000). Sea ice dynamics are described by a viscous–plastic rheology (Hibler 1979), and the thermo-dynamical ice growth rates are calculated from the surface energy balance using the Semtner zero-layer approach following Parkinson and Washington (1979).

River runoff

The discharge of the 42 most important rivers flowing into the Baltic Sea and the Kattegat is prescribed from a monthly mean runoff dataset (Graham 1999; Bergström and Carlsson 1994).

2.2 Coupling

BSIOM is coupled to REMO as a subroutine as described in Hagedorn et al. (2000). The models use different parameterizations to calculate the fluxes at the atmosphere-ocean interface. To be physical consistent, the models are coupled via fluxes, which are all calculated in REMO and the interpolated fields are passed to BSIOM. The necessary surface variables SST, sea ice cover and ice temperature are passed from BSIOM to REMO. The disadvantage of this method is that the resolution of the atmospheric grid is much coarser than the ocean grid. This can be problematic for non-linear fluxes such as the thermal radiation with a forth-order temperature dependence.

2.2.1 Exchanged variables

The following variables are exchanged between REMO and BSIOM at the air-sea interface at an hourly frequency to resolve the diurnal cycle:

REMO → BSIOM

- Sensible and latent heat flux
- Net surface solar and thermal radiation
- Wind stress
- Surface pressure
- Precipitation

BSIOM → REMO

- Sea surface temperature
- Sea ice cover
- Ice surface temperature

Since the grids of the two models are not the same, the exchanged data have to be transformed onto the respective destination grid via bilinear interpolation in the interior and a distance weighted extrapolation at coastal points where the different land-sea masks do not overlap.

2.2.2 Sea ice

The thermo-dynamic sea ice growth is treated differently in the coupled model compared to the stand-alone version. The heat fluxes between the atmosphere and the ocean determine the temperature of ice surface layer T_i, with a fixed thickness of 10cm. The thermo-dynamic growth of the ice thickness H at the ice-ocean interface is then calculated from the conducted heat through the ice layer assuming the water temperature to be at the freezing point T_f:

$$\rho_i L \frac{dH}{dt} = \kappa_i \cdot \frac{T_f - T_i}{H} - Q_w \tag{2.11}$$

where ρ_i is the ice density, L the latent heat of freezing, κ_i the heat conductivity of ice, and Q_w the heat flux from water to ice.

2.3 Performed Experiments

In this work three different model simulations are analyzed for the 20-year period from 1989 to 2008. Two uncoupled simulations serve as reference for the coupled simulation: an atmosphere-only simulation, where REMO was forced with the ERA-Interim reanalysis from ECMWF at the lateral boundaries and at the sea surface. As an ocean-only simulation a simulation run at the Geomar is used, where BSIOM is driven with interpolated synoptic observations from SMHI. This run is also used for the initialization of the 3-dimensional hydrographic field of the coupled run. This coupled simulation also uses ERA-Interim as lateral atmospheric forcing and its sea surface temperatures where the models are not interactively coupled.

2.4 Observational and Reanalysis Datasets

To evaluate the model performance, a variety of different datasets produced by different methods is used, originating from station observations, satellite measurements, reanalysis, or a combination of them. All methods have their advantages and disadvantages. The station data are interpolated onto a geographic grid where the quality of the product depends on the density of the stations and the spatial homogeneity of the variable. The satellite measurements may be limited by cloud cover for example. And the quality of the reanalysis data depends both on the used model and the observations.

The used datasets are shortly introduced in the following:

ERA-Interim The latest reanalysis dataset from the European Centre for Medium-Range Weather Forecasts (ECMWF) is defined on a global grid with a resolution of 0.75° (about 79km) (Dee et al. 2011).

NOCS NOCS Surface Flux Dataset v2.0 from the National Oceanography Centre, Southampton (NOCS). The data are based on VOS observations from the International Comprehensive Ocean–Atmosphere Data Set (ICOADS) Woodruff et al. (1998); Worley et al. (2005) They are defined as monthly means over the global oceans with a resolution of 1° for the period 1973–2009 (Berry and Kent 2009).

OAFlux Objectively Analyzed air-sea Fluxes from the Woods Hole Oceanographic Institution. It uses an optimal blending of satellite retrievals and three atmospheric reanalyses to calculate the fluxes using the COARE bulk flux algorithm 3.0. The resolution is 1° (Yu and Weller 2007; Yu et al. 2008). The short and longwave radiation data are taken from ISCCP.

ISCCP International Satellite Cloud Climatology Project as part of the World Climate Research Programme. The data are monthly means of surface variables over the global ocean with a resolution of 1° from 1958 onwards (Zhang et al. 2004).

COREv2 Coordinated Ocean-ice Reference Experiments (CORE). The data are based on a mixture of the NCEP reanalysis and several satellite products. They are defined over the global oceans with a resolution of 1° Griffies et al. (2009); Large and Yeager (2009).

CRU TS3.10 Climate Research Unit. The dataset consists of monthly means of interpolated station data and is defined over the global land surface with a 0.5° resolution Harris et al. (2013).

BSH Federal Maritime and Hydrographic Agency in Hamburg, Germany (BSH). Sea surface temperatures are derived from infrared high-resolution data of the U.S. NOAA weather satellite series (Siegel et al. 2006).

ASI-SSMI Sea ice concentrations computed at IFREMER by applying the ARTIST Sea Ice (ASI) algorithm to brightness temperatures from the 85 GHz SSM/I and SSM/IS channels. They are available for the polar regions with a resolution of 12.5km from 1992 onward Kaleschke et al. (2001); Spreen et al. (2008).

ICES International Council for the Exploration of the Sea (ICES). This dataset consists of temperature and salinity profiles of the Baltic Sea from the ICES oceanographic database compiled at GEOMAR in Kiel. Depth-specific CTD and bottle measurements. All available measurements between 1970 and 2010 were subsequently aggregated to monthly mean area averages on 5m vertical resolution. Data gaps were closed by linear vertical and temporal interpolation (Lehmann et al. 2014).

SMHI This dataset of the Swedish Meteorological and Hydrological Institute (SMHI) is produced from synoptic station observations interpolated on a regular grid by using a 2D univariate optimum interpolation scheme. It is defined over the Baltic catchment area with a resolution of 1° Omstedt et al. (1997).

Chapter 3

Model Evaluation

In this chapter the model performance of the coupled and uncoupled simulations is evaluated by testing its ability to reproduce observed variables. For this the results of the model simulations are compared to several observational datasets and reanalysis products introduced in Chapter 2 over the land part of the Baltic catchment area and the Baltic Sea surface separately.

3.1 Baltic Catchment Area

The simulated mean circulation over the Baltic region for the different seasons is depicted in Figure 3.1. The Baltic sea is located along the path of the North Atlantic storm tracks (Leppäranta and Myrberg 2009). The circulation is strongly influenced by the North Atlantic oscillation. The highest meridional pressure gradients and thus winds speeds occur during winter. With the mean westerly circulation over the Atlantic and turning southerly at the eastern part of the domain. Also visible is the deflection at the Scandinavian mountain ridge. During summer the pressure gradient is much weaker, resulting in lower wind speeds. This allows for the development of a more local circulation with lower pressure over the Gulf of Bothnia as an imprint of the high frequency of Baltic cyclones in that area.

In this section, the model performance on the land part of the Baltic catchment area is evaluated. The analysis is constraint on some basic climatic variables, namely the 2m temperature, precipitation, evaporation, and runoff. The latter will become important when a river routing scheme will be implemented into the model scheme to have the river discharge consistent within the simulations.

The components of the hydrological cycle over the Baltic catchment area in regional climate models have been subject of several studies, e.g. Hagemann et al. (2004); Graham et al. (2008); Lind and Kjellström (2009). Hagemann et al. (2004) investigated the water

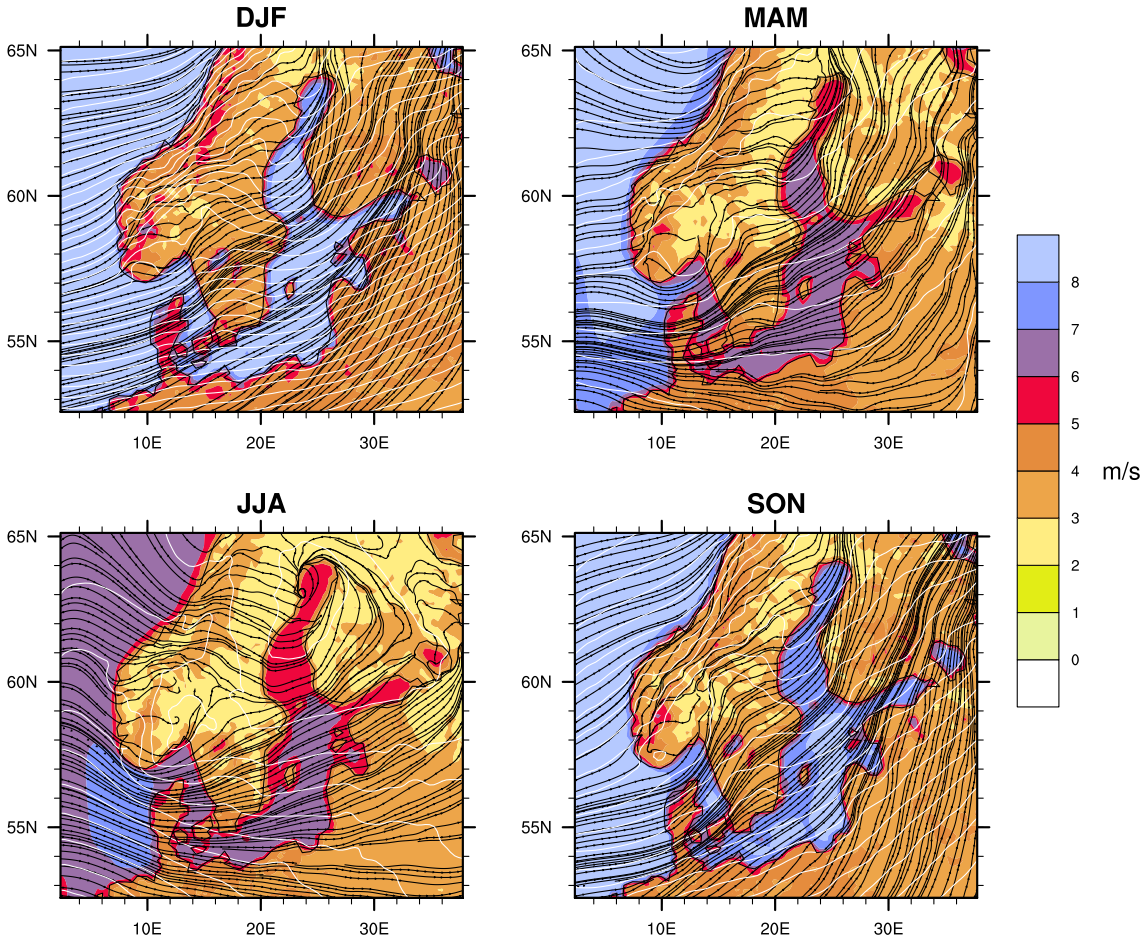

Figure 3.1: Mean circulation in the coupled model simulation in the Baltic region for the different seasons (winter: DJF; spring: MAM; summer: JJA and autumn: SON) for the period from 1989 to 2008. Colors indicate the 10m wind speed, black streamlines the mean flow direction, and white contour lines the mean sea level pressure at a 50mbar interval.

and energy budget in regional climate models over Europe. They found a general overestimation of precipitation throughout the year except for summer. As probable reasons they mentioned deficits in the internal model parameterizations, such as large-scale condensation and convection. The annual cycle is in general well represented Graham et al. (2008).

The atmospheric variables at the surface of the Baltic Sea in an ensemble of regional climate simulations have been investigated by Meier et al. (2011). Precipitation over the Baltic Sea surface is difficult to observe. It has been addressed e.g. by Rutgersson et al. (2001); Hennemuth et al. (2003). BSIOM in its stand-alone version has proven to simulate the physical state of the Baltic Sea realistically (Lehmann et al. 2014).

2m Temperature

In Figure 3.2, the difference of the 2m temperatures of the model run to the CRU data over the land parts of the simulated domain are shown. The highest differences occur during winter with a cold bias of up to 3°C over an extended area in the eastern part of the domain and over Scandinavia and the Finish lakes with a warm bias persisting until spring. The cold bias might be related to the snow cover in regions with a high forest fraction, where the surface albedo might not be calculated realistically. Because of the mainly westerly flow, this does not have a strong impact on the Baltic Sea itself. The reason of the warm biases is probably the treatment of lakes in the model where the temperatures are interpolated from the nearest ocean grid points in this model version. The implementation of a lake module would probably strongly reduce this bias. For the rest of the year, the near-surface temperatures are very well reproduced by the model.

The same can also be seen in the mean annual cycle and the yearly-mean time series of the area averages over the catchment area, as shown in Figure 3.3 where the cold bias shows up in a mean bias in the range of around 1°C.

Precipitation

The next investigated variable is precipitation. Figure 3.4 shows the monthly means of the simulated precipitation for the different seasons of the simulation period from 1989 - 2008. The seasonal cycle is quite different for land and sea: Over land, the highest intensities occur during summer due to convection that follows closely the near-surface temperature and thus the solar radiation. Due to the large heat capacity of the water body, over sea the sea surface temperature has a damped seasonal cycle compared to the air temperature, leading to a more stable atmosphere with reduced convection during spring and summer and the opposite during autumn and winter. Also prominent are the regions with intense orographic precipitation at the Scandinavian mountain chain and at the Alps. There are very high intensities close to the eastern boundary which is a common feature in regional climate simulations over Europe.

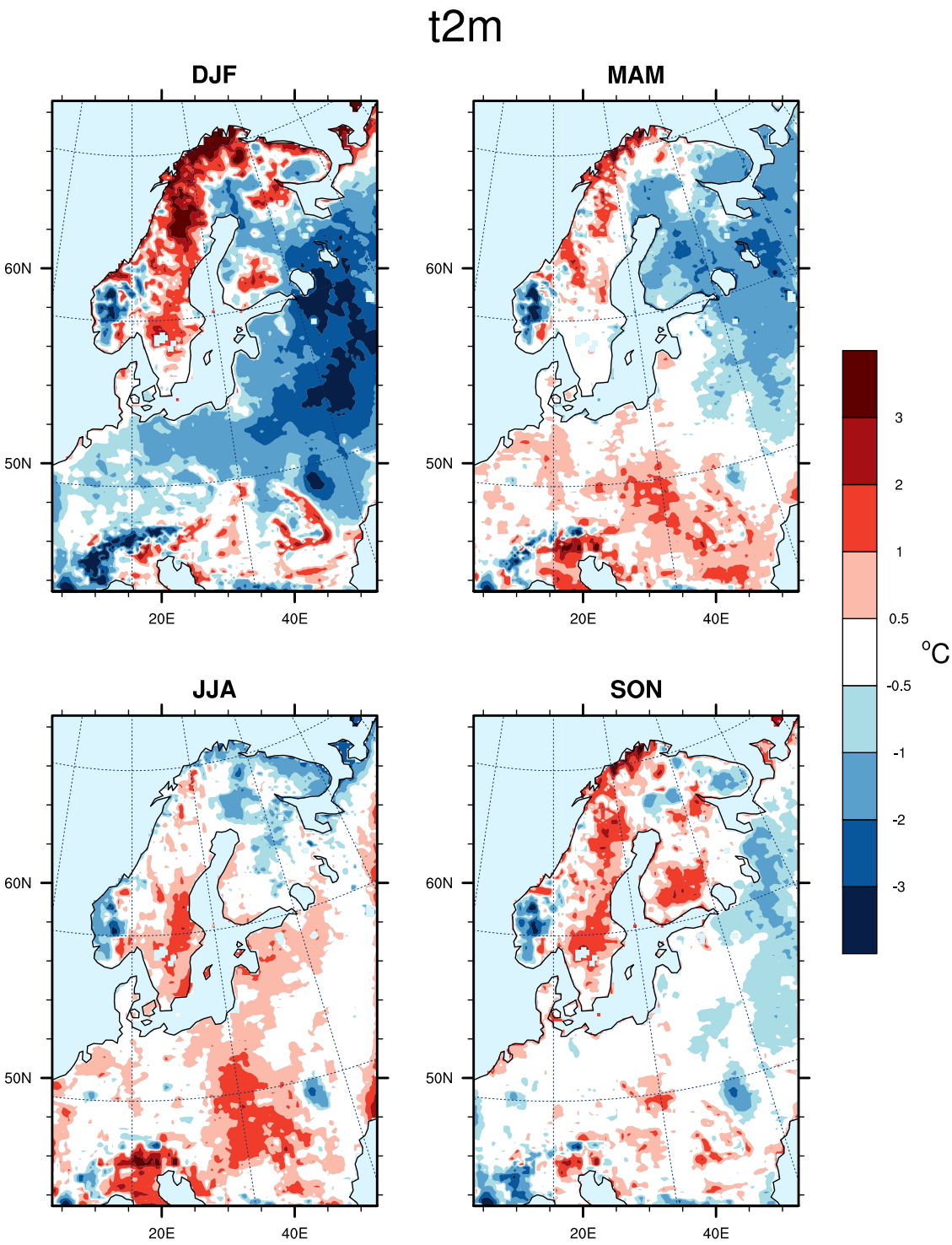

Figure 3.2: Difference of the 2m temperature from the coupled simulation and the CRU observations for the different seasons over the land area of the simulation domain for the period from 1989-2008.

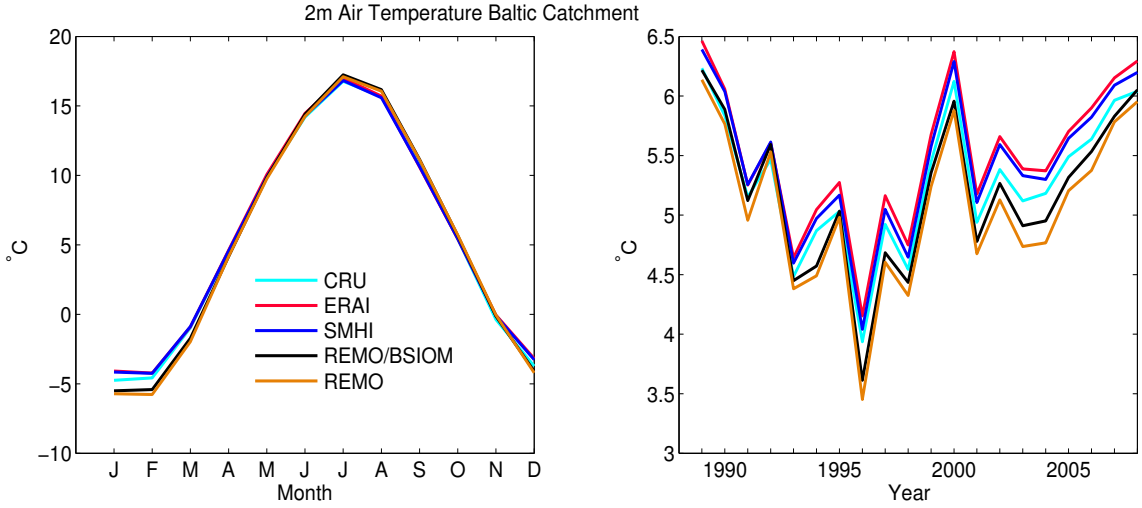

Figure 3.3: 2m temperature as mean annual cycle (left) and annual means (right) averaged over the land part of the Baltic catchment area for the period 1989-2008.

Next, the differences in the seasonal behavior of the simulated precipitation over land and sea are investigated. In Figure 3.5 the contributions from the large scale and the convective parameterizations of precipitation in the model are shown for land and sea separately, both for the whole domain (a) and the Baltic catchment area. This separation is actually a model artifact, which uses different parameterizations for resolved (large-scale) and subgrid-scale (convective) processes. The large scale precipitation (dashed lines) is very similar over land (red) and over water (blue). The main differences come from the convective activities (dash-dotted lines) due to the different thermal inertia. Over land the convective precipitation peaks in July with more than 2mm per day whereas over water the highest convective activity occurs later during summer when the atmosphere starts to cool faster than the ocean due to the large amount of heat stored in the Baltic Sea.

Figure 3.6 depicts the difference between the simulated precipitation and CRU over land. During winter and autumn the differences are relatively low (about 20%) and the spatial structure has common features to the orography. The reason for this similarity might be a too intense orographic precipitation. During spring and summer the biases are stronger (around 40%) and are mainly caused by the convective parameterization. This is a common problem of regional climate models. It might be a problem of double counting mesoscale processes which are already partly resolved by the model, especially at higher resolutions (Jones et al. 2004).

The mean annual cycle as well as the inter-annual variability are captured well by the model simulations as shown in Figure 3.7. However, there is a quite strong wet bias of more than 40% in summer leading to an overestimation of about 30% in the yearly mean (Table 3.1). An investigation by Rubel and Hantel (2001) of systematic errors of rain-gauges in the Baltic catchment area revealed an under catch of more than 20% during winter when precipitation mainly falls as snow and minor corrections of about 5% in

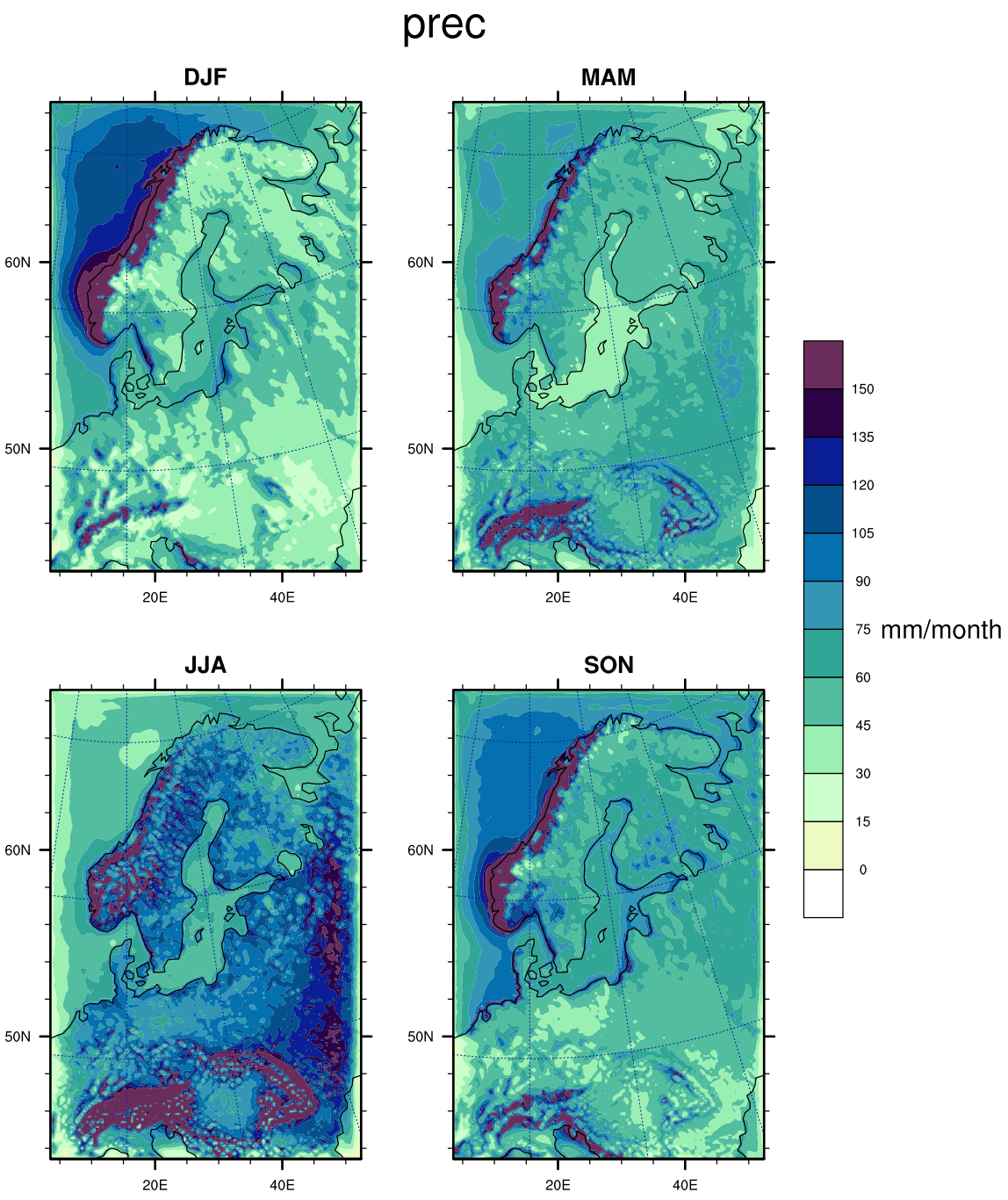

Figure 3.4: Seasonal means of the total precipitation in $^{\mathrm{mm}}/_{\mathrm{month}}$ in the coupled simulation over the simulation domain for the period 1989-2008.

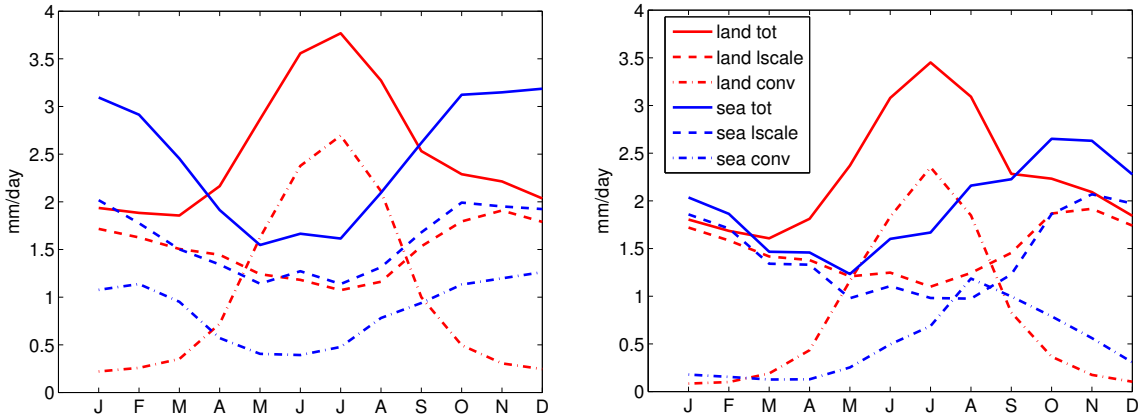

Figure 3.5: Mean annual cycles of precipitation averaged over the whole domain (a) and the Baltic catchment area (b).

summer which have to be taken into account when evaluating the model output. With these corrections in mind, there is a quite good agreement of the precipitation intensities for the winter months suggesting that the large-scale part of the simulated precipitation is realistic. Assuming this, the convective precipitation is overestimated by around 50% throughout the year.

Evaporation

Another important component of the water cycle is the evaporation. Its rate depends mainly on the availability of water at the surface, the available energy to compensate for the related latent heat flux, and the capacity of the lower atmospheric boundary to take up the evaporated humidity. In the Baltic catchment area, the soil is usually moist throughout the year. Therefore the evaporation rate closely follows the net surface solar radiation. Because of its heterogeneity, no gridded observational datasets exit for long time periods. Therefore only the ERA-Interim reanalyses are used as reference. The simulated evaporation has a stronger seasonal cycle compared to ERA-Interim and is about 10% higher on an annual basis as shown in Figure 3.8.

Surface Runoff

Figure 3.9 shows the runoff of the model runs and from ERA-Interim. Data from HELCOM (a combination of observations and modeled data Graham (1999); Kronsell and Andersson (2012)) from the river flow are also shown for comparison. Note that the modeled runoff and the river data are not comparable on a monthly time scale since the former is the local runoff and the latter the flow at the river mouths. In REMO, the peak during spring due to snow melt is in April, one month earlier compared to ERA-Interim. Hagemann et al. (2004) found a statistical relation of the surface runoff and the river discharge with

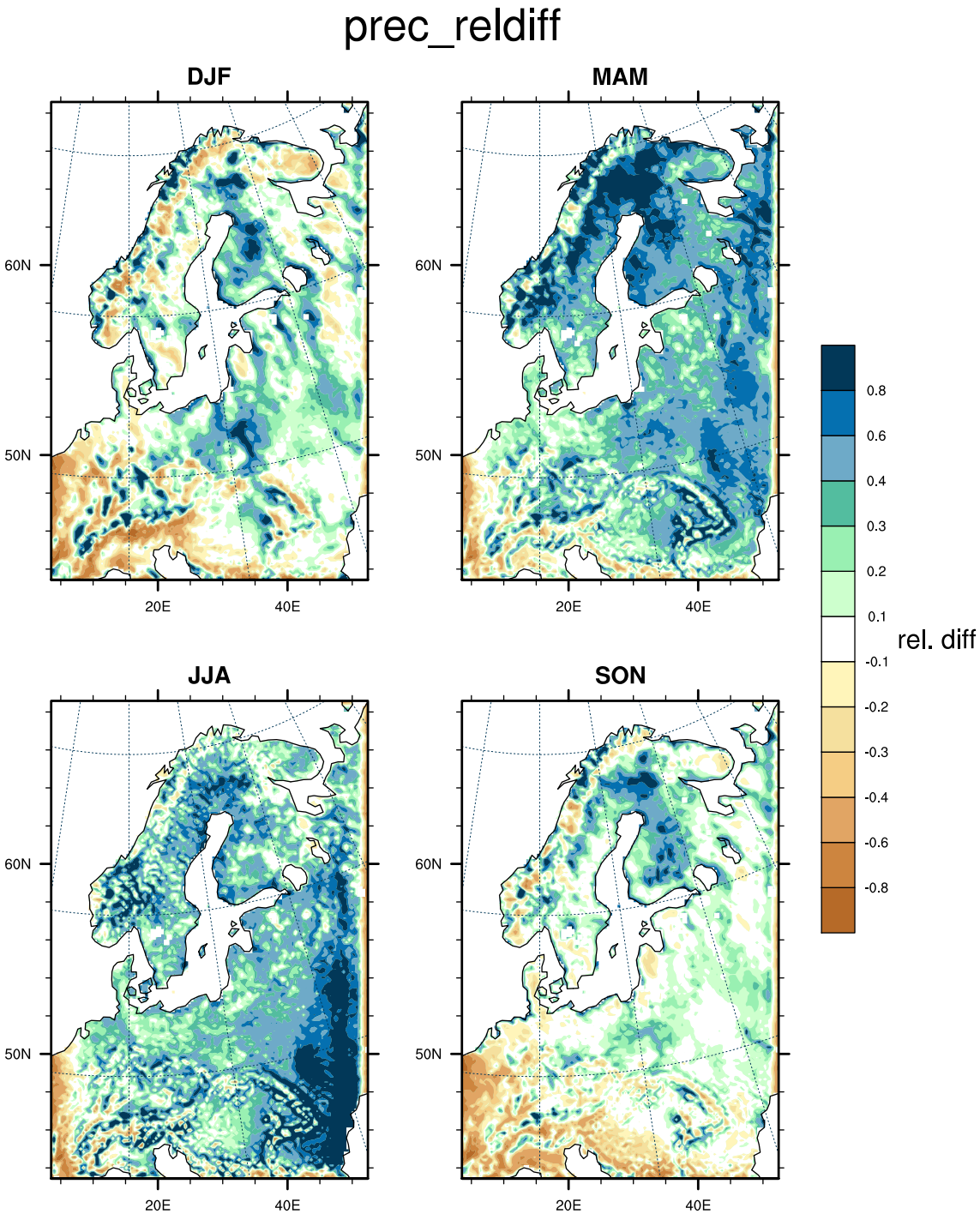

Figure 3.6: Difference of total precipitation from the coupled simulation and the CRU observations for the different seasons over the simulation domain.

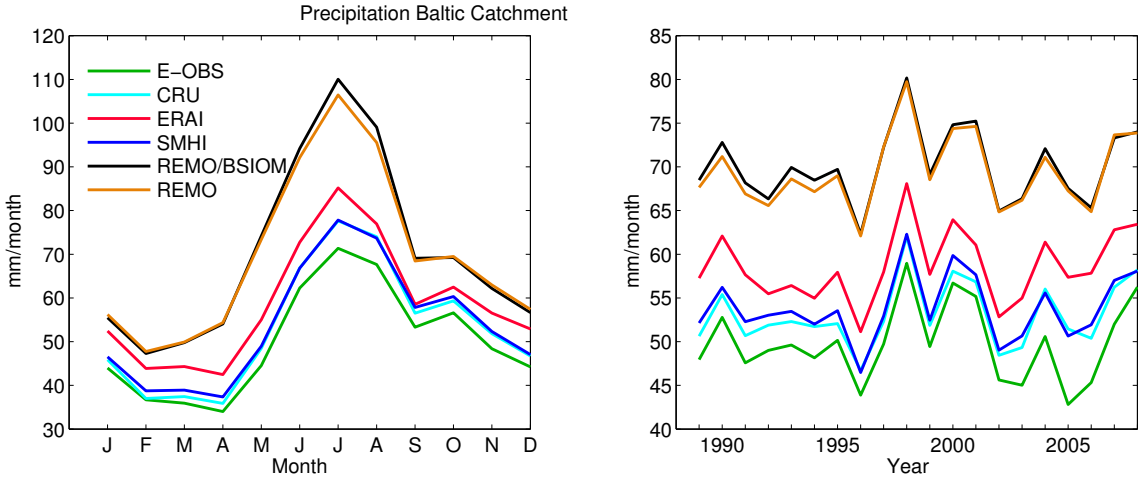

Figure 3.7: Total precipitation from different datasets as mean annual cycle (left) and annual means (right) averaged over the land part of the Baltic catchment area for the period 1989-2008.

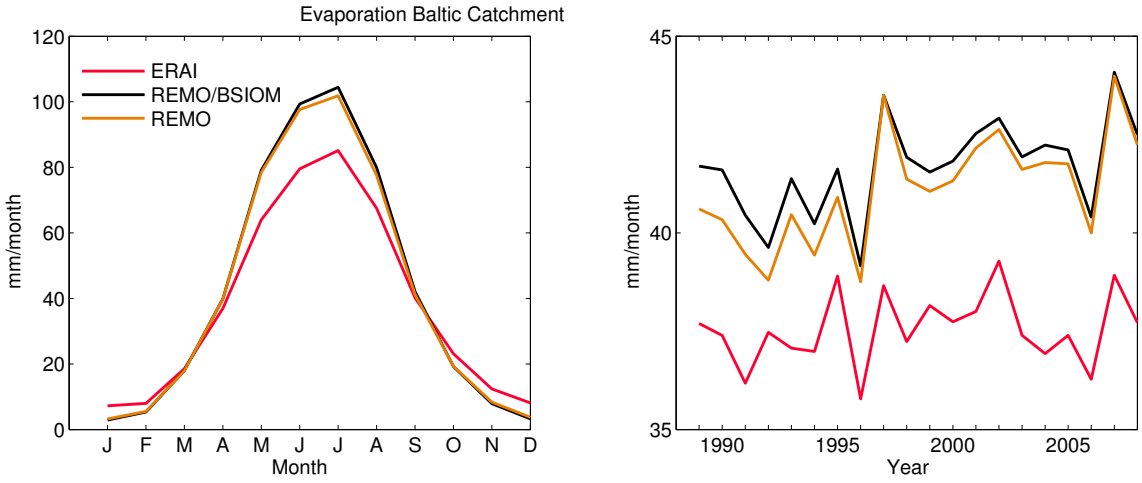

Figure 3.8: Evapo-transpiration as mean annual cycle (left) and annual means (right) averaged over the land part of the Baltic catchment area for the period 1989-2008.

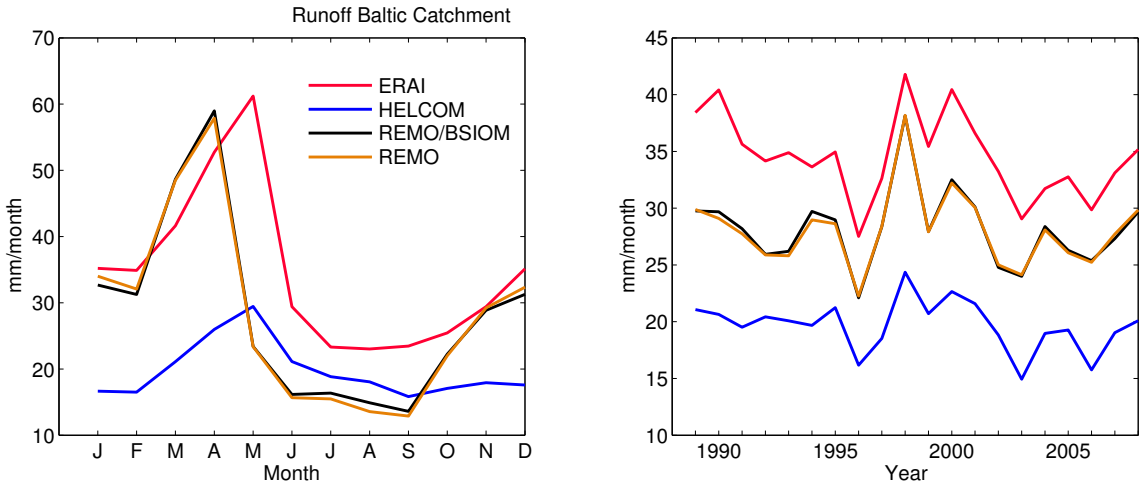

Figure 3.9: Surface runoff as mean annual cycle (left) and annual means (right) averaged over the land part of the Baltic catchment area for the period 1989-2008.

an average delay of about one month which tends to confirm the REMO results. The annual means are about 40% higher compared to the HELCOM data. To use the modeled runoff as input for a coupled river routing scheme to close the water cycle within the model domain would have a strong impact on the salinity of the Baltic Sea (Meier and Kauker 2003).

Surface water balance

Table 3.1 shows a summary of the yearly means of total precipitation, evaporation, and runoff. For precipitation, the spread among the different datasets is relatively large. The simulated precipitation lies above this range. The inter-annual variations are very similar however. The runoff from ERA-Interim has a large bias compared to the observations. The water balance is not closed. The reason for this inconsistency might be the soil-moisture nudging in ERA-Interim (Hagemann, pers. comm.). Because of the too high surface runoff, a river routing scheme is not implemented in the coupled model system. The river discharge into the Baltic Sea is instead prescribed from observations.

3.2 Baltic Sea surface

Next the model performance at the sea surface of the Baltic Sea is evaluated. Note that the different datasets are not always directly comparable since some of them as NOCS are restricted to ice-free conditions. Differences in the land-sea masks resulting from different resolutions can also lead to considerable differences.

Table 3.1: Surface water balance over the Baltic catchment area for the period 1989-2008. Shown are the annual means and their standard deviations for precipitation, evaporation, and runoff in $^{mm}/_{year}$.

	Precipitation	Evaporation	Runoff
E-OBS	598 ±53	-	-
CRU	637 ±46	-	-
ERAI	703 ±49	451 ±11	415 ±45
SMHI	646 ±46	-	-
HELCOM	-	-	236 ±26
REMO/BSIOM	841 ±51	500 ±15	338 ±41
REMO	834 ±52	493 ±17	337 ±40

3.2.1 Atmospheric variables

2m temperature

The 2m temperature is influenced by both the large-scale atmospheric situation and the sea surface temperature. In the model it is an interpolation between the surface temperature and the first model level using the stability functions described in section 2.1.1.

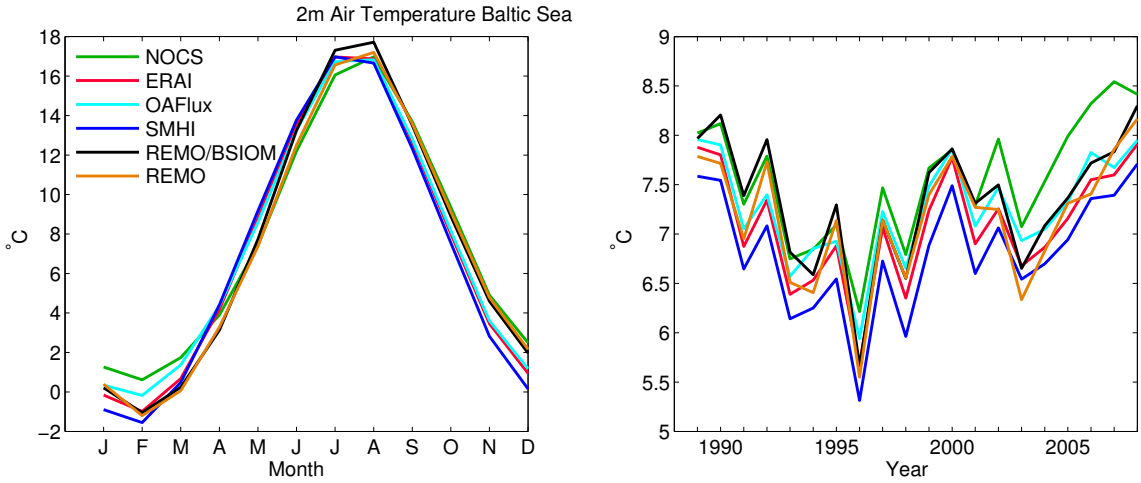

Figure 3.10: 2m temperature as mean annual cycle (left) and annual means (right) averaged over the Baltic sea surface (excluding Kattegat and the Danish Straits) for the period 1989-2008.

Figure 3.10 shows the mean annual cycle and the annual-mean time series of the 2m temperatures for the period from 1989 to 2008. During winter, the results from the coupled model simulation are within the range of the other datasets. During spring, the temperatures derived from the simulations are increasing more slowly than the others. Several explanations are possible for this: different stability parameterizations of the atmospheric

boundary layer, and/or lower advection of heat from land to the Baltic Sea. During summer and autumn, the model has a warm bias of about half a degree. These differences will be discussed later in 3.2.2.

Regarding the different observational datasets, NOCS shows too high temperatures during winter due to the restriction of the data to ice-free conditions. During spring they are similar to the modeled temperatures. The SMHI temperatures are colder during winter and warmer during spring than the other datasets. This probably comes from the extrapolation of the synoptic observations situated mainly over land. Apart from a relatively constant offset, the inter-annual variations is quite similar in the simulations and the observational datasets.

Specific humidity

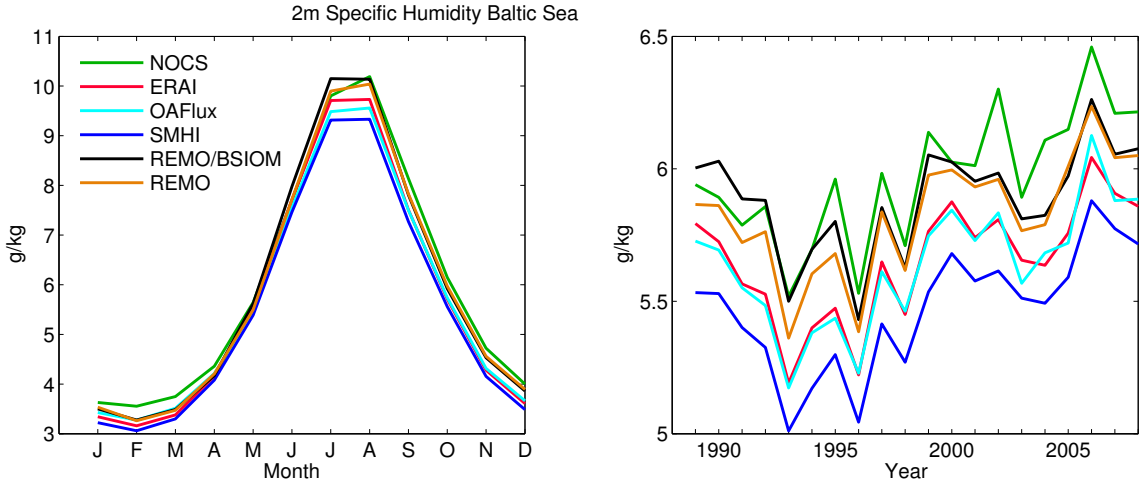

Figure 3.11: Specific humidity as mean annual cycle (left) and annual means (right) averaged over the Baltic sea surface (excluding Kattegat and the Danish Straits) for the period 1989-2008.

The specific humidity is strongly related to the 2m temperature that determines the saturation vapor pressure according to the Clausius–Clapeyron relation. It also depends on other factors like the evaporation, the atmospheric stability, and the advection. The mean seasonal cycle and the annual means of the specific humidity over the Baltic Sea are depicted in Figure 3.11. The annual cycle resembles to that of the 2m temperatures. But there is a larger spread among the different datasets. The year-to-year variations do not correlate very well with temperature showing the importance of the other factors mentioned. It is very similar among the different datasets with a nearly constant bias along the years. Similarly to the 2m temperature the coupled models shows the highest values in specific humidity during the summer period. The SMHI data have the lowest values throughout the whole year. Again, this might be due to the use of land stations where the relative (and thus the absolute) humidity is typically lower.

Precipitation

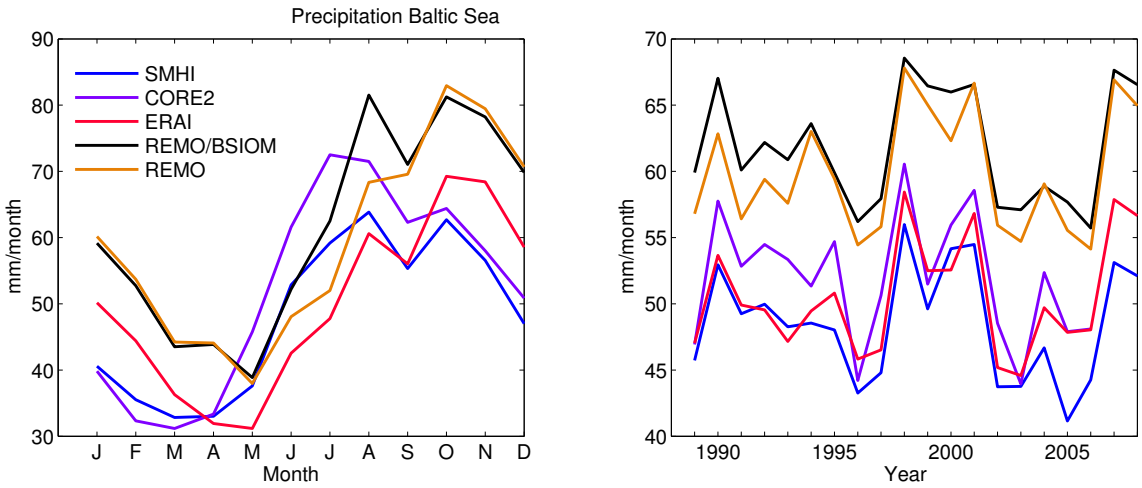

Figure 3.12: Precipitation as mean annual cycle (left) and annual means (right) averaged over the Baltic sea surface (excluding Kattegat and the Danish Straits) for the period 1989-2008.

Figure 3.12 shows the mean annual cycle and the yearly means of precipitation averaged over the surface area of the Baltic Sea for the period from 1989 to 2008. Consistently in all datasets, a distinct annual cycle is visible, with its minimum at about $40^{\mathrm{mm}}/_{\mathrm{month}}$ per month during spring and its maximum at about $80^{\mathrm{mm}}/_{\mathrm{month}}$ in late summer and autumn. This can be explained by the large heat capacity of the water masses of the Baltic Sea that causes a delayed annual cycle of the SSTs compared to the near-surface temperatures of the atmosphere, which are influenced by the large-scale advection of heat. During spring the atmosphere warms up faster than the water, which leads to a high stability of the atmospheric boundary layer and thus reduced convective activity, and in the end less convective precipitation. During late summer when the atmosphere starts to cool down, the opposite effect with a relatively unstable boundary layer and enhanced convective precipitation occurs. This peak coincides with the maximum of large scale precipitation during autumn.

This behavior is different compared to the precipitation over the land part of the catchment where the surface temperatures are in phase with the near-surface air temperatures. There the highest convective activity is in mid-summer (see Figure 3.7). Compared to the observations, the model shows good skills in reproducing the inter-annual variability, with a wet bias of about 20% as seen previously in the analysis of the precipitation for the whole catchment area. The coupled model simulates more precipitation than the stand-alone REMO in summer due to the higher SSTs (see 3.2.2) and thus more convection.

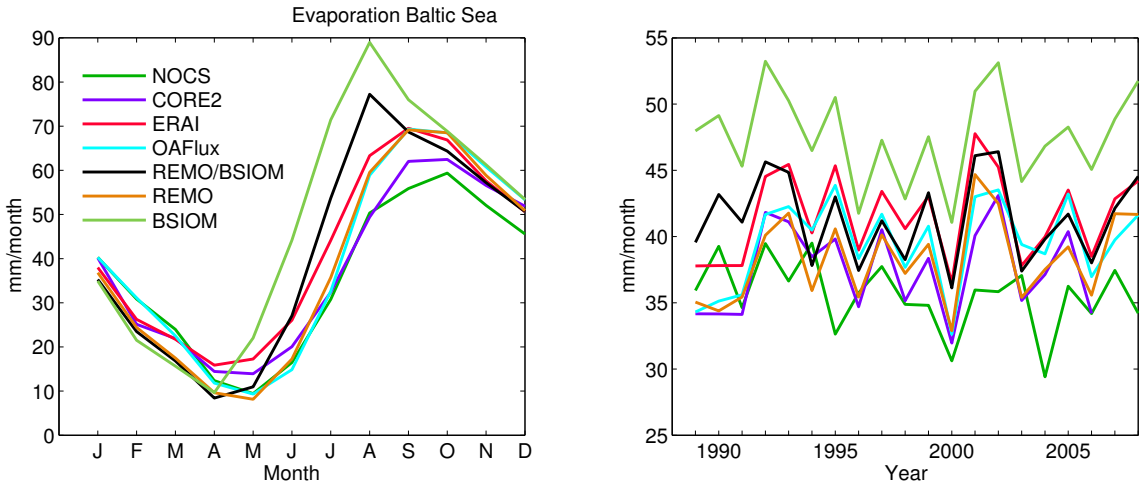

Figure 3.13: Evaporation as mean annual cycle (left) and annual means (right) averaged over the Baltic sea surface (excluding Kattegat and the Danish Straits) for the period 1989-2008.

Evaporation

The evaporation rate is depicted in Figure 3.13. It is determined by the difference in vapor pressure at the surface and the atmosphere, the wind speed and the atmospheric stability (compare Equation 2.2). Due to its dependence on the stability of the atmospheric boundary layer, the evaporation rate shows a similar annual cycle as precipitation, but with stronger variations since large-scale effects are less important. The coupled model agrees well with the observations, except during summer when it shows enhanced evaporation. This can be explained by the higher SSTs. BSIOM has an even stronger bias because of the low specific humidity in the prescribed SMHI observations that cannot react to this enhanced evaporation as seen in the coupled simulation. In contrast to the coupled run, the evaporation rate of the uncoupled REMO simulation is significantly lower compared to ERA-Interim during spring and summer. The difference in the 2m specific humidity can probably only partly explain this.

Net freshwater flux

The difference between precipitation and evaporation gives the net freshwater flux to the Baltic Sea. It has a direct impact on the salinity and also on the stratification as it represents a buoyancy flux due to the lower density of the fresh water. As can be seen in Figure 3.14, there are considerable differences among the datasets. Most of them (except CORE2) have a distinct annual cycle with a minimum during late summer when the evaporation rate has its maximum.

Table 3.2 shows the averages over the simulation period from 1989 to 2008 of precipitation,

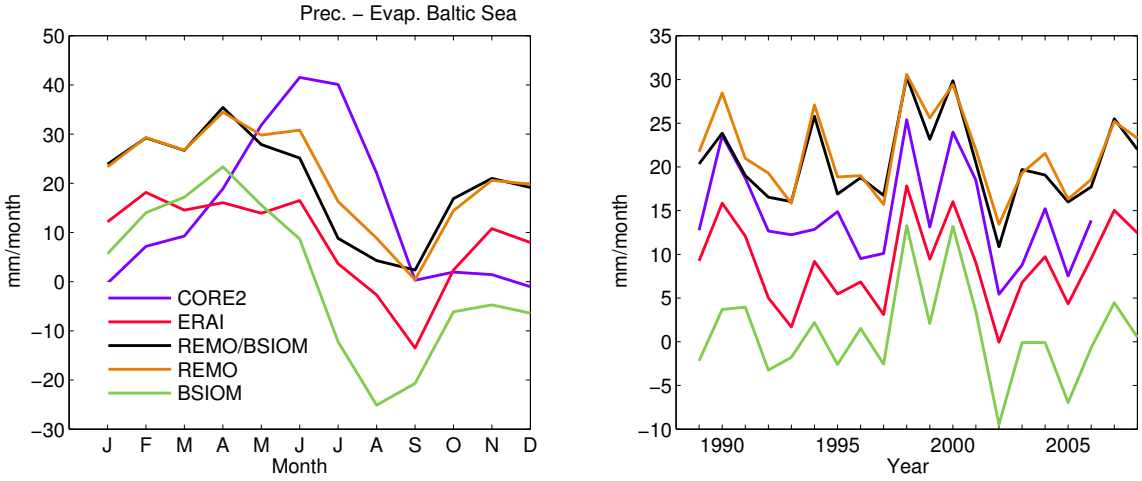

Figure 3.14: Precipitation minus Evaporation as mean annual cycle (left) and annual means (right) averaged over the Baltic sea surface (excluding Kattegat and the Danish Straits) for the period 1989-2008.

Table 3.2: Surface water balance over the Baltic Sea (excluding Kattegat and the Danish Straits) for the period 1989-2008. Shown are yearly means and their standard deviations for precipitation, evaporation and the resulting freshwater flux. Units are $^{mm}/_{year}$.

	Precipitation	Evaporation	P - E
NOCS	-	427 ±32	-
SMHI	582 ±52	-	-
CORE2	622 ±57	450 ±40	173 ±68
ERAI	606 ±52	499 ±40	107 ±59
OAFlux	-	474 ±40	-
REMO/BSIOM	742 ±52	497 ±39	245 ±58
REMO	719 ±55	460 ±39	259 ±58
BSIOM	583 ±52	571 ±42	11 ±66

evaporation and their differences. This fluxes will become important for the closure of the water budget of the Baltic Sea in Chapter 4.

Surface Pressure & Atmospheric Circulation

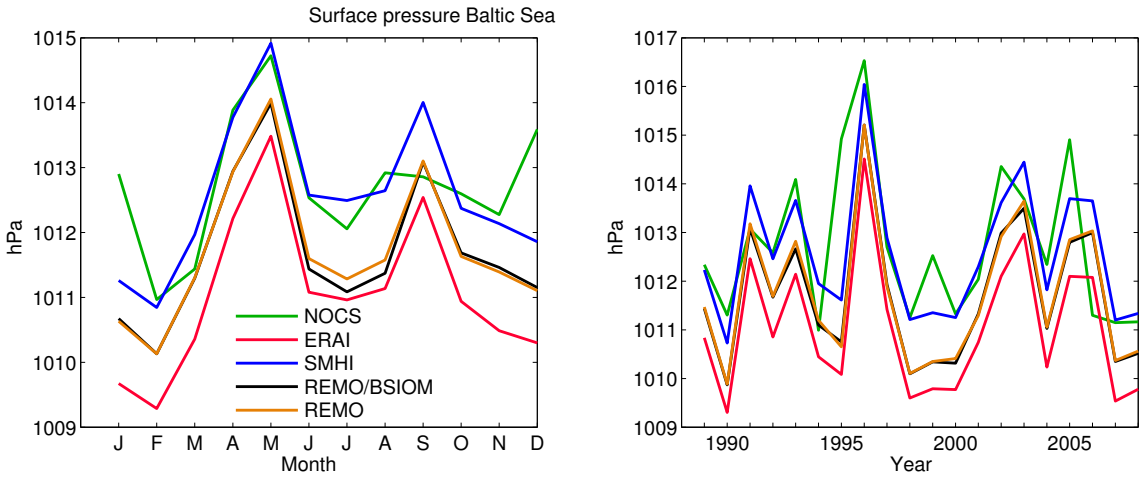

Figure 3.15: Surface pressure as mean annual cycle (left) and annual means (right) averaged over the Baltic sea surface (excluding Kattegat and the Danish Straits) for the period 1989-2008.

The mean sea-level pressure somehow represents the large-scale atmospheric situation. All datasets show a distinct mean annual cycle with maxima in May and September (Figure 3.15). Except for the NOCS dataset, there exists a quite good agreement for the annual cycle as well as the annual means of sea-level pressure, apart from a constant offset.

For the turbulent surface fluxes the near-surface wind speed is very important. In the Baltic region, wind speed is determined by cyclonic activity and related changes in the air pressure (Leppäranta and Myrberg 2009). Figure 3.16 shows the mean annual cycle and the yearly-mean time series of the 10m wind speed averaged over the Baltic Sea surface for the simulation period. The near-surface wind speed has a strong annual cycle with high velocities of about 8$^{m}/_{s}$ during winter and lower values of about 5-6 m/s in summer. The inter-annual variability is relatively low with annual means around 6.8 $\pm 0.2^{m}/_{s}$.

The different datasets agree within a range of 1$^{m}/_{s}$, except for OAFlux which shows much lower velocities during spring and summer.

The velocities in the coupled simulation are very similar to those existing in the ERA-I forcing dataset but with a slight shift in the seasonal cycle towards earlier months. The differences might partly come from differences in the stability of the atmospheric boundary layer.

For BSIOM the neutral 10m wind calculated from the geostrophic wind as described in Bumke and Hasse (1989) is shown, not taking the stability corrections into account. This is

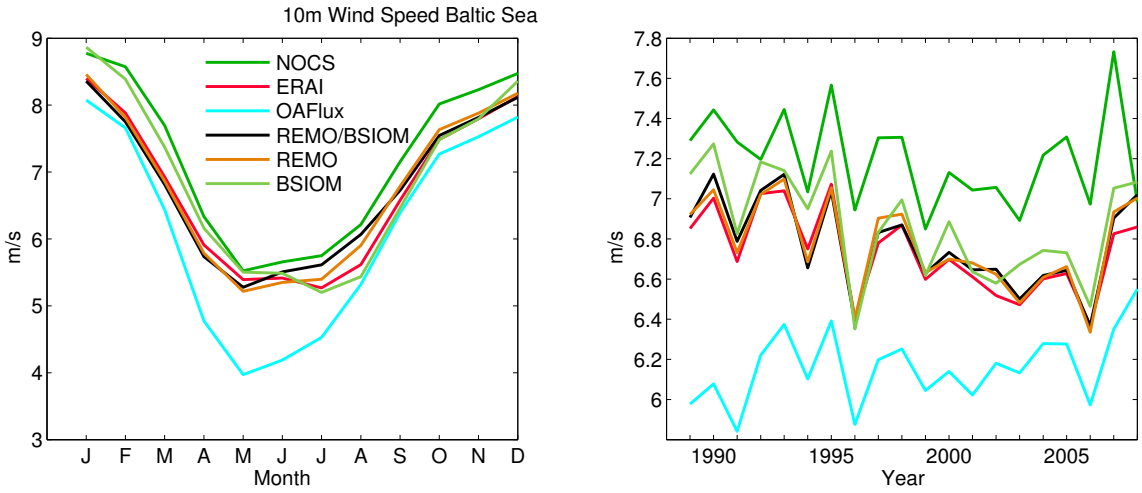

Figure 3.16: 10m wind speed as mean annual cycle (left) and annual means (right) averaged over the Baltic sea surface (excluding Kattegat and the Danish Straits) for the period 1989-2008.

the reason for the shift in the annual cycle with higher velocities during winter and spring when the marine atmospheric boundary layer (MABL) is relatively stable and lower values during late summer and early autumn when the MABL tends to be unstable.

The NOCS velocities deduced from ship observations are slightly higher than the other datasets.

3.2.2 Oceanic variables

Sea Surface Temperature

The SST is the most relevant variable to evaluate the performance of the coupled model system. It is determined by several factors. The most important ones are the fluxes between the ocean and the atmosphere. The surface heat fluxes affect the water masses within the mixed-layer depth which is mainly determined by mechanical wind mixing from wind and convective processes. For the SST different kinds of observations are available: measurements from satellites, ships and buoys. Figure 3.17 shows the mean annual cycle and the yearly-mean time series of the SSTs averaged over the Baltic Sea area (excluding Kattegat). Overall, the coupled model shows a reasonable seasonal cycle (left) and also the inter-annual variability is captured well. During winter, the SSTs lie within the range of the observations. During the heating period from May to August, however, there exists a warm bias of about 1°C. The reason for this is mainly based on the too shallow thermocline, which will be explained later. In the spatial distribution of the SST (not shown), the values of the coupled simulation are larger in summer near the coast. The reason is the coarser resolution of the atmospheric grid in REMO compared to the oceanic grid, since the surface

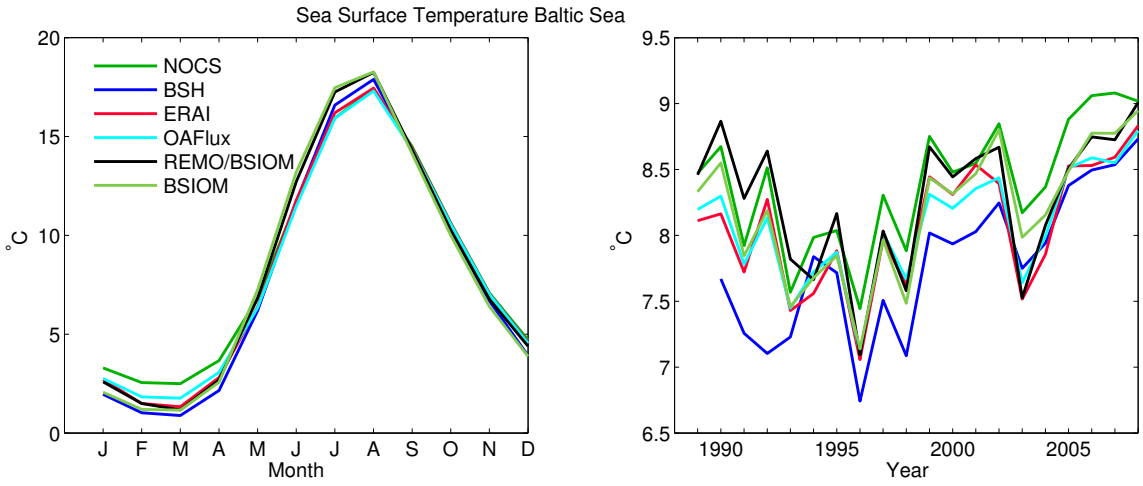

Figure 3.17: Sea surface temperature as mean annual cycle (left) and annual means (right) averaged over the Baltic sea surface (excluding Kattegat and the Danish Straits) for the period 1989-2008.

fluxes are calculated in REMO. The 4th-order dependence of the thermal upward radiation is problematic in this context and leads to larger SSTs in shallow areas (Döscher et al. 2002).

There is a relatively large spread among the observational datasets, especially during winter where the NOCS SSTs show more than 1°C larger temperatures than the other datasets. Most of this deviation is due to the assembling of the NOCS data based on ice-free conditions only (Berry and Kent 2009).

The satellite observations from the BSH indicate colder SSTs during winter and slightly warmer during summer. The cold bias might come from the fact that the measurements are taken under cloud-free conditions. The warm bias during summer might come from a diurnal thermocline in the upper layer leading to relative large differences between the skin temperature measured by the satellite and the bulk SST. The plot of the yearly-mean time series shows that the differences disappear from the year 2003 on.

It is worth to note that the simulated SSTs are a clear improvement compared to the old BALTIMOS model system, where Bennartz et al. (2009) found a generally too weak seasonal cycle with a delayed heating during spring. This bias to higher SSTs during winter lead to an underestimation of the ice extend.

Sea Ice

Sea ice is another important variable. Since ice can only form when the water temperature falls below the freezing point, it is very sensitive with regard to the SST. This leads to a high inter-annual variability.

In Figure 3.18 the sea-ice fraction is depicted. The annual cycle is well simulated with the start of the freezing in December, the maximum ice extend in March, and the end of the

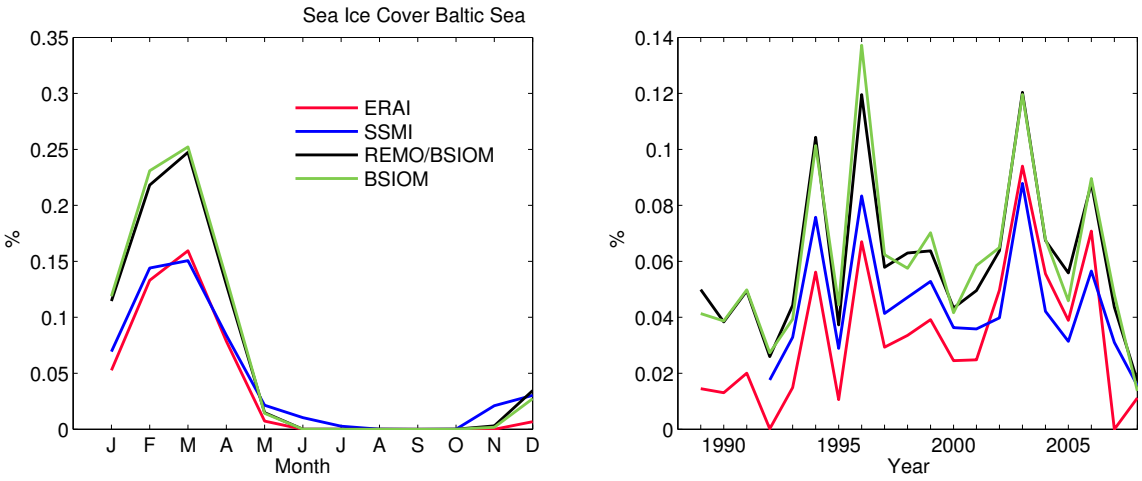

Figure 3.18: Sea ice concentration as mean annual cycle (left) and annual means (right) averaged over the Baltic sea surface (excluding Kattegat and the Danish Straits) for the period 1989-2008.

ice period in May. However, the simulated ice-covered area is overestimated by about 60%. The year-to-year changes are also in good agreement with the observations. The results from the coupled run and the uncoupled BSIOM run are very similar indicating that the sea ice cover is mainly determined by the parameterization of the sea-ice dynamics which are identical in the two simulations.

The SSM/I observations suffer from the contamination of the satellite observations from land areas (Bennartz 1999; Maaßand Kaleschke 2010). This can lead to an artificial detection of ice near the coast. Therefore there is an artificial extended sea ice period in this dataset.

In contrast to the old version of BALTIMOS where the sea ice concentrations were highly underestimated, there is an improvement over the old model system with too little ice extent and motion (Bennartz et al. 2009). The results are very sensitive to some key parameters in the sea-ice model. Some simple sensitivity simulations applying changes for these parameters indicate the possibility to improve the sea-ice representation in the model. Although this is beyond the scope of this project it seems worthwhile to mention it.

Temperature and Salinity

Figure 3.19 shows the mean salinity of the Baltic Sea for the simulation period from 1989 to 2008 (averaged over the whole basin excluding Kattegat and the Danish Straits). The coupled model simulation is drifting towards a freshwater lake.

Since the river discharge is identical in the two simulations, the reason for the differences must come from the atmospheric fluxes at the surface. One possibility is the enhanced

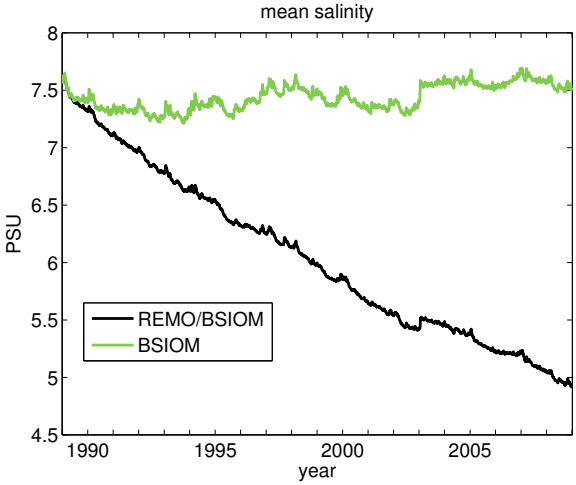

Figure 3.19: Mean salinity of the Baltic Sea averaged over the whole basin excluding Kattegat and the Danish Straits derived from different model simulations.

net freshwater flux in the coupled simulation compared to the uncoupled one as was found in Section 3.2. To investigate the influence of the freshwater flux on the salinity inflow, a sensitivity study for the year 1989 has been conducted where the precipitation in the coupled model was artificially reduced by one third to get a net freshwater flux similar to that in the uncoupled BSIOM simulation. The mean salinity averaged over the whole basin of the Baltic Sea of the three simulations is shown in Figure 3.20. It can be deduced that the differences in the freshwater flux can at least partly explain the reduced salinity.

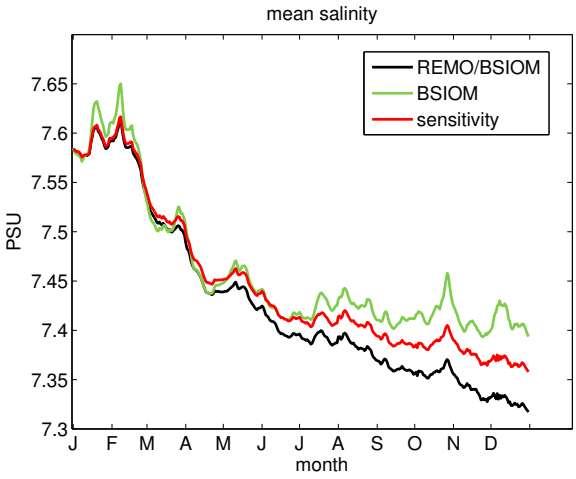

Figure 3.20: Mean salinity for the year 1989 of the coupled model (red), the uncoupled BSIOM (black) and from a sensitivity experiment with an artificial reduction of the precipitation over the Baltic Sea (green).

ICES subdivisions

To evaluate the model performance area averages of the vertical profiles are compared to observations from the ICES database. The ICES subdivisions for the Baltic Sea are shown in Figure 3.21.

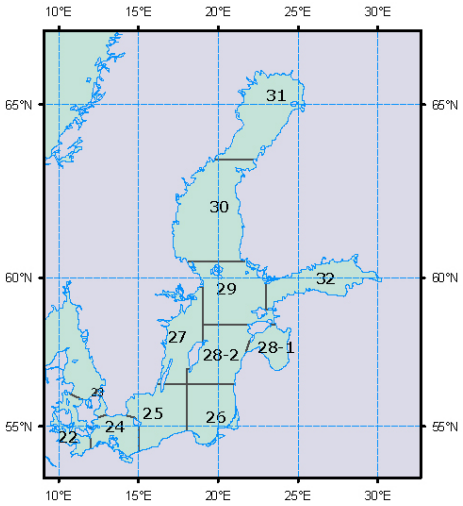

Figure 3.21: Map of the Baltic Sea showing the ICES subdivisions of the Belt, the Sound, and the Baltic Sea (from http://www.fao.org/fi/figis/area/data/assets/images/faoarea27_3.jpg).

Figure 3.22 shows the mean annual cycle of the area-averaged temperature profile for the ices region 28. The difference plot shows that the thermocline is too shallow during spring and summer leading to too high surface temperatures and too low temperatures just below the thermocline. During autumn the mixed-layer depth seems to deepen too rapidly.

In Figure 3.23 a comparison of the salinity profiles is shown. In the ICES area 25 close to the entrance of the Baltic Sea the bottom salinity decreases quickly in the model simulation. A strong stratification is only visible during strong inflow events. This leads to a too low inflow of highly saline water into the basins of the central Baltic Sea where the salinity decreases steadily (3.23b).

3.2.3 Sea level

On decadal time scales, the mean sea level (MSL) in the Baltic Sea is mainly influenced by the global sea level rise and the uplift of the land due to the post-glacial rebound.

The mean sea level and its variability of the Baltic Sea basin is influenced by several factors. Samuelsson and Stigebrandt (1996) developed a model to calculate the barotropic

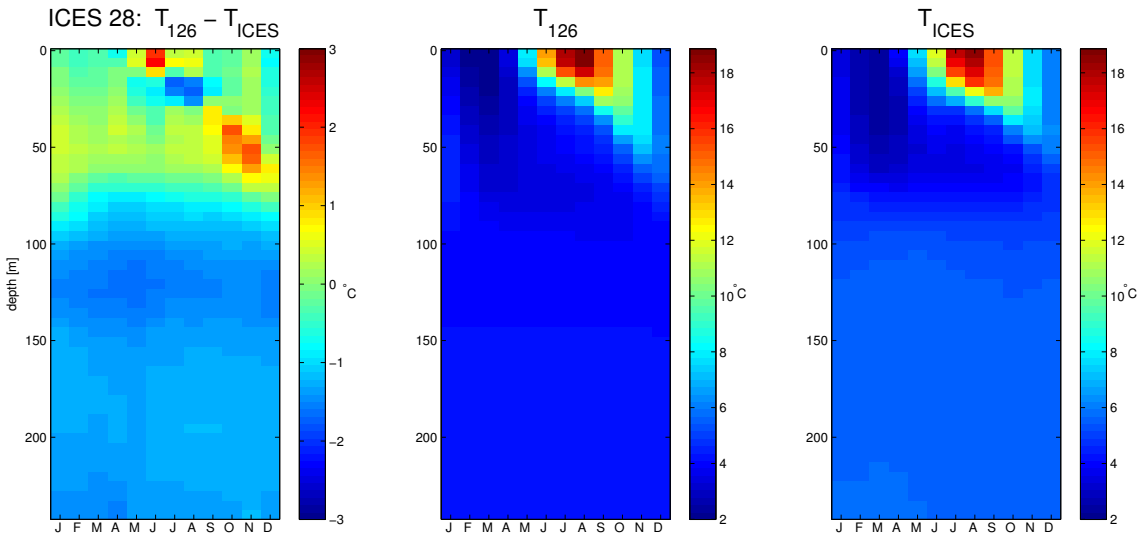

Figure 3.22: Comparison of temperature profiles

flow through the narrow channels of the Danish Straits with the Kattegat using the sea level difference between the Kattegat and the Baltic Sea.

The sea level Figure 3.24 shows the monthly mean time series of the sea level at Landsort for the period from 1989-2008 from the coupled model simulation (blue line) and from observations (red line). The modeled sea level follows the observations quite closely on a monthly time scale. This shows that the method of using the BSI to define the external forcing in the North Sea works quite well. The extreme values are a bit overestimated however. This is also visible in the spectral representation of the daily time series shown in Figure 3.26.

Since the sea level at Landsort is a good estimator of the mean sea level of the whole Baltic Sea, its daily changes can be seen as a good measure of the water exchange with the North Sea through the Danish straits. A comparison of the daily changes from the model simulation and from observations is depicted in Figure 3.25. The model seems to reproduce the observations adequately indicating that the barotropic exchange between the Baltic and the North Sea is simulated realistically. This means that the reduced salinity inflow must have other reasons like a wrong baroclinic flow or wind stirring in the Danish straits or the Kattegat.

EOF analysis of the sea level

In order to investigate the spatial variations, an EOF-analysis from the daily values of the simulated sea surface elevation has been performed (Janssen 2002). The spatial patterns and the explained variability of the first three principle components is shown in Figure 3.27.

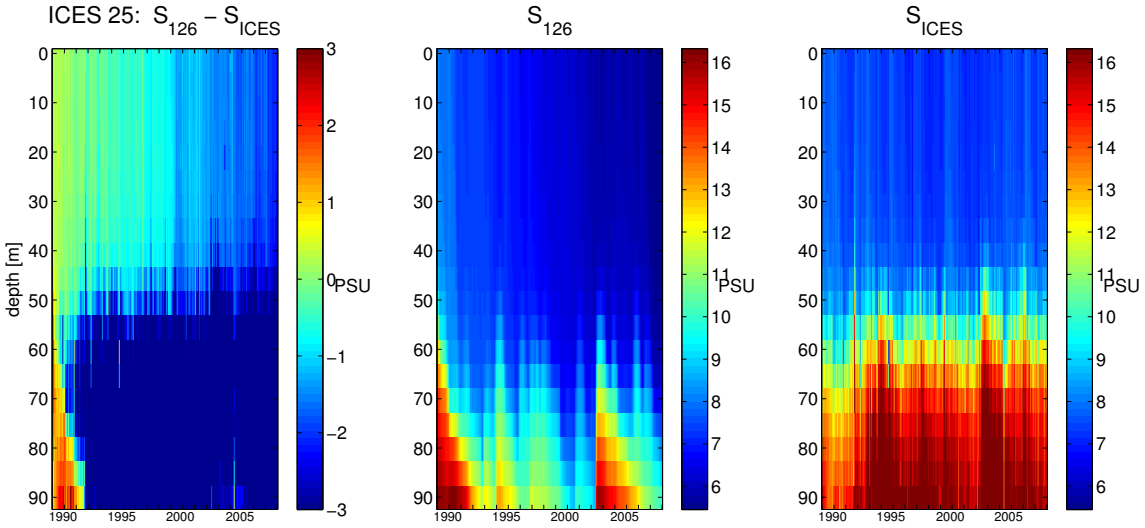

(a) ICES 25

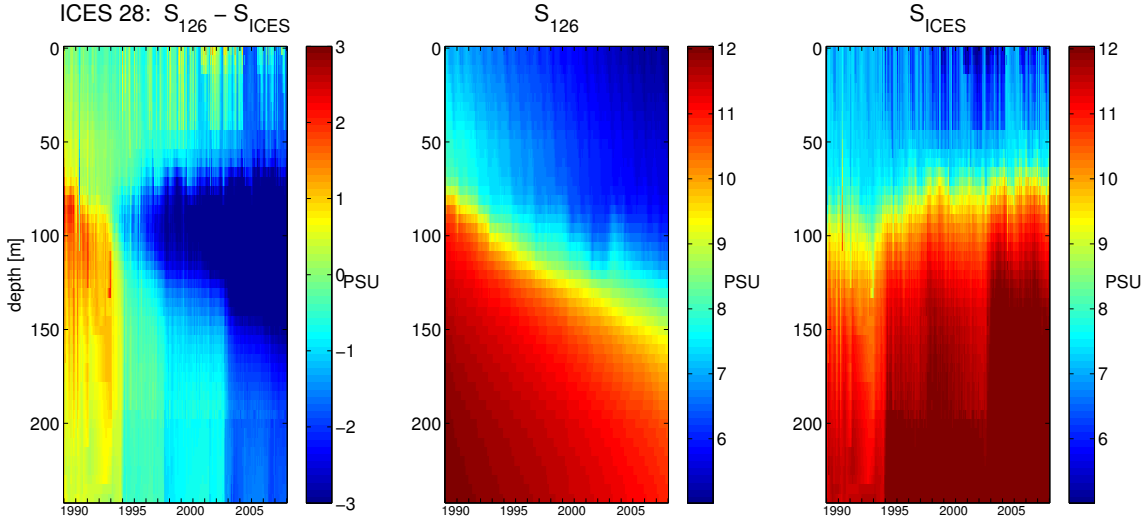

(b) ICES 28

Figure 3.23: Comparison of salinity profiles

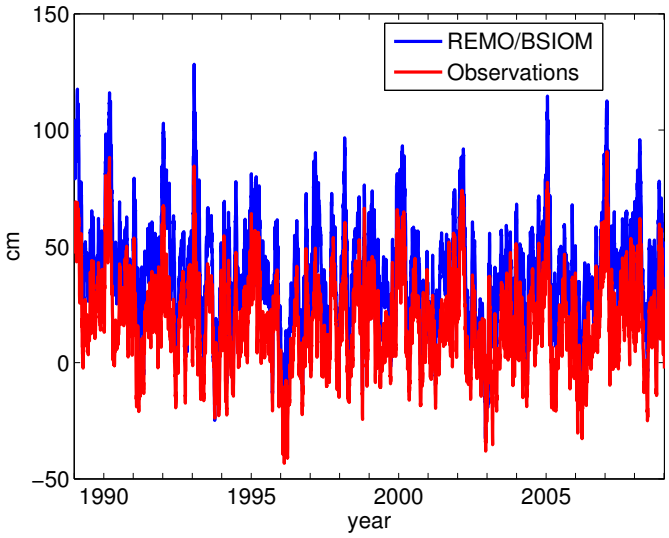

Figure 3.24: Time series of the monthly-mean sea level at Landsort for the period from 1989-2008 from the coupled model simulation (blue line) and from observations (red line)

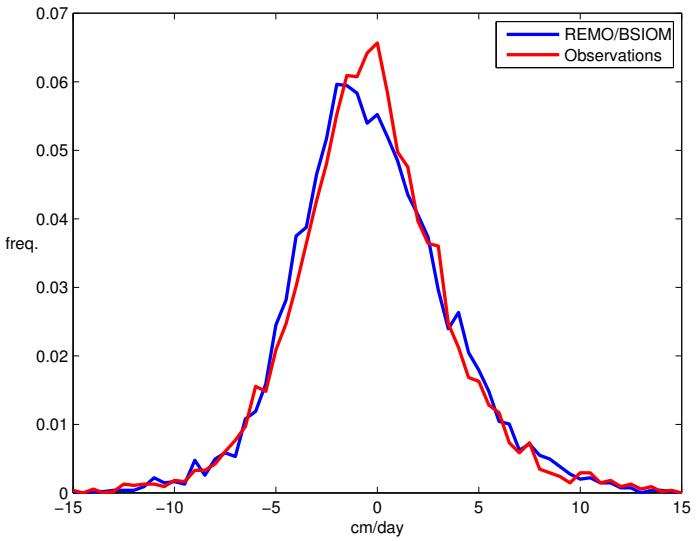

Figure 3.25: Histogram of the daily change in sea level at Landsort for the period from 1989-2008. The model simulation is shown in blue and the observations in red. TODO:Bin size??

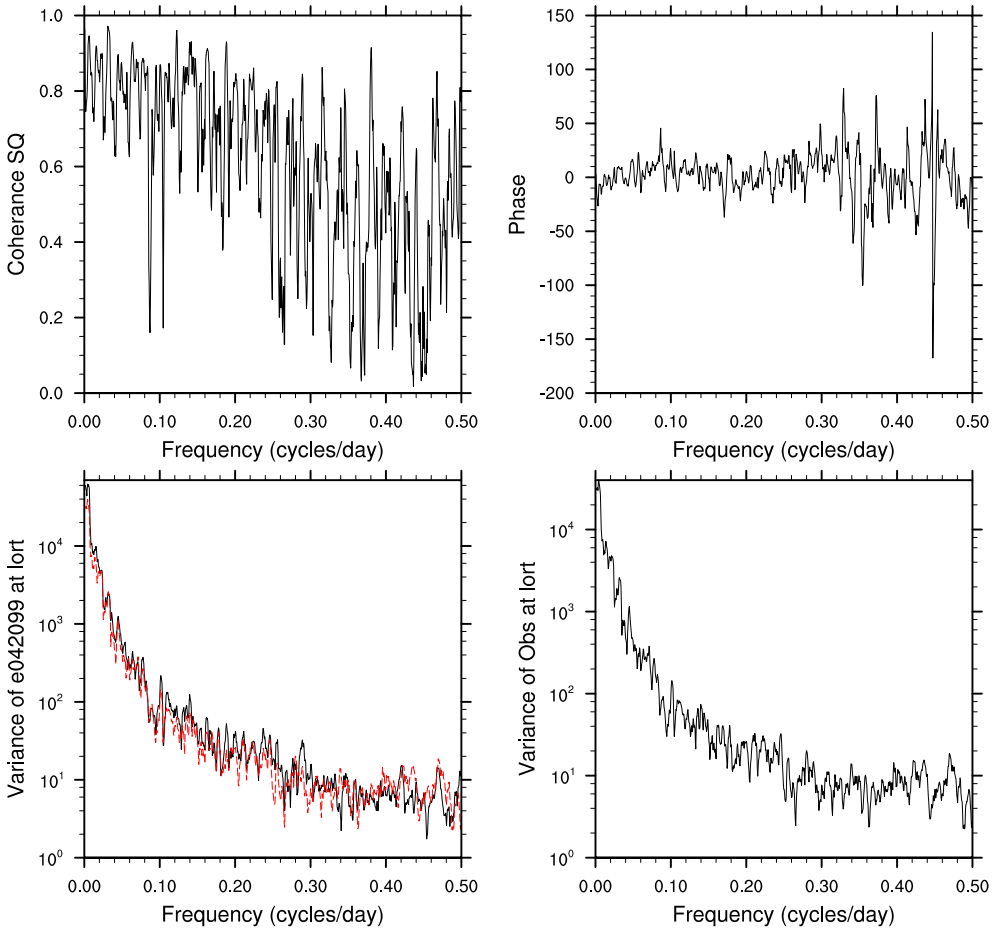

Figure 3.26: Coherence and power spectra of the modeled sea level and observations

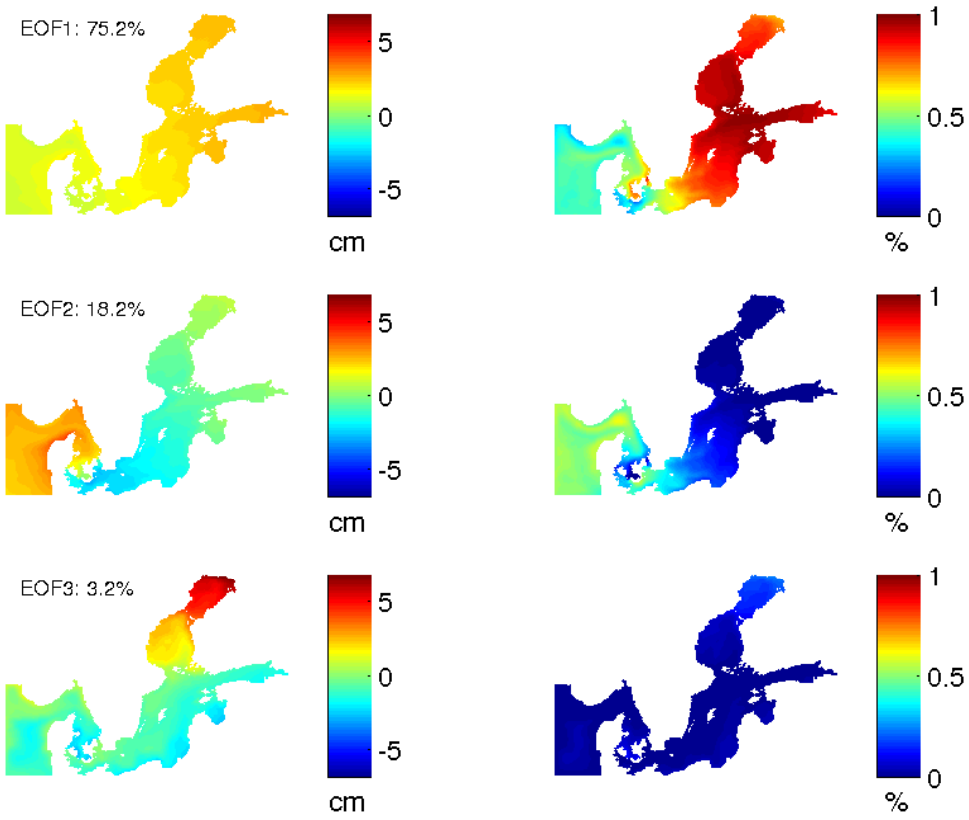

Figure 3.27: EOF analysis of daily sea level time series from the coupled model simulation for the period from 1989-2008.

The first principal component has the imprint of an open basin where the sea-level oscillations are in phase in the whole Baltic Sea with the amplitude increasing with the distance from the entrance area. It explains about 75% of the total variability and almost all variability at the node of the first seiche oscillation of the Baltic Sea (Neumann 1941).

3.3 Conclusions

In this chapter, the ability of the model system to reproduce some observed variables has been evaluated. Over land REMO simulates the 2m temperatures reasonably well with a cold bias of up to 3°C in the eastern part of the domain during winter which might be related to the surface-albedo parameterization for snow-covered forests. The simulations also show warm biases over the Finish lakes and in the Scandinavian mountain ridge. An implementation of a lake model would probably help to reduce these biases.

More problematic for a potential regional earth system model is the overestimation of precipitation of about 30%. Potential reasons are a too high horizontal moisture flux in the forcing boundary data from ERA-Interim. Also the convection parameterization might play a role. These issues have to be solved before the next step toward of a full regional earth system model by including a river routing scheme to close the water cycle within the model domain.

The simulated SSTs are in relative good agreement with the observations. From May to August the temperatures are about 1°C too high which could be explained by a too shallow seasonal thermocline. Therefore the parameterization of turbulence is another important topic that needs further improvement in the model system.

The seasonal cycle and the inter-annual evolution of the sea ice cover is simulated realistically, with a considerable overestimation of the ice extend of about 60% however. The reason is probably that the ice is too rigid in the model.

The major deficiency of the model system is the inability to simulate the salinity correctly. In the current configuration the Baltic Sea seems to drift toward a fresh-water lake. Parts of the weak salinity inflow can be explained by the high net precipitation over the Baltic Sea in REMO. Given the horizontal and vertical resolution of the model, one can probably not expect to resolve the complex process of salt exchange sufficiently. A pragmatic solution could be the artificial deepening of the entrance area. Other approaches are the nesting of a model with higher resolution at the channels (Tian et al. 2013) or adoptive grids (Hofmeister et al. 2011). To make the model system usable for longer simulations this problem has to be solved first.

The barotropic flow and connected to it the variability of the sea level are simulated realistically. The model could be used for sea-level-change studies.

Chapter 4

Water & Energy Budget of the Baltic Sea

4.1 The BALTEX box

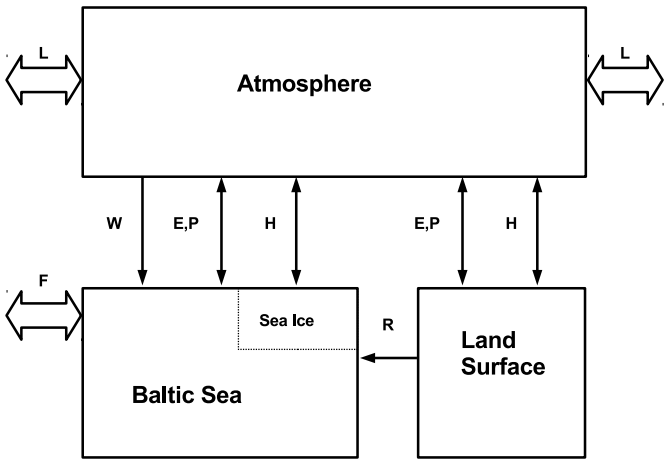

Figure 4.1: Schematics of the three components of the Baltic earth system and the coupling among them: atmosphere, continental surfaces and Baltic Sea. E evaporation, P precipitation, F in- and outflow through the Danish Straits, H heat and energy flux at the air-sea and air-land interfaces, including radiation, L lateral heat exchange with the atmosphere outside the Baltic catchment area, R river runoff, W wind stress at the sea surface. Adapted from Omstedt and Nohr (2004); IBS (1995).

The topic of this chapter are the water and energy cycles of the Baltic Sea. This was one of the major topics in BALTEX Raschke et al. (2001). Several studies have been conducted using observations or numerical models.

Due to its semi-enclosed nature, the Baltic Sea is almost in thermo-dynamic balance with the atmosphere (Omstedt and Rutgersson 2000).

Figure 4.1 shows the BALTEX box IBS (1995) illustrating the three main components of the earth system of the Baltic catchment area and its interaction among them. The focus of this work lies on the Baltic Sea itself. The sea ice has been included into the budget because of the variety of different processes involved in ice freezing and melting, like ice growth in open water or melting of ice that is advected to warmer areas. This is different to other studies like those of Omstedt and Rutgersson (2000) or Omstedt and Nohr (2004) where the cryosphere was not part of the budget.

The Baltic Sea is connected with the atmosphere above through the radiative and turbulent heat fluxes, evaporation and precipitation, and wind stress, to the land part of the catchment area through the river discharge, and to the North Sea through the in- and outflows via the Danish Straits. In the following all fluxes and their contribution to the energy and mass budgets of the Baltic Sea are investigated.

Meier and Doscher (2002) investigated the water and energy cycles in the coupled model system RCAO.

4.2 Surface Fluxes at the Baltic Sea

The most important components are the fluxes at the air-sea interface of the Baltic Sea. The mean annual cycles and yearly-mean time series averaged over the Baltic Sea surface (excluding Kattegat and the Danish Straits) are analyzed by comparing the coupled and uncoupled simulations to the observational and reanalysis datasets. Note that the comparison of the area averages might hide considerable differences on smaller scales like coastal effects for example (Hagedorn et al. 2000).

The fluxes of BSIOM in the uncoupled configuration have been compared with observations in Rudolph and Lehmann (2006).

4.2.1 Heat Fluxes

As mentioned above, the budget of the Baltic Sea including sea ice is investigated. Therefore the analyzed fluxes are those at the atmosphere-water and atmosphere-ice interface respectively.

Solar radiation

The solar irradiance is the most important driver of the climate system. Due to its location at high latitudes of the Baltic Sea with its northern part almost lying at the polar circle, the solar irradiation at the Baltic Sea surface has a very strong seasonal cycle. The strong

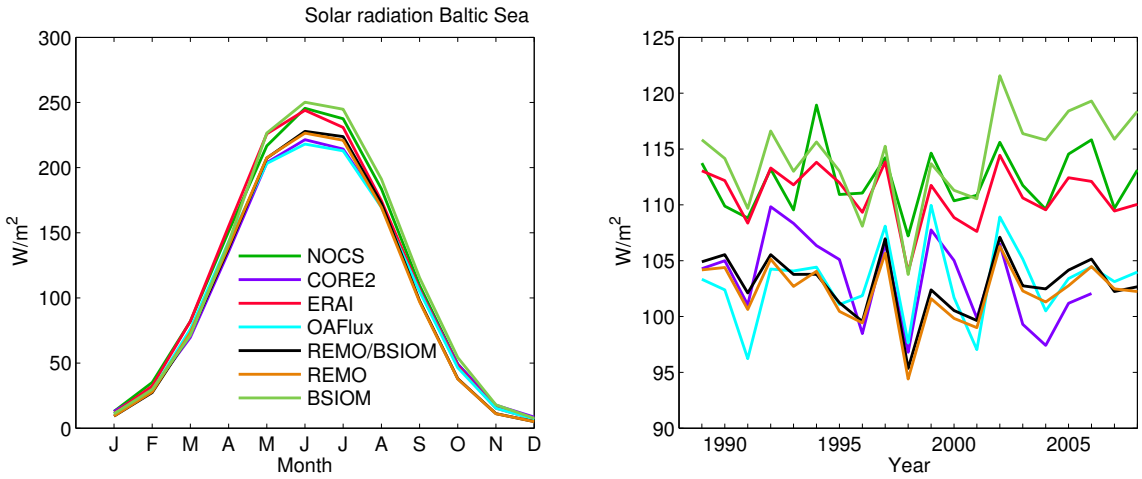

Figure 4.2: Net surface solar irradiance as mean annual cycle (left) and annual means (right) averaged over the Baltic sea surface (excluding Kattegat and the Danish Straits) for the period 1989-2008.

dependence on cloud cover causes a relative high variability on various time scales. The mean annual cycles and the annual means for the simulation period from 1989-2008 are shown in Figure 4.2. The different datasets show a remarkable spread of more than $20\frac{W}{m^2}$ in summer resulting in differences of about $10\frac{W}{m^2}$ in the annual means with the model results sitting at the lower end of the spread. There seem to be two families. The different products use different methods to calculate the radiation including full radiative transfer model and fully empirical parameterizations, but cloud cover is the most important factor for all of them. However, cloud cover is not a very well defined quantity. Its mean annual cycle and the yearly means are depicted in Figure 4.3. It also shows a distinct annual cycle with high coverage during winter and lowest values in summer as well as a relatively high inter-annual variability. Here again, there are two groups of data with a lower cloud cover of the two REMO simulations and ERA-Interim. This somehow counterintuitive since REMO also has the lowest irradiation which emphasizes the importance of the different radiation models. The reason of the relatively low correlation between the annual means of cloud cover and solar irradiance is that the latter is mainly determined by the cloud cover in summer.

Thermal radiation

The thermal radiation is a net flux resulting from a downward flux from the atmosphere and an upward flux from the sea surface following Stefan-Boltzmann's law.

The mean net thermal radiation averaged over the Baltic Sea (excluding Kattegat and the Danish Straits) is depicted in Figure 4.4. The different datasets differ quite strongly in both the annual cycle (left) and the yearly means (up to 15 W/m^2) (right). They also show large differences in the inter-annual variability.

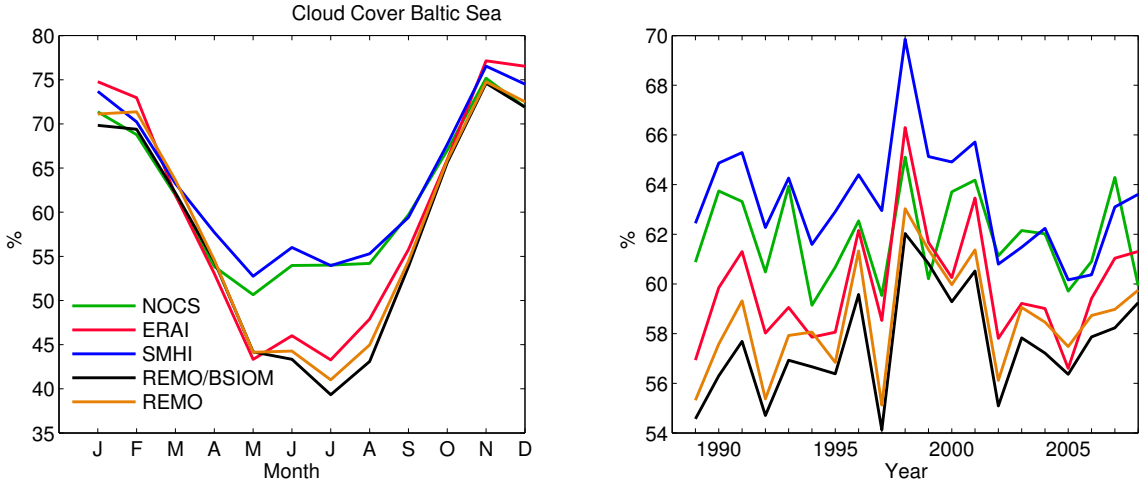

Figure 4.3: Cloud cover as mean annual cycle (left) and annual means (right) averaged over the Baltic sea surface (excluding Kattegat and the Danish Straits) for the period 1989-2008.

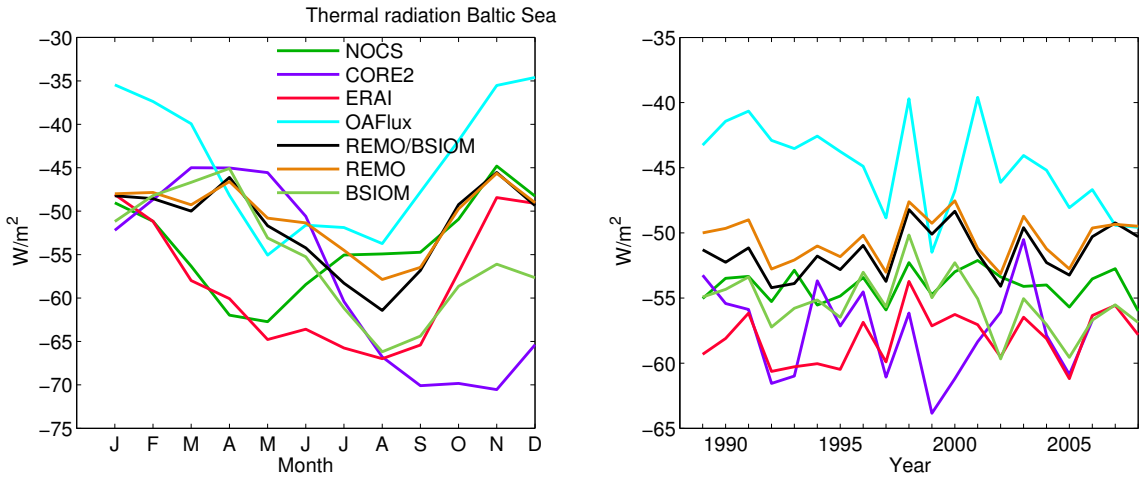

Figure 4.4: Net surface thermal radiation as mean annual cycle (left) and annual means (right) averaged over the Baltic sea surface (excluding Kattegat and the Danish Straits) for the period 1989-2008.

The upward and downward components are analyzed separately. For this, only the ERA-Interim reanalysis is used as reference. The upward thermal radiation is depicted in Figure 4.5 and the downward component in Figure 4.6.

The upward radiation in the coupled simulation is slightly higher during summer compared to the stand-alone REMO simulation which comes from the higher SSTs. Due to their common SSTs, the upward radiation is almost identical in the uncoupled REMO simulation and ERA-Interim. In the uncoupled BSIOM simulation, the upward radiation is lower than in the coupled simulation by about $6 W/m^2$ despite the very similar SSTs. This is due to the lower emissivity of water in BSIOM of $\sigma = 0.985$ compared to $\sigma = 0.997$ in REMO.

Regarding the downwelling thermal radiation, the coupled and uncoupled values in REMO are almost the same showing that it is determined by the large-scale atmospheric conditions. In BSIOM the radiation is about 10 W/m^2 lower which is almost constant throughout the different years. The mean annual cycle is also different with largest deviations during winter. Except in winter, the downward radiation from ERA-Interim is considerably lower compared to the REMO simulations with differences of up to 15 W/m^2 in spring. These differences originate most likely from differences in the vertical structure of temperature and humidity.

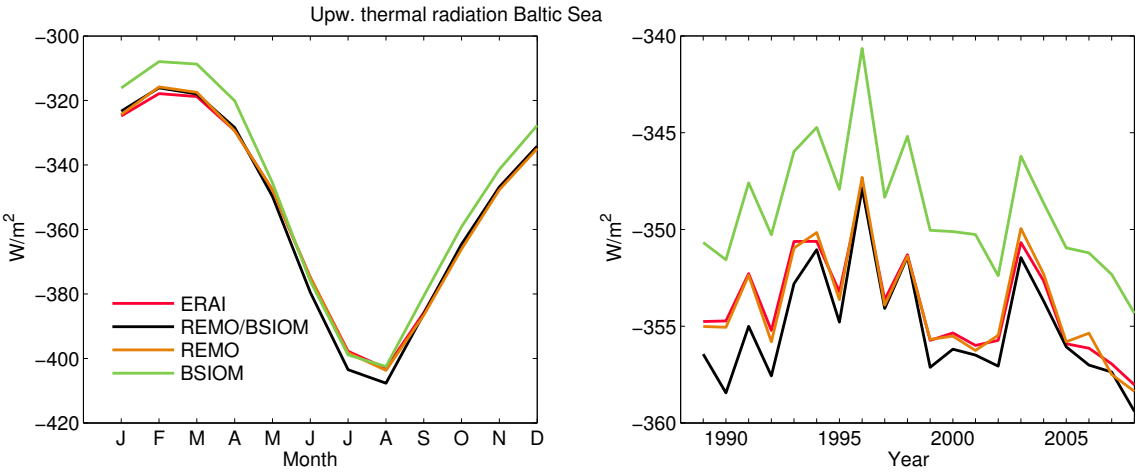

Figure 4.5: Upward thermal radiation as mean annual cycle (left) and annual means (right) averaged over the Baltic sea surface (excluding Kattegat and the Danish Straits) for the period 1989-2008.

The temporal averages of the the components are given in Table 4.1.

Sensible heat flux

Figure 4.7 shows the sensible heat fluxes. It is determined by the temperature difference of the sea surface and the lower atmospheric boundary layer, the near-surface wind speed, and the stability of the atmospheric boundary layer (as parameterized in Equation 2.2). The

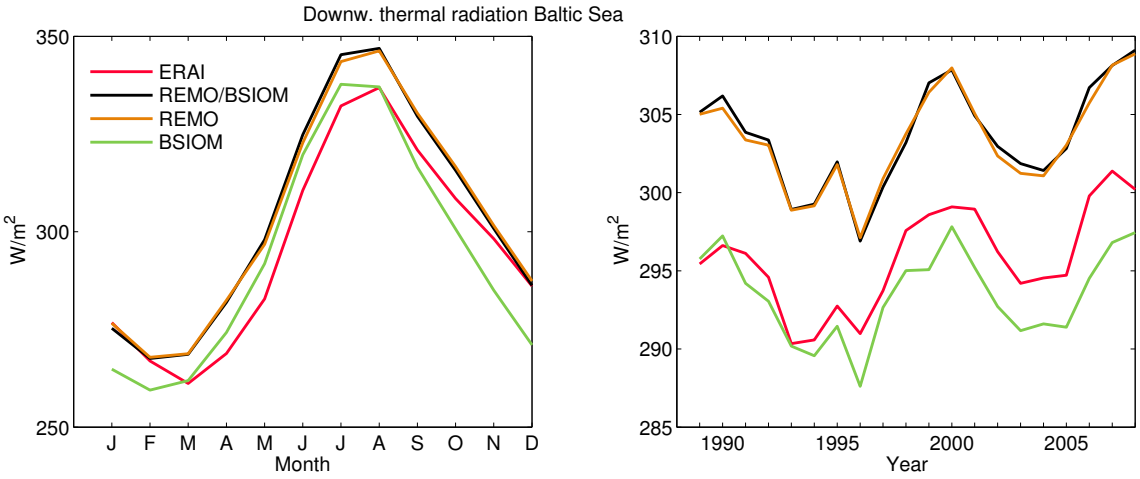

Figure 4.6: Downward thermal radiation as mean annual cycle (left) and annual means (right) averaged over the Baltic sea surface (excluding Kattegat and the Danish Straits) for the period 1989-2008.

Table 4.1: Temporal means and its standard deviations of the net (LWR), upward (LWU), and downward thermal radiation (LWD) in the model simulations for 1989-2008.

	LWR	LWU	LWD
ERAI	-58.0 ±2.0	-353.9 ±2.6	295.8 ±3.2
REMO/BSIOM	-51.5 ±1.9	-355.1 ±2.9	303.6 ±3.3
REMO	-50.5 ±1.7	-353.9 ±2.8	303.4 ±3.2
BSIOM	-55.4 ±2.2	-349.0 ±3.2	293.5 ±2.8

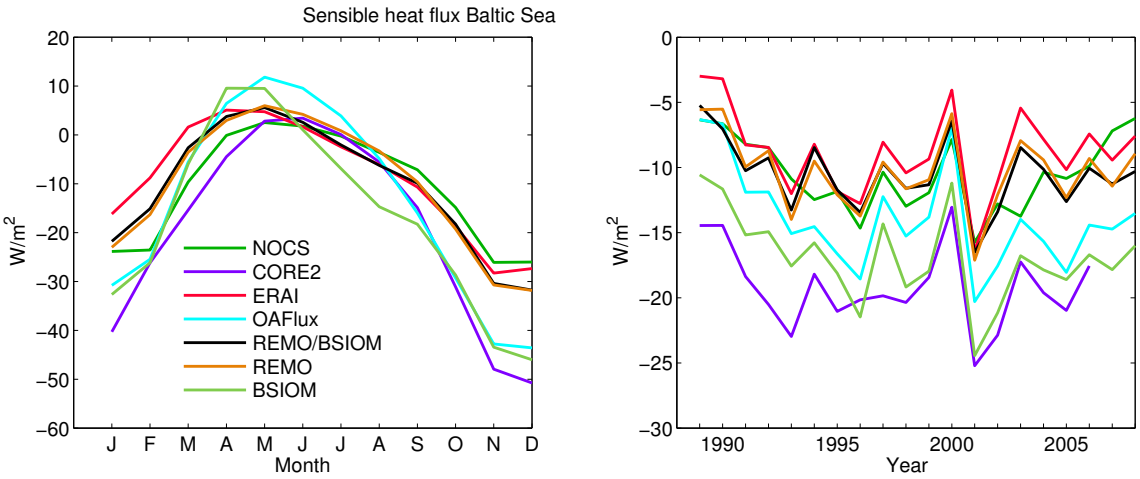

Figure 4.7: Sensible heat flux as mean annual cycle (left) and annual means (right) averaged over the Baltic sea surface (excluding Kattegat and the Danish Straits) for the period 1989-2008.

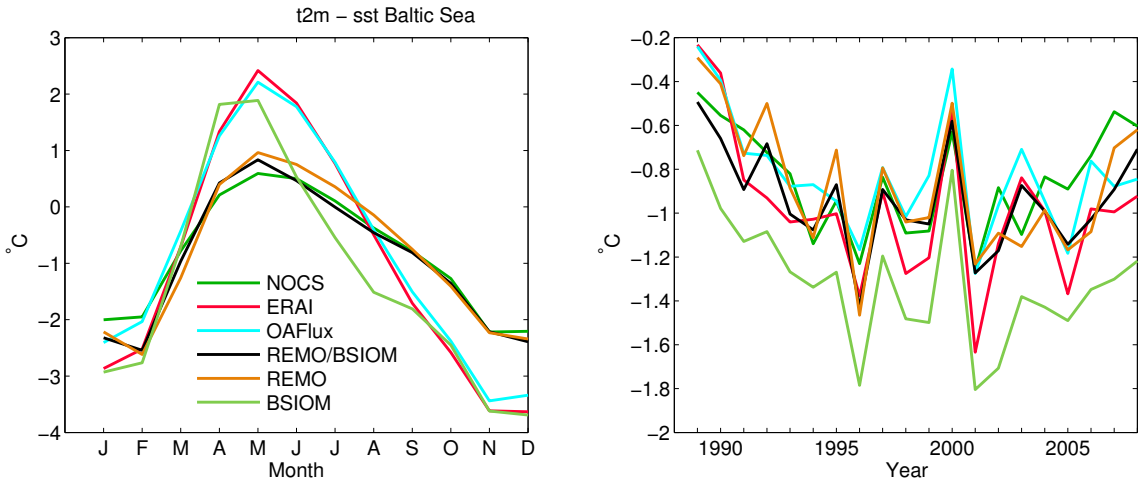

Figure 4.8: Difference in 2m temperature and SST as mean annual cycle (left) and annual means (right) averaged over the Baltic sea surface (excluding Kattegat and the Danish Straits) for the period 1989-2008.

highest fluxes occur during winter. Then the temperature difference is largest, the wind speed highest and the atmosphere is most unstable. Therefore both the mean annual cycle and the annual means closely follow the difference of the 2m temperature and the SST as shown in Figure 4.8. The fluxes in REMO and REMO/BSIOM are similar, also to those in ERA-Interim and NOCS. The similarity with ERA-Interim is surprising, considering the differences in the annual cycle in the air-sea temperature difference.

In Figure 4.8 it can be seen that in REMO and REMO/BSIOM the differences between the T_{2m} and the SSTs are very similar despite their different SSTs. Both agree also very well with the difference in the NOCS dataset. Since the respective T_{2m} and SST in REMO and NOCS are rather different and measured independently in NOCS, this tends to give some confidence to the REMO results.

Latent heat flux

The other turbulent heat flux is the latent heat flux associated with evaporation and sublimation of water and ice. Its rate depends on the water vapor pressure difference between the surface and the lower atmospheric boundary layer, the near-surface wind speed, and the stability of the atmospheric boundary layer. It is depicted in Figure 4.9. It has a distinct annual cycle with its lowest rates during spring when warmer air advected from land sits over the still quite cold sea surface which leads to a relatively stable atmosphere. During autumn, the opposite situation occurs with high SSTs leading to a high vapor pressure at the sea surface and also to a relatively unstable boundary layer. BSIOM shows the highest evaporation rates during summer among all datasets due to its high SSTs and the low specific humidity of the SMHI observations (Figure 3.11). Here again, it might

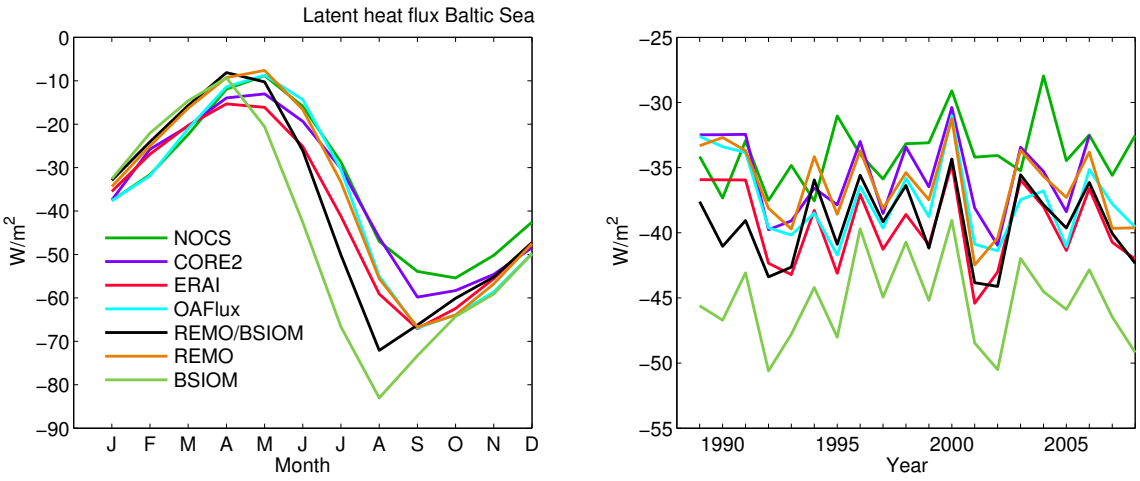

Figure 4.9: Latent heat flux as mean annual cycle (left) and annual means (right) averaged over the Baltic sea surface (excluding Kattegat and the Danish Straits) for the period 1989-2008.

play a role that these observations are mainly derived from synoptic stations over land.

Total energy flux

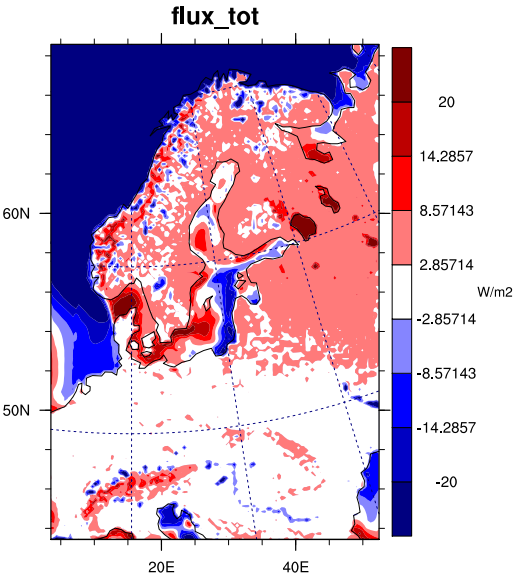

Figure 4.10: Total heat flux at the surface in the coupled model simulation as temporal mean over the simulation period from 1989 -2008.

Figure 4.10 shows the mean total energy flux in the coupled simulation for the period 1989-2008. Blue colors indicate a mean energy flux from the ocean to the atmosphere and red colors from the atmosphere to the ocean. In the central Baltic Sea a clear east-west

gradient exists. This is mainly caused by the mean surface circulation transporting warm water northward at the east coast leading to relatively higher SSTs and vice versa at the west coast. The upwelling regions along the Swedish coast are also clearly visible. The colder SSTs enhance the heat uptake of the ocean there. In the Gulf of Finland there is a similar circulation-caused dipole pattern.

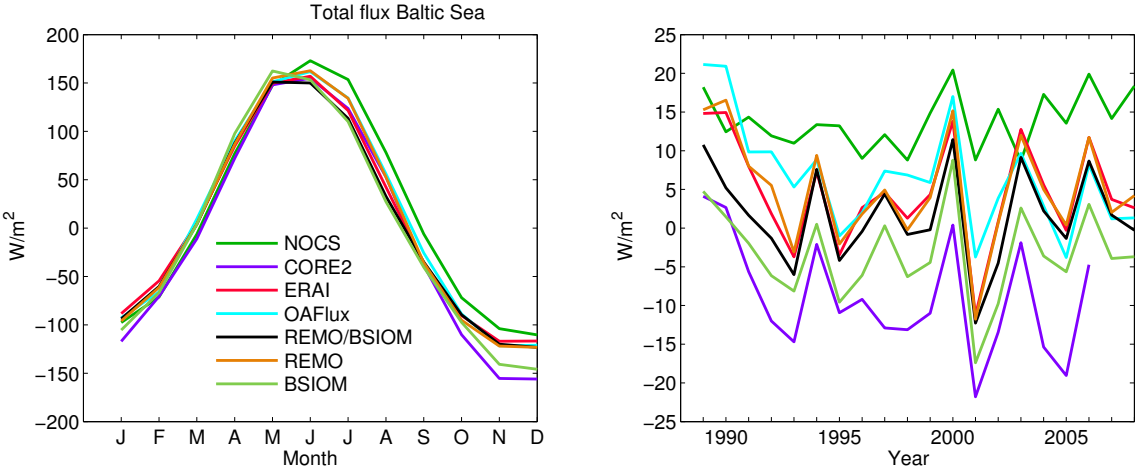

Figure 4.11: Net surface heat flux as mean annual cycle (left) and annual means (right) averaged over the Baltic sea surface (excluding Kattegat and the Danish Straits) for the period 1989-2008.

Figure 4.11 shows the mean annual cycles and the yearly means of the total energy flux averaged over the Baltic sea surface. There is a quite large spread among the different observational/reanalysis datasets both in the annual cycle and in the yearly means of more than $20\frac{W}{m^2}$.

A strong inter-annual variability is also visible. Prominent is the drop from the year 2000 to 2001 of about $20\frac{W}{m^2}$. The main differences between this years lie mainly in the sensible and latent heat caused by a much larger temperature difference between the atmosphere and the ocean. In 2001 the atmosphere is relatively colder (compared to 2000) than the ocean surface below (Figure 4.8). This leads to a more unstable atmosphere and thus to enhanced turbulent fluxes.

Table 4.2 shows the surface energy balance over the Baltic Sea (excluding Kattegat) for the period 1989-2008. One has to keep in mind that the different datasets are not fully comparable. NOCS is defined for the ice-free ocean for example. The different land-sea masks might also lead to considerable differences. One cannot expect the energy budget of the atmosphere-ocean interface to be closed especially not at shorter time scales when variations of the total heat content of the Baltic Sea play a role. Heat transport related to the exchange with the North Sea has to be considered, as well as the heat of the river discharge to mention the most important factors. A detailed analysis of the full energy budget is shown in Section 4.8. For ERA-Interim Berrisford et al. (2011) found a surface

Table 4.2: Surface energy balance over the Baltic Sea (excluding Kattegat) for the period 1989-2008. Shown are the annual means and the standard deviation of the total flux, the net solar radiation (SWR), the net thermal radiation (LWR), the sensible heat flux (SHF), and the latent heat flux (LHF). The fluxes are defined as positive downwards in $\frac{W}{m^2}$.

	Total Flux	SWR	LWR	SHF	LHF
NOCS	13.8 ±3.7	112.2 ±2.9	-54.1 ±1.2	-10.5 ±2.8	-33.9 ±2.5
CORE2	-8.9 ±7.4	103.4 ±4.0	-57.5 ±3.5	-19.2 ±3.1	-35.6 ±3.2
ERAI	4.6 ±6.8	110.9 ±2.6	-58.0 ±2.0	-8.7 ±3.3	-39.5 ±3.2
OAFlux	6.7 ±7.0	103.1 ±3.6	-44.9 ±3.4	-13.9 ±3.8	-37.6 ±3.1
REMO/BSIOM	1.6 ±6.1	102.9 ±2.8	-51.5 ±1.9	-10.5 ±2.7	-39.3 ±3.1
REMO	5.0 ±7.1	102.2 ±2.8	-50.5 ±1.7	-10.3 ±2.9	-36.4 ±3.1
BSIOM	-3.3 ±6.0	114.5 ±4.2	-55.4 ±2.2	-16.9 ±3.5	-45.3 ±3.4

energy imbalance over water of 6.9 $\frac{W}{m^2}$ globally.

Even in the coupled model there is a small imbalance of the atmospheric heat fluxes of more than $1\frac{W}{m^2}$. In the following the fate of this remainder is investigated.

4.3 Exchange North Sea - Baltic Sea

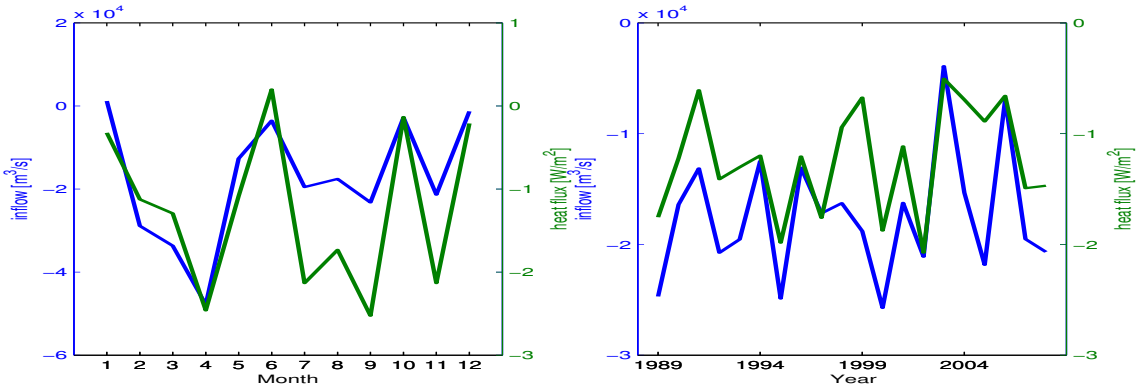

Figure 4.12: Water exchange of the Baltic Sea with the North Sea through the Danish Straits (blue line) and its associated heat flux (green line) for the period from 1989 to 2008 as mean annual cycle (left) and annual means (right).

Model of the sea level & exchange with North Sea

The (change of the) mean sea level of the Baltic Sea is mainly determined by the change of the water mass which is the sum of the flow through the Danish Straits, the freshwater

supply from the rivers, and the precipitation minus evaporation Lisitzin (1967). Other factors like thermal expansion and salinity contraction are negligible at least on an annual time scale (Stigebrandt 2001; Omstedt et al. 2004).

$$A\frac{\mathrm{d}h_B}{\mathrm{d}t} = Q + Q_f \tag{4.1}$$

where h_B is the sea level in the Baltic Sea, A the surface area of the Baltic Sea, Q the exchange between the Baltic Sea and the North Sea, and Q_f the net freshwater supply.

The barotropic flow Q through the Danish Straits can be modeled from the difference in sea level Δh between the two sides of the channel using a simple model from Stigebrandt (1980):

$$Q^2 = \frac{1}{\Phi}\Delta h \tag{4.2}$$

where Φ is a strait-specific coefficient of the flow resistance.

A linear regression analysis to estimate the simulated barotropic flow using the sea-level difference between the Kattegat and the Baltic Sea has been performed. A resistance coefficient of $\Phi = 5.6 \cdot 10^{-10}\mathrm{s}^2/\mathrm{m}^5$ leads to a correlation of 86%. This means that this simple model can explain about 74% of the variability. When the wind stress at the Kattegat is included, even 85% of the variability can be explained.

4.4 Rivers

Due to the large catchment area of the Baltic Sea compared to its surface river discharge plays a key role in the physical system. The total river discharge with an average of about $450\,\mathrm{km}^3/\mathrm{year}$ corresponds to approximately 2% of the total volume of the Baltic Sea. Besides its water mass, the river discharge carries a certain amount of heat. In the model the rivers do not have a temperature defined, yet. The model therefore attributes the sea surface temperature at the location of the river mouth which might deviate considerably from the actual temperature. Even the state-of-the-art discharge models only consider the mass flow. They represent a considerable heat flow, however. Figure 4.13 shows the mean annual cycles and the annual means of the river discharge and its associated heat fluxes in the coupled model simulation from 1989 to 2008. Due to the strong annual cycle of the SSTs (and thus the assumed temperatures of the rivers), the advected heat flux has its peak in summer and not in May when the volume discharge has its maximum. However, they are highly correlated on an inter-annual time scale. The mean heat flux is $1.2\pm0.2 W/m^2$ and the mean temperature of the rivers is 7.5°C ±0.4°C.

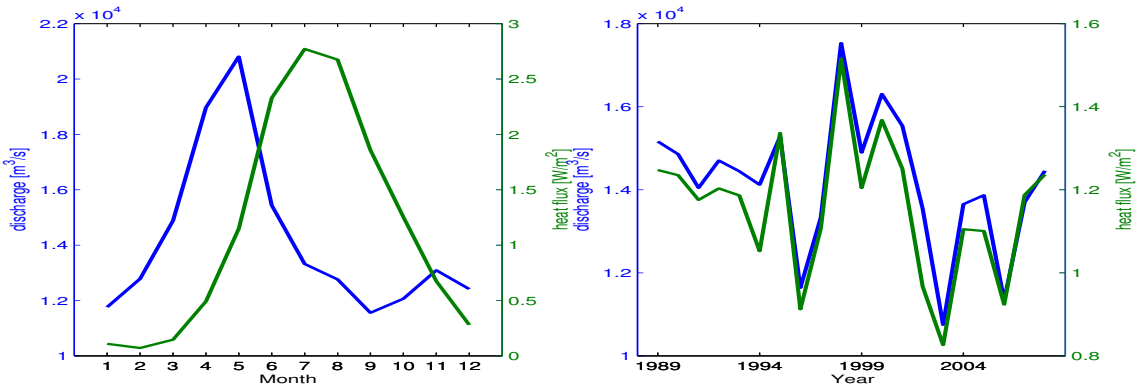

Figure 4.13: River discharge (blue line) and its associated heat flux (green line) from all rivers flowing into the Baltic Sea (excluding Kattegat and the Danish Straits) for the period from 1989 to 2008 as mean annual cycle (left) and annual means (right).

4.5 Precipitation & Evaporation

Precipitation and evaporation play an important role in both the water and energy balances. The associated mass/volume fluxes have already been discussed in Section 3.2.

Concerning the energy budget: Besides the heat change related evaporation, the latent heat due to the phase change of liquid or frozen water to vapor, there is also a heat flux associated with the mass flux of the water that occurs at a certain temperature. Since precipitation and evaporation more or less balance each other, the resulting net flux is relatively small.

Another flux is the latent heat related to snow that falls onto the water or the ice where it melts immediately or after the underlying ice has melted. In the coupled simulation snow fall amounts to about $97 \pm 24\,\mathrm{mm/year}$. This corresponds to a latent heat flux of $F_{snow} = -0.9 \pm 0.2\mathrm{W/m^2}$. In the coupled model, however, only total precipitation is passed to the ice-ocean part, not distinguishing between rain and snow. Thus precipitation is only considered as snow when it falls onto ice and the air temperature is lower then 0°C. Precipitation falling on open water is always considered as rain. Figure 4.14 depicts the latent heat flux associated with snow fall into the Baltic Sea. Shown are both the simulated snow fall REMO (dashed lines) and what BSIOM diagnoses as snow (solid lines). In the simulation this still corresponds to a latent heat flux of $F_{snow} = -0.3 \pm 0.1\mathrm{W/m^2}$.

4.6 Storage changes

The mean sea level exhibits large seasonal and inter-annual variability. The associated changes in the total water volume are very important for the investigation of the water budget of the Baltic Sea, as Lehmann and Hinrichsen (2001) have stated.

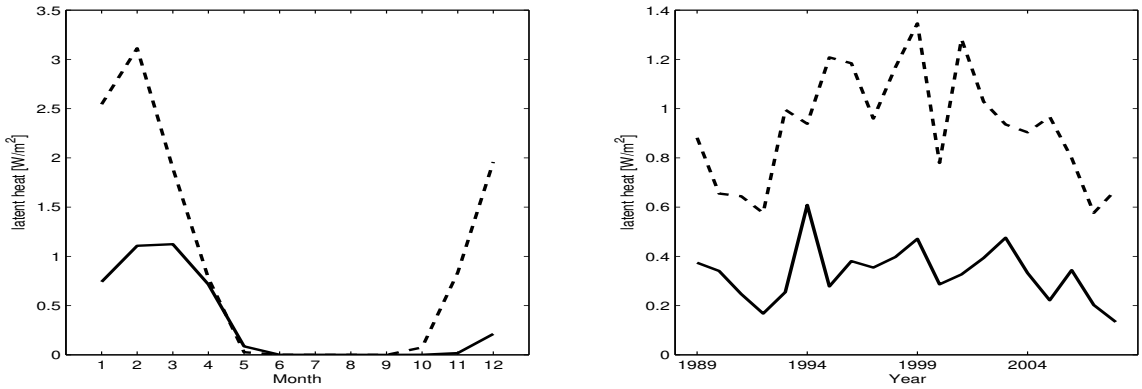

Figure 4.14: Latent heat flux related to snow fall into the Baltic Sea (excluding Kattegat and the Danish Straits) for the period from 1989 to 2008 as mean annual cycle (left) and annual means (right). Dashed lines indicate the snow fall as in REMO, solid lines diagnosed snow in BSIOM.

The mean sea level is depicted in Figure 4.15. There is a distinct annual cycle with maxima during winter and summer and minima during spring and autumn. It seems to correlate highly with the annual cycle of the mean sea level pressure (see Figure 3.15 on page 32). Also the annual mean time series resemble each other. (The inverse barometric effect can only explain around 15%). This shows the close connection of the atmospheric circulation (which mainly determines the sea level) and the surface pressure.

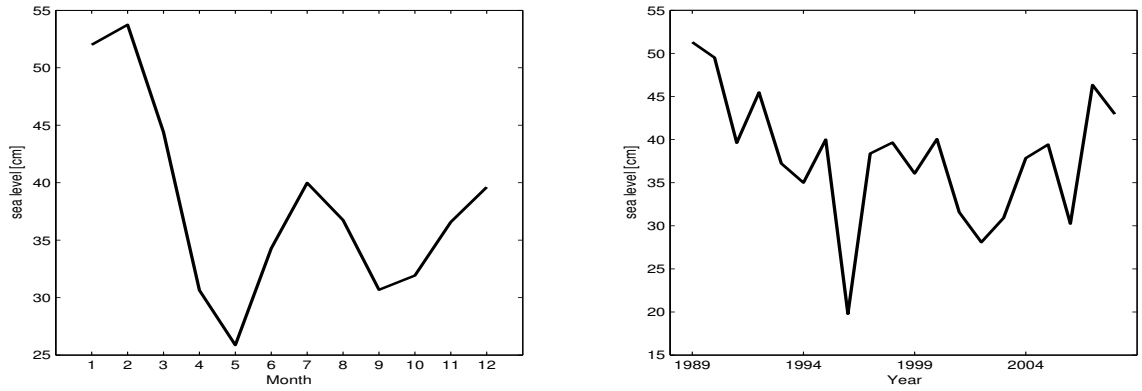

Figure 4.15: Mean sea level of the Baltic Sea (excluding Kattegat and the Danish Straits) for 1989 -2008 as mean annual cycle (left) and annual means (right).

The mean heat content is shown in Figure 4.16 as an equivalent temperature, where the latent heat of freezing from ice and snow is subtracted. The differences to the actual temperature are actually only minor and reach up to 0.1°C during the simulation period.

As mentioned earlier, the Baltic Sea is in close blanc with the atmosphere above. For this reason the changes in the total heat content are closely following the heat fluxes at the sea surface as shown in Figure 4.11 on page 53. In Section 4.8 it will investigate how close

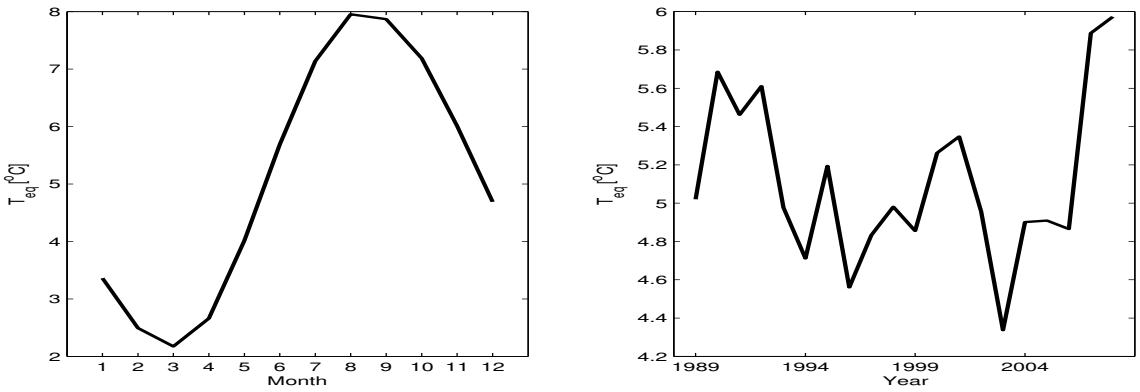

Figure 4.16: Mean equivalent temperature of the Baltic Sea (excluding Kattegat and the Danish Straits) for 1989 -2008 as mean annual cycle (left) and annual means (right).

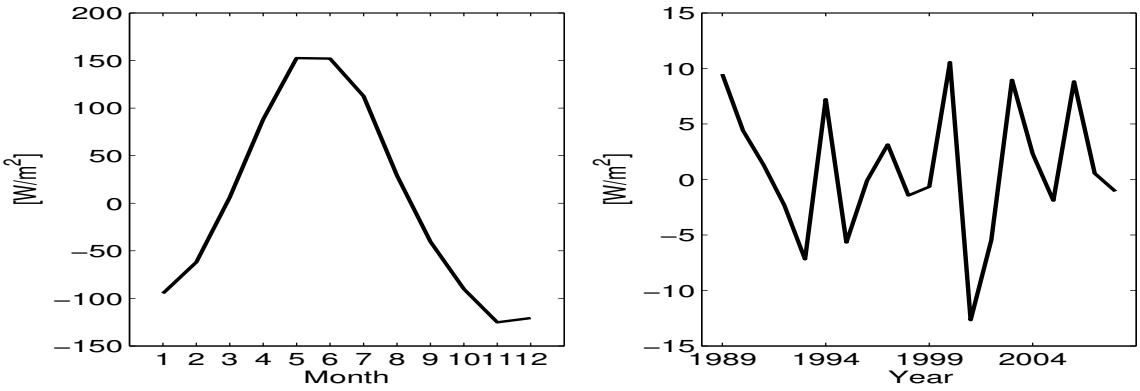

Figure 4.17: As in Figure 4.16 but for the change in the total heat content converted into a mean flux over the Baltic sea surface area.

they actually are and where possible differences come from.

4.7 Closure of the Water Budget

The Baltic Sea water balance follows from the conservation of volume Omstedt and Rutgersson (2000):

$$A_s \frac{dz_s}{dt} = Q_i - Q_o + (P - E)\, A_s + Q_{riv} - Q_{ice} + Q_{rise} + Q_T + Q_S + Q_g \tag{4.3}$$

where A_s is the surface area of the Baltic Sea, z_s the averaged water level, Q_i and Q_o the in- and outflows through the Danish straits, P and E the precipitation and evaporation rates, Q_{riv} the river (and direct) runoff , Q_{ice} the volume change due to ice advection through the Danish straits, Q_{rise} the volume change due to land uplift, Q_T and Q_s the volume changes due to thermal expansion and salt contraction, and Q_g the ground water inflow.

The last five terms on the right-hand side are small compared to the total volume changes (Omstedt and Nohr 2004) (and not in the model anyway) and thus not considered in the analysis. The main components of the water budget of the Baltic Sea are summarized in Table 4.3.

Table 4.3: Mean water balance of the Baltic Sea (excluding Kattegat and the Danish Straits) in km3/year. The flows are denoted as storage change $A_s \frac{dz_s}{dt}$, inflows Q_i, outflows Q_o, precipitation P, evaporation E, Baltic sea surface area A_s, and river dischargeQ_{riv}.

$A_s \frac{dz_s}{dt}$	$Q_i - Q_o$	Q_i	Q_o	$(P-E)\cdot A_s$	$P \cdot A_s$	$E \cdot A_s$	Q_{riv}
-9	-550	1156	1706	96	287	191	447
±155	±174	±108	±136	±22	±20	±14	±50

4.8 Closure of the Energy Budget

With the major components presented now, it should be possible to close the energy balance of the Baltic Sea. Sea ice contributes as negative heat since energy is needed for melting. The total heat content H of the Baltic Sea is then:

$$H = \int \rho_w c_p T dV_w - \int \rho_i L_f dV_i + \int \rho_i c_{p,i} T dV_i \tag{4.4}$$

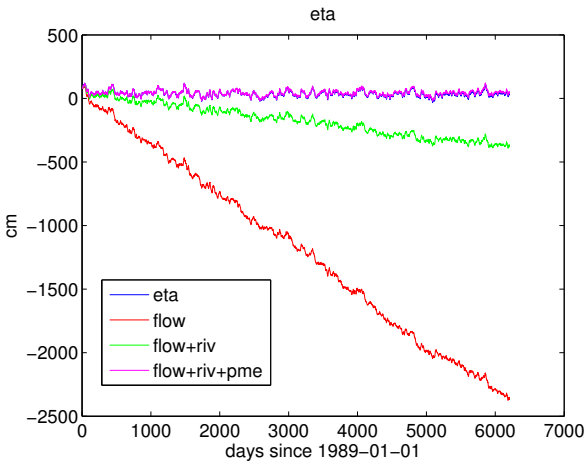

Figure 4.18: Water budget

where ρ_w and ρ_i are the densities of water and ice (which is assumed to be constant ignoring slight dependencies on temperature and salinity), c_p and $c_{p,i}$ the specific heat of water and ice, T the temperature, L_f the latent heat of freezing (neglecting the slight salinity dependence), and V_w and V_i the volumes of the water body and the ice. Eventual snow cover is added to the ice volume.

$$\frac{dH}{dt} = F_h + (F_i - F_o) + F_{riv} + F_{prec} + F_{snow} + F_{ice} \tag{4.5}$$

where F_h is the net surface heat flux from the atmosphere to the open water, F_i and F_o the heat fluxes associated with in- and outflows through the Danish straits, F_{riv} the heat content of the river discharge, F_{prec} the heat flux associated to rain, F_{snow} the latent heat due to snow fall, and F_{ice} the latent heat flux related to in- and outflow of ice through the Danish Straits.

In the analysis, advection of sea ice through the Danish Straits is neglected. The individual components and the standard deviations of the yearly means for the simulation period from 1989 to 2008 are given in Table 4.4. Almost all factors are within the same order of magnitude of around $1\,\mathrm{W/m^2}$.

The right hand side of Equation 4.5 sums up to $1.4\,\mathrm{W/m^2}$, compared to a total heat change of $0.9\,\mathrm{W/m^2}$. This means that about $0.5\ \mathrm{W/m^2}$ are missing in the balance which could be considered as being small. However this would accumulate to a differences of the mean temperature of about 1.3°C over the 20 year period. One reason for this unbalance could be that energy conservation is violated regarding the sea ice temperature. Numerical effects or simply model errors could also play a role.

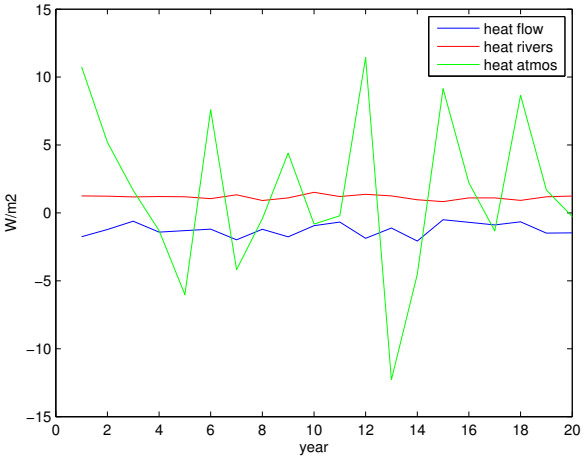

Figure 4.19: Energy budget

Table 4.4: Energy budget of the Baltic Sea (excluding Kattegat and the Danish Straits) in the coupled simulation for the period from 1989 - 2008 in W/m². The fluxes are denoted as storage change $\frac{dH}{dt}$, surface heat flux F_h, heat flux associated with in- and outflows F_i and F_o, heat flux associated with precipitation and evaporation F_{prec} and F_{evap}, advected heat from river discharge F_{riv}, latent heat from snow fall F_{snow}.

$\frac{dH}{dt}$	F_h	$F_i - F_o$	F_i	F_o	$F_{prec} - F_{evap}$	F_{prec}	F_{evap}	F_{riv}	F_{snow}
0.9	1.6	-1.2	3.4	-4.7	0.1	0.8	0.7	1.2	-0.3
±6.1	±6.1	±0.5	±0.3	±0.6	±0.1	±0.1	±0.1	±0.2	±0.1

4.9 Conclusions

In this chapter the BALTEX box has been revisited and the water and energy cycles of the Baltic Sea have been analyzed.

It could be shown that the coupled model is able to reproduce the radiative and turbulent fluxes at the surface of the Baltic Sea (despite its deficits with respect to the salinity). As the other heat fluxes are relatively small, the change in the total heat content of the Baltic Sea water/ice system has to be almost balanced by these surface fluxes. In the analysis, this is only the case for the coupled model simulation. The other simulations and datasets seem to suffer from some inconsistencies. In the uncoupled atmospheric simulation, the prescribed SSTs act as an infinite heat reservoir which allows the energy conservation being violated.

Unfortunately, it was not possible close the heat budget of the Baltic Sea completely, leaving a small residual heat flux unexplained. One can still conclude, however, that one cannot generally assume that occasional imbalances in the radiative and turbulent heat fluxes at the sea surface are balanced by the exchange with the North Sea through the Danish Straits, since the associated heat flux is almost balanced by the advected heat from the river discharge. The latter and other factors as the latent heat in snow fall should be considered as well.

Further the analysis confirms that the Baltic Sea is almost in thermo-dynamic balance with the atmosphere on decadal time scales. In order to use the model system for a detailed analysis of the heat budget the inconsistencies regarding snow fall and ice should be removed.

Chapter 5

Differences between the Coupled and the Stand-Alone Version

In this chapter the influence of the coupling on the atmosphere is analyzed. The differences come from the interactively calculated SSTs, sea ice cover and sea ice temperature. In the uncoupled simulation the SST, SIC and SIT are from ERA-Interim that are originally at a resolution of around 70km and interpolated to the model resolution (and extrapolated at coastal grid points where the land sea masks do not overlap). The analysis begins with the presentation of these differences and then evaluates how these differences affect the above atmosphere. The process of physical upwelling will be discussed separately.

5.1 Temporal mean

SST

The differences in SST between the coupled and uncoupled simulation for the different seasons for the simulation period from 1989 to 2008 are shown in Figure 5.1. During winter the coupled simulation is colder along the coastline with differences about 1°C and warmer in the inner parts. During spring the SSTs agree very well. During summer the coupled simulations has a higher SSTs almost everywhere especially at the coastline with differences up to 3°C. The main reason is that the fluxes are calculated on the grid of REMO with a resolution of about 18.6km which is much coarser than the BSIOM grid with a resolution of about 2.5km. The fluxes are thus calculated on grid boxes that aggregate around 55 grid boxes of BSIOM neglecting the variations at the grid scale of the ocean. This is problematic for the upward thermal radiation with its fourth order dependence on SST. This effect is especially relevant for shallow areas near the coast and occurs almost

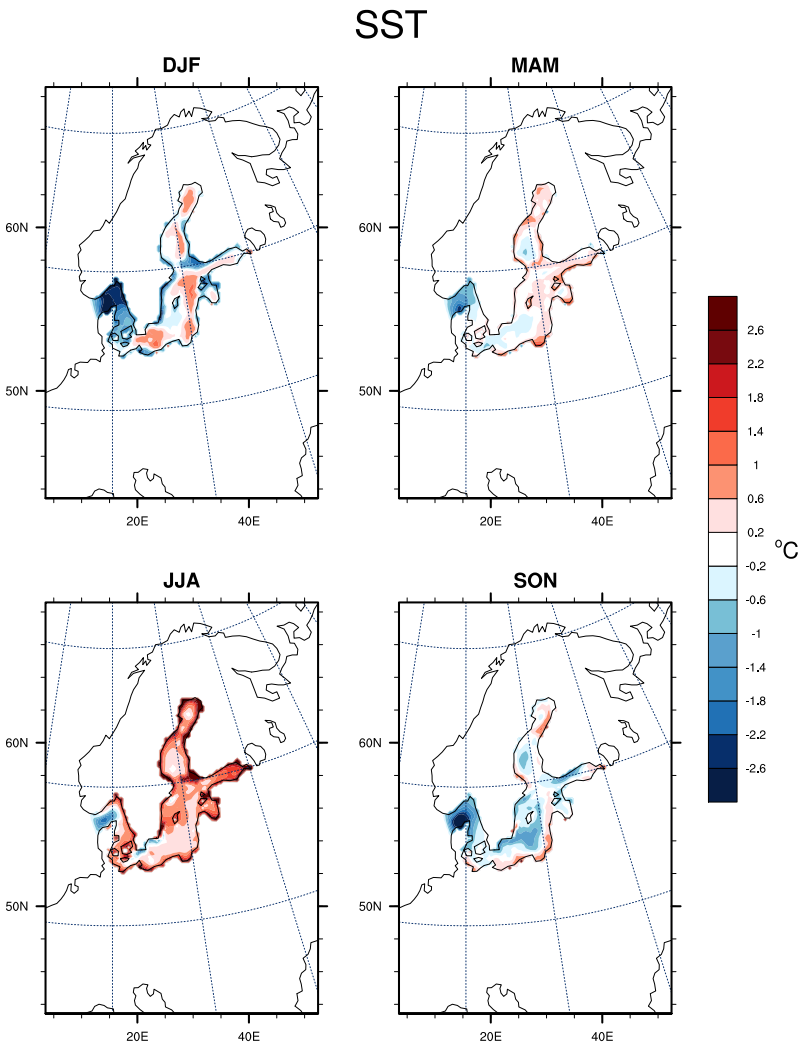

Figure 5.1: Difference in SST between coupled and uncoupled run for the simulation period 1989-2008.

all along the coastline. The only exception is the upwelling region at the Southern coast of Sweden where the SST is colder in the coupled simulation. In autumn the the SST agree fairly well.

Sea ice cover

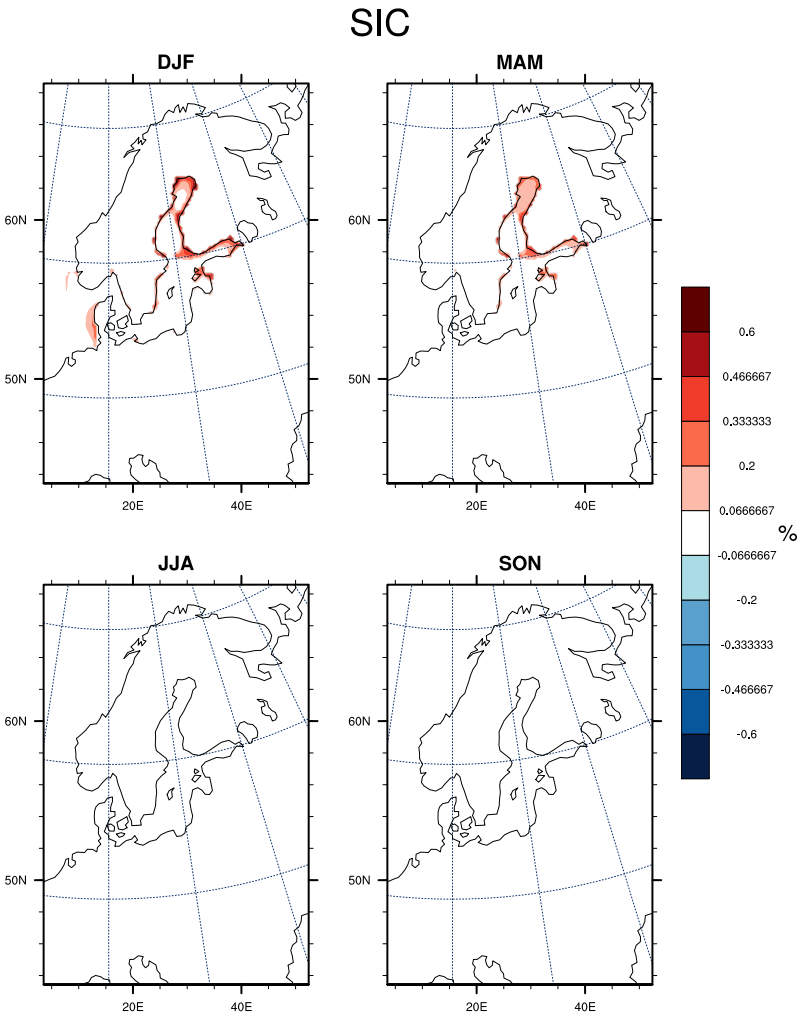

Figure 5.2: Difference in SIC between coupled and uncoupled run for the simulation period 1989-2008.

The sea ice cover is also simulated within the interactively coupled area. The differences between the two simulations are also mainly in the coastal areas of the Gulf of Bothnia and the Gulf of Finland with higher concentrations in the coupled model simulation as depicted in Figure 5.2.

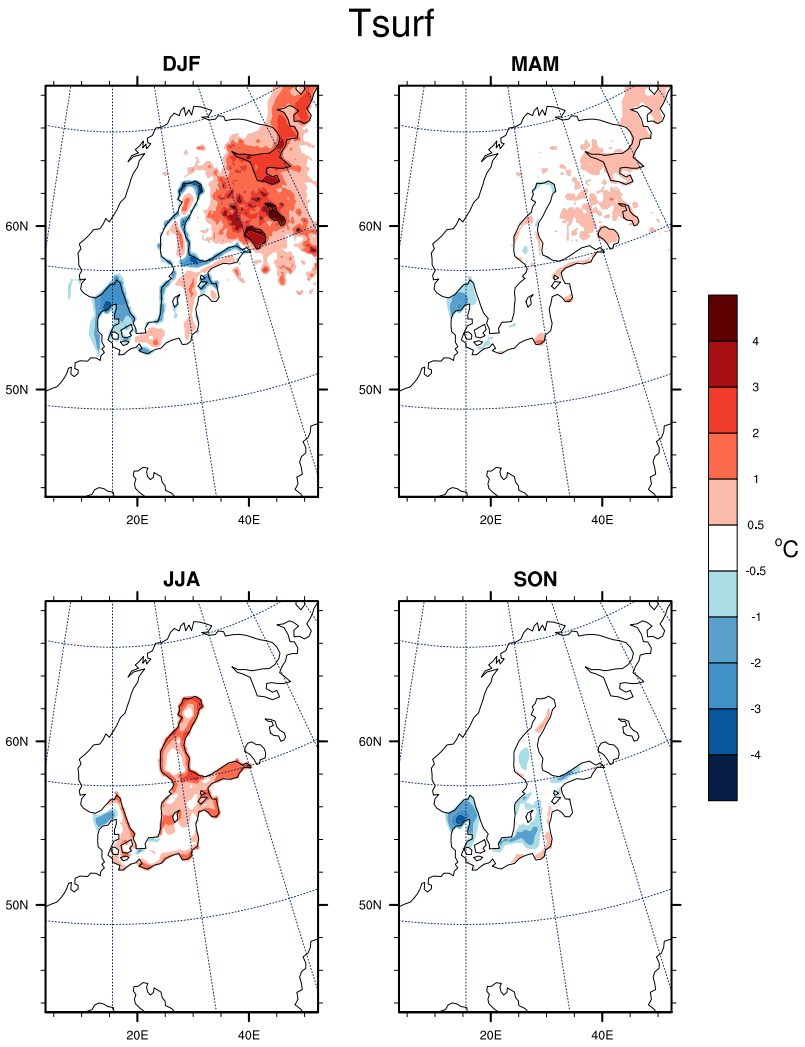

Figure 5.3: Difference in surface temperature between coupled and uncoupled run for the simulation period 1989-2008.

Surface temperature

Sea ice cover is an important element for the air-sea interactions. Where the temperature of the open water is limited to the freezing point of the water, the temperature of the sea ice does not have this constraint and can fall far below 0°C. It can also drastically change the dynamic roughness length of the surface. In areas with higher SICs in the coupled model, the surface temperatures can differ more strongly as in the Northern Bay of Bothnia where the surface temperatures are up to 5°C lower compared to the temperatures deduced from ERA-Interim (Figure 5.3).

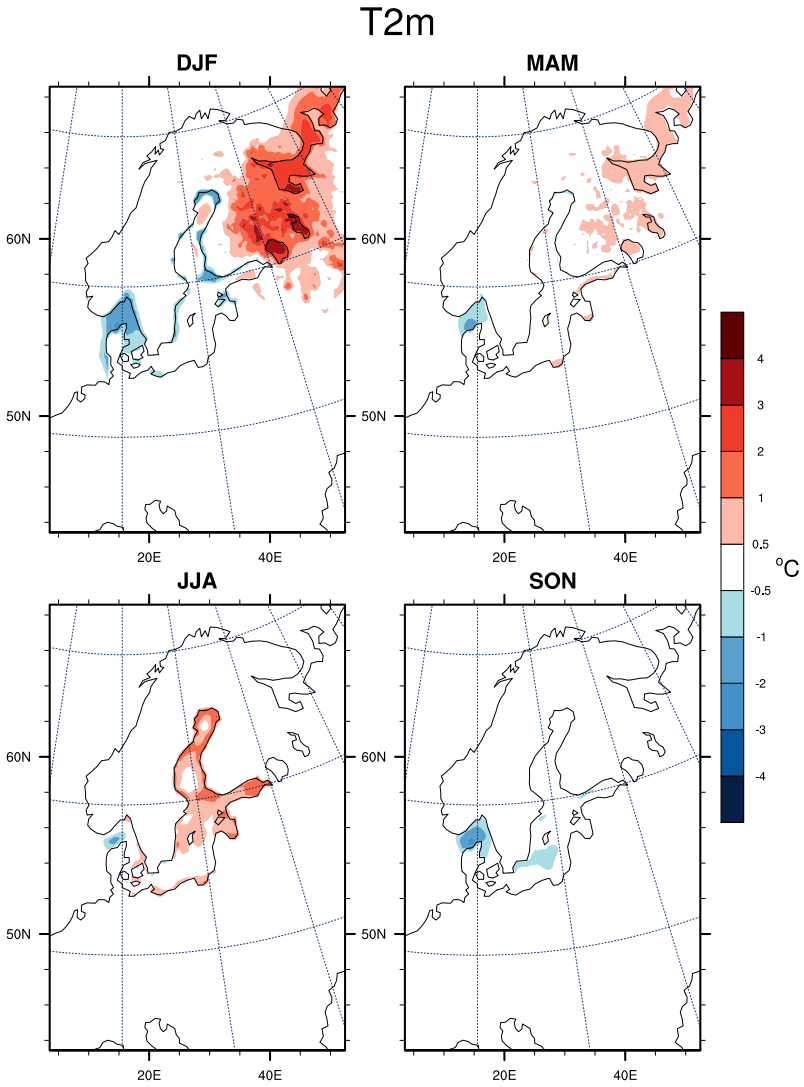

Figure 5.4: Difference in 2m temperature between coupled and uncoupled run for the simulation period 1989-2008.

2m temperature

Figure 5.4 shows the differences in 2m temperature between the coupled and uncoupled REMO simulation. Due to its tight coupling to the surface temperature, the difference in 2m temperature basically shows a spatially smoothed pattern of the surface temperature differences (with lower absolute differences).

Near-surface wind speed

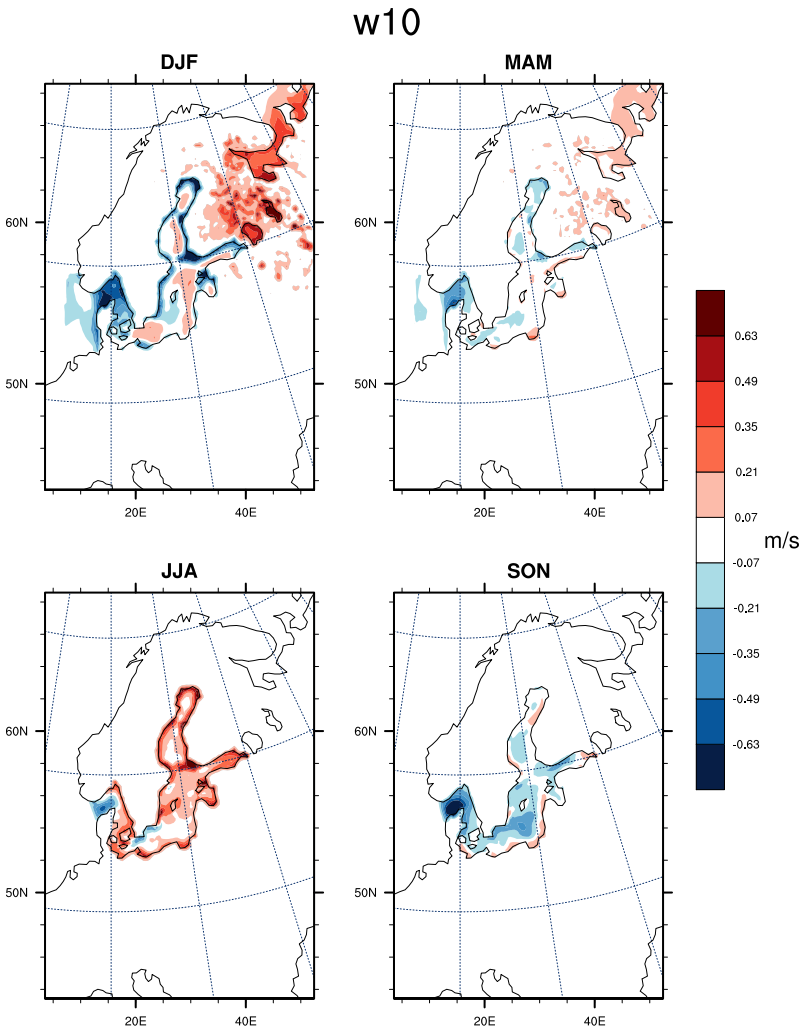

Figure 5.5: Difference in 10m wind between coupled and uncoupled run for the simulation period 1989-2008.

The dampened response of the atmospheric temperature differences compared those of the surface has a direct impact on the stability of the atmospheric boundary layer. Higher surface temperatures lead to a reduced stability (or increased instability), which increases

the momentum transport toward the surface, and thus to higher near-surface wind speeds. The opposite holds for colder surface temperatures. The resulting differences in the 10m wind speed are depicted in Figure 5.5. As consequence the differences in the near-surface wind speed have the same pattern as those of the surface temperatures. These differences have different origins: The increased velocities over the higher surface temperatures can be at least partly considered as an artifact because of the coarse resolution of the heat fluxes, especially of the thermal radiation. The reduced velocities over the upwelling region, however, result from a dynamical effect, that is not sufficiently represented in the uncoupled simulation. This feedback process will be investigated later in this chapter.

Surface Fluxes

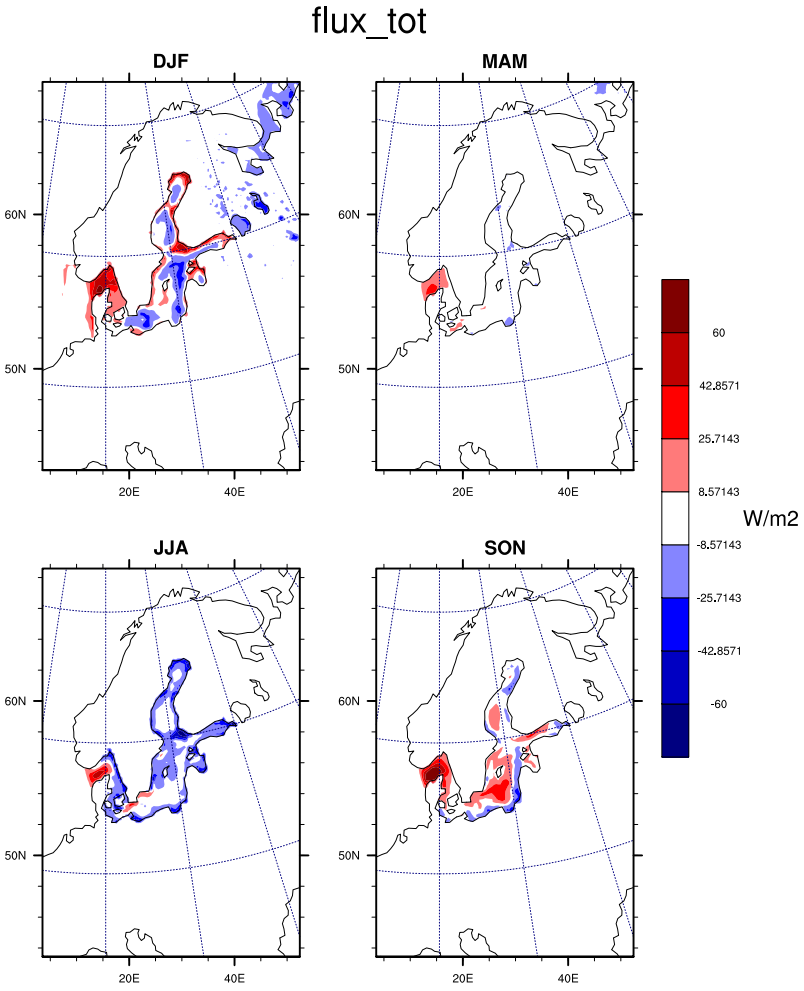

Figure 5.6: Difference in total surface flux between coupled and uncoupled run for the simulation period 1989-2008.

The differences in the surface fluxes basically follow those of the SSTs as can be seen in

Figure 5.6.

5.2 Effect of Coastal Upwelling

In this chapter the process of coastal upwelling in the model system is investigated. Upwelling is one of the most important physical processes in the Baltic Sea. Due to its strong stratification, it is important for vertical mixing and can replenish the surface layers with nutrients which is important for the primary biological productivity (Svansson 1975). A review is given by Lehmann and Myrberg (2008).

Observational studies using in-situ measurements have been conducted for example by Palmén and Laurila (1938); Hela (1946); Sjöblom (1967); Walin (1972b,a); Svansson (1975). These were spatially and temporally limited. When satellite measurements were available, spatial studies became feasible, e.g. Horstmann (1983); Gidhagen (1987); Bychkova and Viktorov (1987). Satellite observations are only available under clear-sky conditions. A useful tool to fill the observational gaps are numerical model. Studies have been performed e.g. by Fennel and Seifert (1995); Jankowski (2002); Lehmann et al. (2002); Myrberg and Andrejev (2003). The uncoupled version of BSIOM has shown to simulate the main upwelling regions of the Baltic Sea correctly(Lehmann et al. 2012).

The effect of SST on mesoscale wind anomalies for the Californian upwelling system was investigated by Boé et al. (2011) using a regional coupled model. They found that upwelling considerably affects the coastal circulation even in the presence of complex orography. Gurova et al. (2013) investigated the influence of upwelling on the wind stress in SAR satellite observations and in an uncoupled simulation of BSIOM. The aim of the present analysis is to investigate a possible feedback of the upwelling-induced SST changes onto the atmosphere.

5.2.1 Physical mechanism

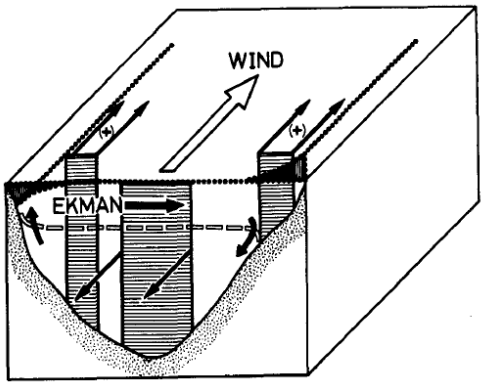

Figure 5.7: Schematic of wind-induced currents in an elongated basin (from Krauss and Brügge (1991))

Figure 5.8

The upwelling process can be divided into two parts, an active phase and a relaxation phase (Zhurbas et al. 2008). The dynamic phase can conceptually be described as the response of a stratified elongated basin to constant wind along the the coast (Krauss and Brügge 1991):

The wind stress causes an Ekman transport in the direction of 90° to the right. This causes an offshore transport on that side where the sea sits on the right-hand side of the wind direction and a decrease in sea level at the coast. The surface water is then mainly replaced by waters from deeper layers. A reverted downwelling process occurs on the opposite side of the coast. During the stratified season, and when the upwelling is strong enough, also relatively colder water from below the thermocline can reach the surface, creating horizontal temperature (and thus density) gradients. The offshore extend of the affected region is scales by the internal Rossby radius, which varies within the range from 1.5 to 10 km depending on the thermal stratification (Fennel et al. 1991).

The inclination of the sea level and the horizontal density gradients create barotropic and baroclinic coastal jets along both coasts in wind direction and a slow compensating flow in the central area of the basin. The coastal jets are meandering along the coast as Kelvin waves, being deflected by coastal irregularities (Lehmann and Myrberg 2008).

After the active phase, the relaxation phase starts and lasts until the SST anomaly disappears. During this phase the dynamic upwelling process including the sea surface anomalies is over, but the SST anomalies still exist. The coastal jet is only baroclinically driven. Due to baroclinic instabilities, filaments, squirts and whirls are often formed, contributing to

the horizontal mixing and thus the relaxation of the temperature anomaly (Zhurbas et al. 2008).

5.2.2 Upwelling Regions

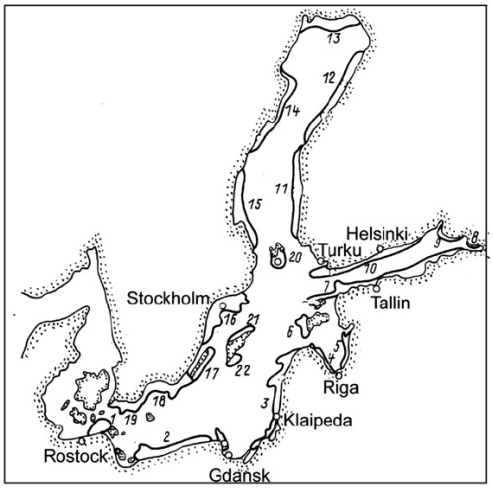

Figure 5.9: Main upwelling regions in the Baltic Sea after Bychkova et al. (1988)

Due to its complex coastline coastal upwelling can be caused by winds from almost all directions on different locations of the coast. Bychkova et al. (1988) classified the main upwelling regions in the Baltic Sea according to specific large-scale circulation patterns as shown in Figure 5.9.

5.2.3 Detection Method

An automatic upwelling detection algorithm similar to Lehmann et al. (2012) has been developed to detect upwelling from daily SST maps. They calculated a zonal anomaly by subtracting the zonal mean for each latitude. Upwelling was detected when the anomaly exceeded a fixed threshold (2°C worked best). This method has its limitations when the zonal mean is mainly calculated parallel to the coast as in the Gulf of Finland, and when there is a temperature gradient between the coastal areas and the open sea. To tackle the first problem, the zonal mean is smoothed over 50 grid boxes before it is subtracted. The second problem is reduced by calculating the anomaly to all grid points with approximately the same distance to the coast. Upwelling is detected when the negative anomaly is lower than −5°C. The advantage of this method is that it only uses only temperature of a single SST map. Thus it is insensitive to missing data for example.

5.2.4 Spatial upwelling distribution

This method was applied to the daily SSTs on the BSIOM grid from the coupled simulation. The seasonal mean occurrence frequencies are depicted in Figure 5.10. With the thermal stratification as a prerequisite, the highest frequencies occur in summer. In summer, the major upwelling regions at the Swedish coast of the Baltic Proper are well represented with upwelling frequencies of up to 30%. In the Bothnian Bay off-shore upwelling is relatively frequent with frequencies above 10%. This upwelling is driven by wind-stress curl and not the topic of this work. In winter, the algorithm falsely detects upwelling due to ice cover, especially in narrow and shallow bays as between Öland and the Swedish mainland (which represents an artificial bay in the model) and in the Gulf of Riga. The following analysis is therefore restricted to the period from March until October.

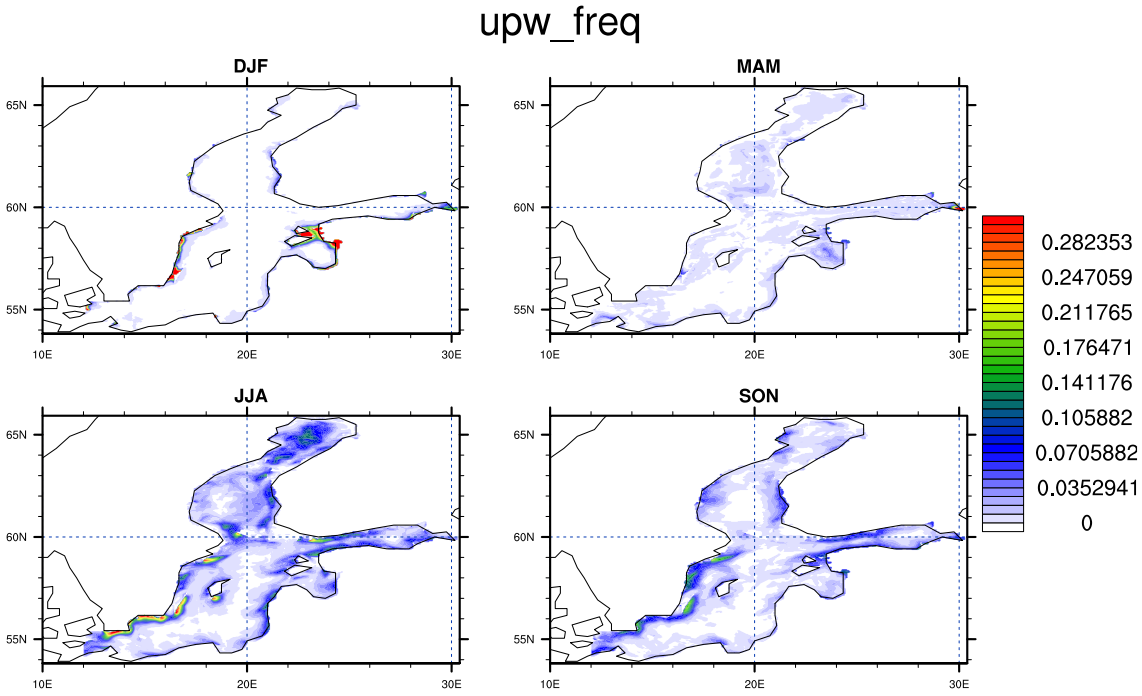

Figure 5.10: Detected upwelling frequency using a threshold of 5°C for the different seasons.

The following analysis focuses on upwelling region 3. This region is chosen because of its relatively long strait coastline in North-South direction where adequate northerly winds can cause upwelling affecting a relatively large area (not too frequently to dominate the local oceanic circulation). In this area, the upwelling season lasts from May to September with highest frequencies in July when on average upwelling is detected in 20% of the time (Figure 5.11a). These events occur irregular in time as they are very sensitive to suitable stratification and wind conditions. During the simulation period from 1989 to 2008, 47 individual upwelling events are detected with an average length of around 8 days. The

distribution of the duration is depicted in Figure 5.11b. About one third of the events is only detected on a single day. The longest event lasts for 41 days. In the following, both the temporal mean situation and the temporal evolution of the upwelling situations are analyzed.

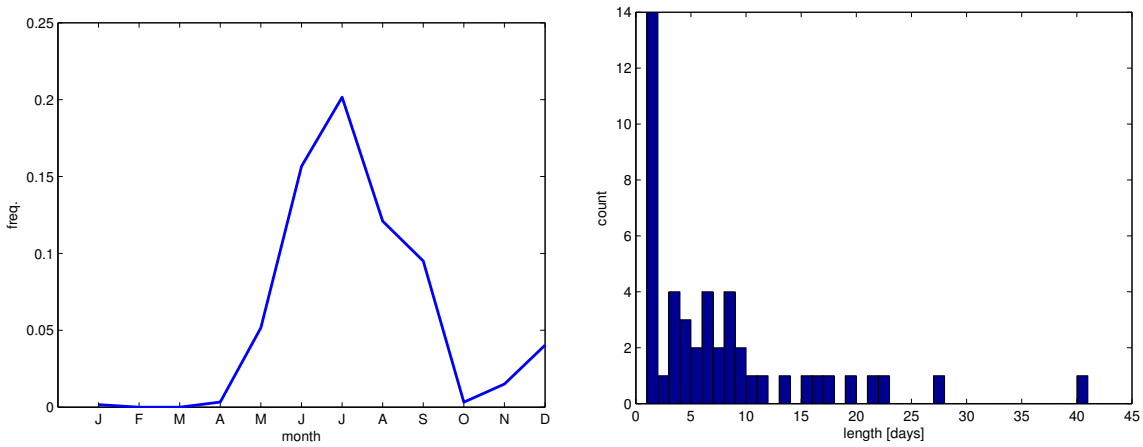

Figure 5.11: Statistics for detected upwelling in region 3: The annual cycle of the upwelling frequency (left) and the histogram of the length of the upwelling events during March to October (right)

5.2.5 Temporal Mean

The temporal mean of all days when upwelling is detected during the simulation period are calculated. As consequence, events of longer duration have a higher weight.

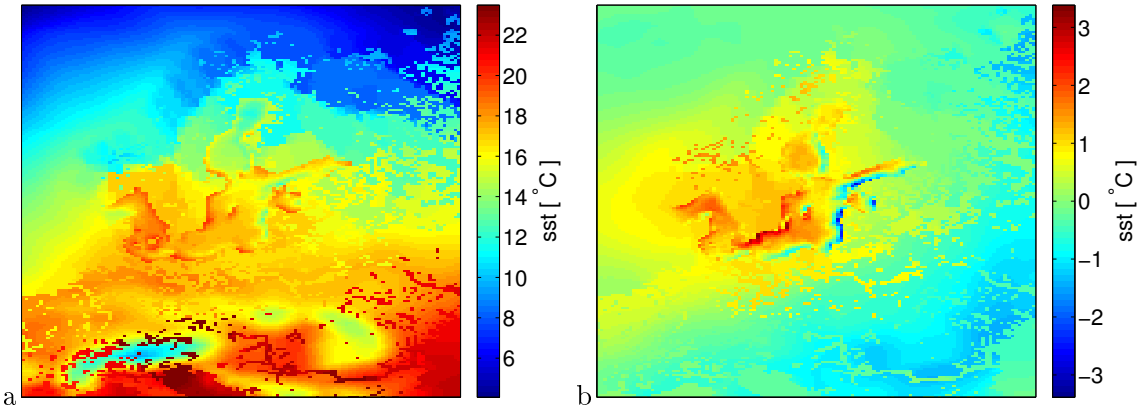

Figure 5.12: Sea surface temperature (left) and the corresponding anomaly (right) for detected upwelling in region 3 during the period from 1989-2008.

The mean SST for all days when upwelling is detected in area 3 during the period from 1989 to 2008 is depicted in Figure 5.12a. The upwelling area is clearly visible. The

picture becomes even clearer when the anomaly to a climatology is regarded. The latter is calculated by averaging over all julian days of the 20-year period for which upwelling is detected at least at one day during this period. These anomalies are about -3°C along the coast. Upwelling in this region also seems to coincide with upwelling at the southern coast of the Gulf of Finland and along the coast of Germany and Poland. This shows that certain circulation types can trigger upwelling in several regions as stated by Bychkova et al. (1988). Also visible are the positive temperature anomalies at coasts opposite to the upwelling areas. This shows that the Baltic Sea behaves as an elongated stratified basin as explained in Krauss and Brügge (1991). They stated that upwelling has to be considered as a 3-dimensional process that also affects the opposite coast and the central area of the basin.

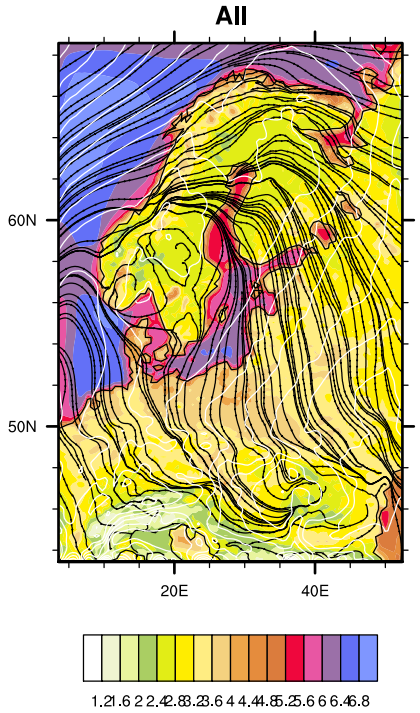

Figure 5.13: Mean near-surface circulation for detected upwelling in area 3 during the period from 1989-2008

The mean atmospheric circulation during detected upwelling is depicted in Figure 5.13. The upwelling is associated with anti-cyclonic circulation caused by high pressure over the North Sea and the Baltic Sea. Note that this is only the mean circulation. The actual circulation that causes an upwelling event can look completely different, including cyclonic circulation.

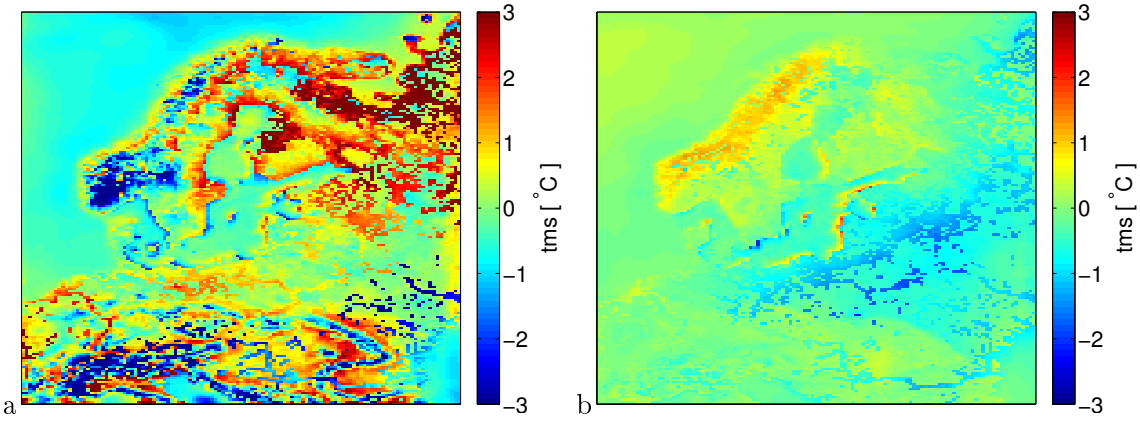

Figure 5.14: Difference between SST and 2m temperature (left) and the corresponding anomaly (right) for detected upwelling in region 3 during the period from 1989-2008.

The question is whether the reduced SST has an influence on the atmosphere above. The colder SST leads to an increase of the sensible heat fluxes from the atmosphere to the ocean, which causes a reduction of the near-surface temperatures (not shown). However, the atmospheric temperature response is not as strong as that of the SST, because of advection for example. The difference between the 2m temperature and the SST is shown in Figure 5.14a. Over the upwelling region, the air is warmer than the underlying sea surface which increases the stability of the atmospheric boundary layer. A more stable boundary layer leads to a reduced momentum transport from the free atmosphere to the surface. This leads to a lower near-surface wind speed (Sweet et al. 1981). The wind speed anomaly for detected upwelling in area 3 is depicted in Figure 5.15. Over the upwelling region the velocities are considerably lower than the climatological mean with differences of up to $1^{m}/_{s}$ above the coldest SSTs at the coast. This has to be compared with an only slight negative anomaly over the unaffected regions of the Baltic Sea which comes from the specific weather conditions that lead to the upwelling process.

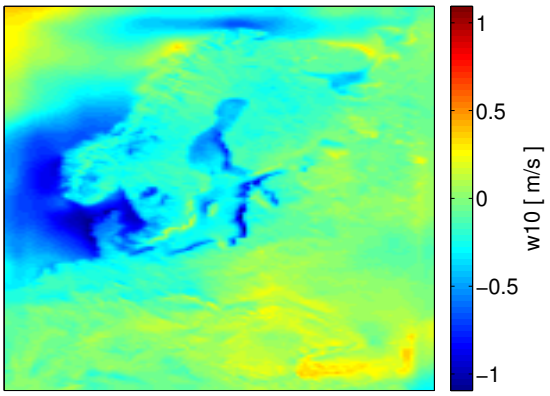

Figure 5.15: 10m wind speed anomaly for detected upwelling in region 3 during the period from 1989-2008.

Differences coupled-uncoupled

To separate the local effect of the change SST on the near-surface simulation more clearly from the large-scale influence, the comparison to the uncoupled REMO simulation is used, since both simulations have basically the same large-scale circulation. It has also been shown how the climatological differences in the SSTs cause differences the near-surface winds via the stability effects. Here, the differences in the anomalies during upwelling are examined (5.16). The SST difference reach up to -4°C, whereas the 2m temperature response is only about half the magnitude. The resulting higher difference in the difference between the 2m temperature and the SST are the reason for the lower wind speed of up to $0.6^{m}/_{s}$ in the coupled simulation all along the east coast of the Baltic Proper.

5.2.6 Temporal Evolution

To investigate the temporal evolution of the upwelling effects, the 61 day periods including 30 days before and after the initial detection of the individual upwelling events are investigated. The analysis is done at a point in the upwelling region with a strong response. The time series of all upwelling events are temporally averaged. For comparison, a climatology is calculated in the same way as for the temporal means in the previous section. The time series for both the coupled and uncoupled REMO simulation for several variables are shown in Figure 5.17.

Before the average upwelling event, the SST is increasing faster than the climatology developing a positive anomaly of about 1.5°C. During the active phase of the upwelling events, the SST drops then by more than 2.5°C within two days. During the relaxation phase afterwards, the SST is rising quickly towards its climatological value. This phase lasts on average about two weeks.

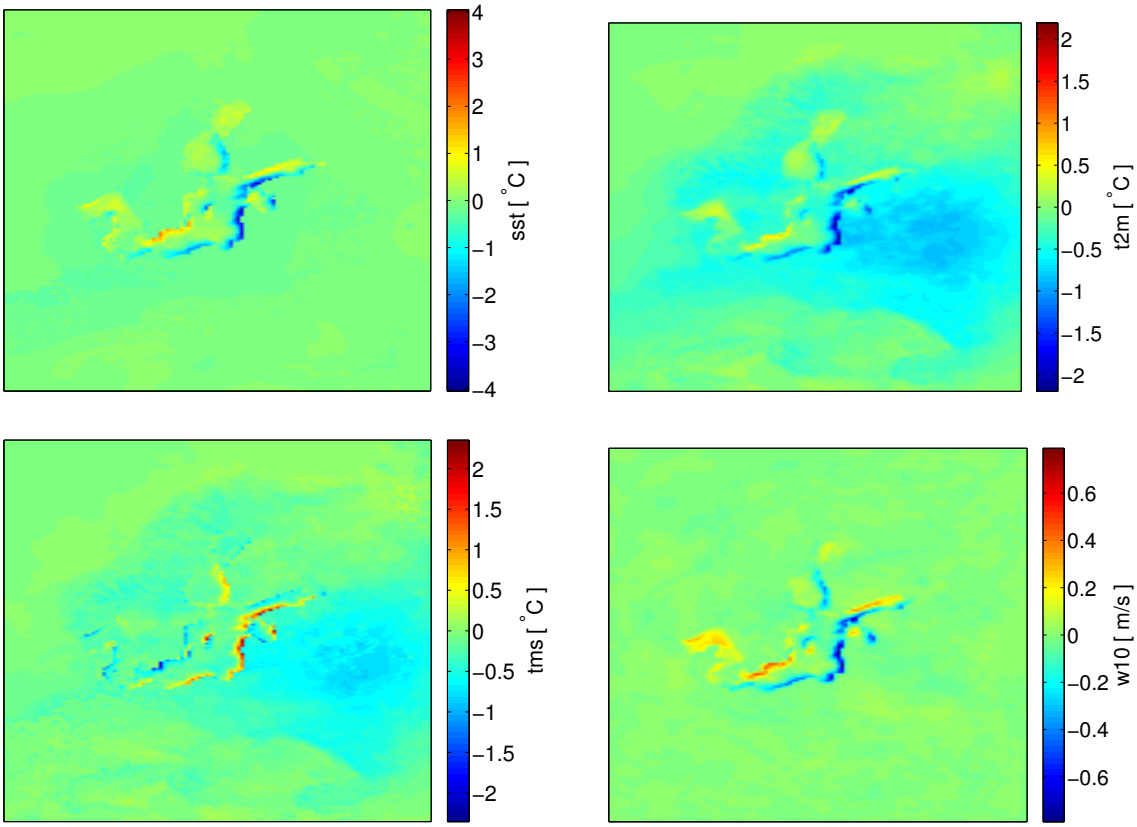

Figure 5.16: Temporal mean differences between the anomalies of the coupled and the uncoupled simulations in SST (a), 2m temperature (b), the difference between the 2m temperature and the SST (c), and 10m wind (e) for detected upwelling in region 3 during the period 1989-2008.

The near-surface wind is the main driver in the dynamical process of coastal upwelling. Before the upwelling event, the wind speed is relatively low with values of about $1^m/_s$ below its climatological mean. This favors the development of a relatively shallow mixed-layer depth which as consequence causes relatively fast rising SSTs. The upwelling event is then triggered by a strong wind pulse from North of more than $8^m/_s$ immediately before and during the upwelling process. During the relaxation phase, the velocities fall again below its climatological mean. As already mentioned, this anomaly is partly a large-scale phenomenon. The effect attributed to the enhanced stability of the atmospheric boundary layer can be seen in the differences between the coupled and uncoupled simulations. During the phase with reduced SSTs, the 10m wind speed is significantly lower in the coupled simulation. The anomaly of the difference between the 2m temperature and the SST as an indicator of the atmospheric stability is shown in Figure 5.18. During the phase with reduced SSTs, these difference reach up to 1°C and cause considerably lower wind speeds up to $0.8^m/_s$ immediately after the upwelling event as shown in Figure 5.19.

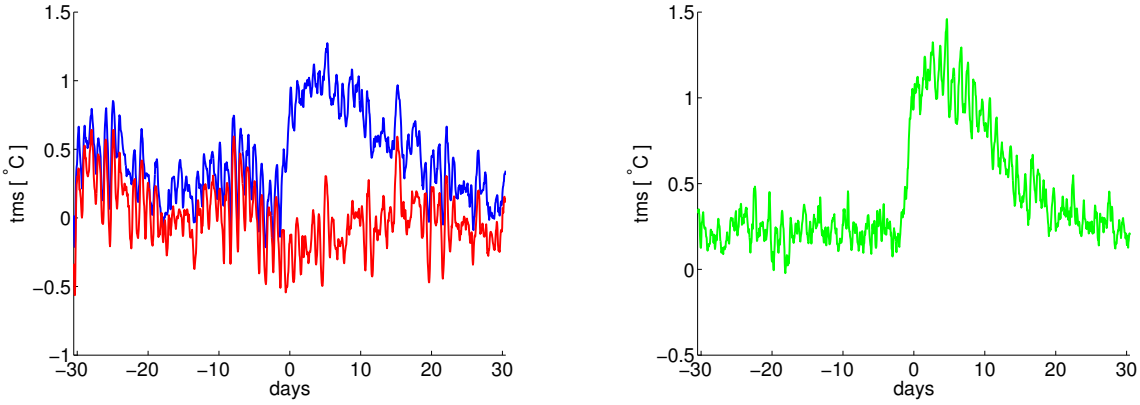

Figure 5.18: Anomaly of the difference between the 2m temperature and the SST for the coupled (blue line) and uncoupled (red line) simulation (left) and the difference between the two simulations (right) for detected upwelling in region 3 during the period 1989-2008.

5.3 Conclusions

In this chapter, the differences between the coupled and uncoupled simulations has been investigated. The interactive coupling mainly affects the atmosphere above the Baltic Sea surface. The different SSTs directly affect the turbulent heat fluxes between the ocean and the atmosphere and thus the near-surface air temperature. This as consequence changes the stability of the atmospheric boundary layer and therefore the vertical momentum transport from the free atmosphere toward the surface. This results in considerably different near-surface wind speeds.

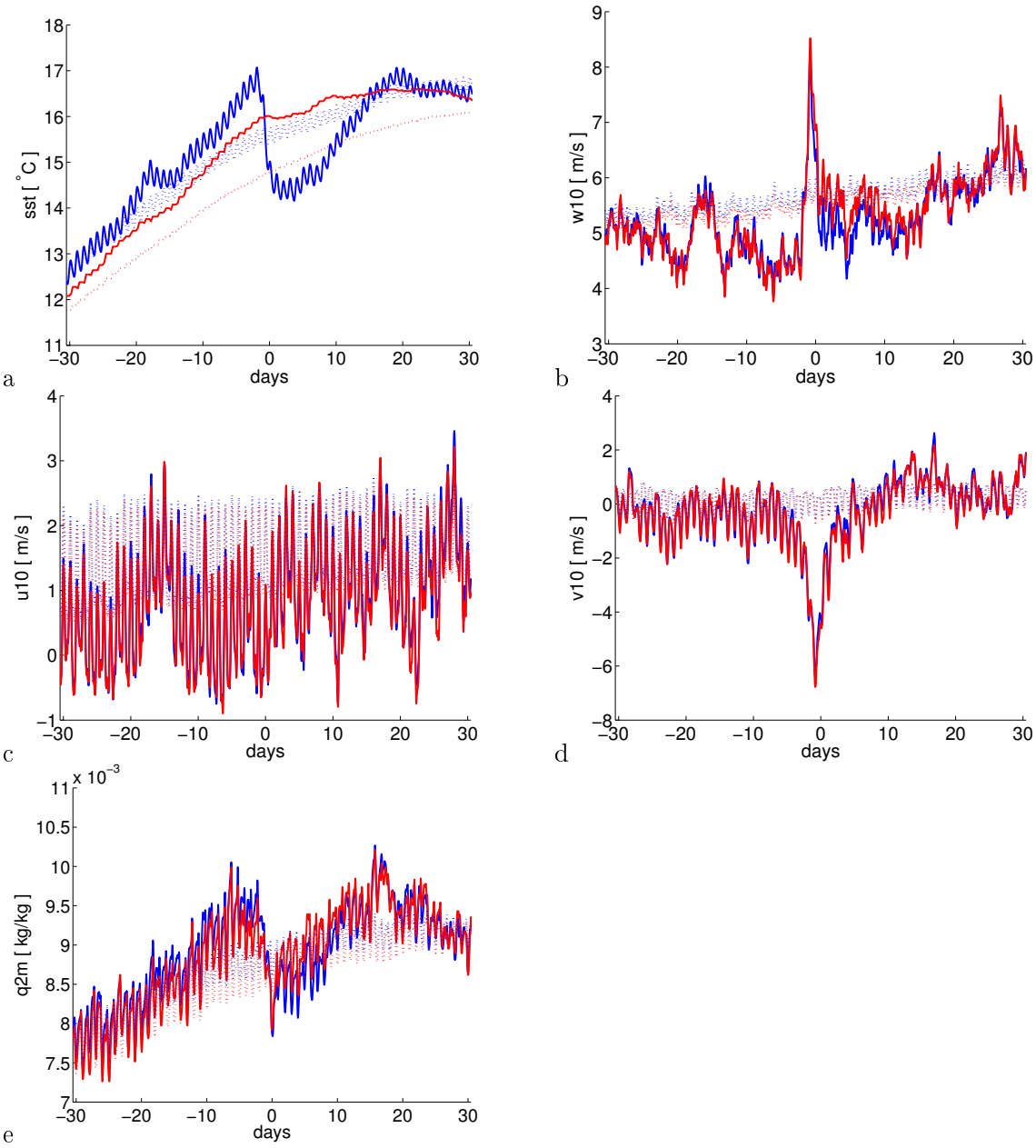

Figure 5.17: Time series of several variables for detected upwelling in region 3 for the period 30 days before and after an upwelling event has been detected initially. The depicted variables are the SST (a), the 10m wind speed (b) , and its U- and V-component (c) and (d), and the 2m specific humidity (e). Blue lines indicate the coupled simulation, red lines the uncoupled atmospheric simulation. Solid lines stand for the mean time series of all upwelling events detected during the period from 1989-2008 and dashed lines indicate the corresponding climatological time series.

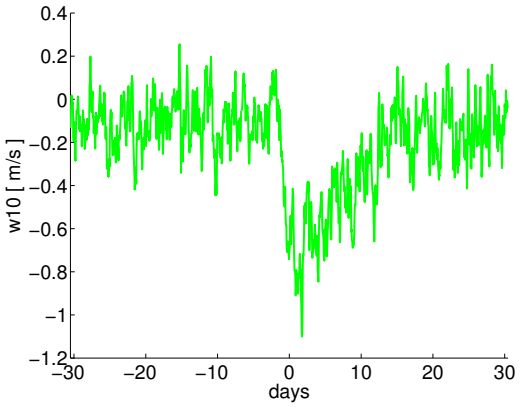

Figure 5.19: Difference of the anomalies of the 10m wind speed from the coupled and the uncoupled simulation for detected upwelling in region 3 during the period 1989-2008.

The process of coastal upwelling has been investigated in the coupled model system. A statistical method has been applied to detect upwelling from SSTs. It could be shown that the model is able to reproduce the major upwelling regions of the Baltic Sea realistically. The underlaying processes have been investigated for one upwelling region at the East coast of the Baltic Proper. The atmospheric conditions to trigger upwelling are as expected from Ekman's theory. It has also been investigated how the changed SSTs feed back on the atmospheric circulation via changes of the stability of the atmospheric boundary layer. It has been shown that the near-surface wind speed is considerably reduced over the upwelling region. This feedback is only represented in a coupled regional climate model.

Chapter 6

Conclusions & Outlook

6.1 Conclusions

In this thesis, the water and energy cycles of the Baltic Sea have been investigated using a coupled regional climate model. For this purpose, the regional atmospheric model REMO has been coupled to the Baltic Sea ice ocean model BSIOM, using the coupling interface of the existing model system BALTIMOS.

The model system was used to downscale the ERA-Interim reanalysis data for the period from 1989 to 2008. A comparison with several observational datasets showed that the model is able to reproduce the atmospheric climate in the Baltic Sea region quite realistically. However, precipitation was overestimated by about 30%. Due to the high sensitivity of the Baltic Sea to fresh-water input, this bias can be seen as problematic, especially when the simulated runoff should be used as input for a river routing scheme in a regional earth system model with an internally closed water cycle. This bias is a common feature for regional climate model simulations over Europe (Jones et al. 2004). This problem might be at least partly explained by the use of parameterization which were originally developed for global climate models with a much coarser resolution. The regional model might resolve mesoscale processes which leads to unrealistic effects when the parameterizations are not adjusted adequately.

Concerning the simulations of the Baltic Sea itself, the model showed an ambivalent performance. The model is able to reproduce the annual cycle of the SST fairly well, with only slightly too high values in summer. This bias is related to a too shallow mixed-layer depth during spring and summer, which in turn is determined by the vertical turbulent mixing. Turbulence is a rather complicated process, especially in the Baltic Sea with its complex bathymetry, and stratification. It is one of the most important ongoing research topics for the Baltic Sea. Also the evolution of the sea ice is reproduced rather realistically, with a considerable overestimation of the sea ice extend however. An optimization of the parameters for the sea ice dynamics could lead to a considerable improvement, considering the realistically simulated SSTs during winter.

In contrast to the stand-alone simulation of BSIOM, the coupled model is not able to simulate the salinity correctly. The inflow of high saline water from the North Sea through the Danish Straits is too weak in general; especially so called major inflows are not simulated. Here again, the turbulent mixing is one of the key factors. The too high net freshwater flux due the exceeding precipitation is also partly contributing. This issue has to be solved before the model can be used for longer simulations including climate change studies.

The model is able to reproduce the main upwelling regions in the Baltic Sea during the stratified season adequately. A potential feedback has been investigated, namely the stability effect of the reduced SST over the upwelling regions on the near-surface wind speed. This effect leads to a considerable reduction of the 10m wind speed in the order of $0.5^{m/s}$ during upwelling phases. This shows the importance of the coupling for short-term wind forecasts, which is essential with regard to the offshore wind-energy plans.

The answers to the major research questions are the following:

- How large are the major components in the water and energy cycles of the Baltic Sea?

Due to the reasons mentioned above, the water cycle is not represented adequately in the coupled model simulations. The energy cycle is simulated realistically. Only in the coupled model simulation, the heat budget is almost closed on longer time scales, with an imbalance of about $1.6^{W/m^2}$at the sea surface over the simulation period that go from the atmosphere into the ocean. This agrees well with values from other studies as Omstedt and Rutgersson (2000); Omstedt and Nohr (2004); Meier and Doscher (2002). The uncoupled simulations and the observational and reanalysis datasets suffer from inconsistencies regarding the energy cycle. One major reason is the prescribed SSTs, which lead to missing feedbacks. This study tries to explain the imbalance of the heat fluxes. A large part ($0.9^{W/m^2}$) is stored as additional heat. The common explanation was that the remainder is advected through the Danish straits into the North Sea. In the present study, this advective flux amounts to $1.2^{W/m^2}$. However, this flux is completely balanced by the heat flux that is advected with the rivers that flow into the Baltic Sea. The latent heat flux associated with snow fall was identified to contribute considerably to the heat balance in the order of $1^{W/m^2}$. Due to inconsistencies, it only contributed with about $0.3^{W/m^2}$ in the model simulation. About $0.5^{W/m^2}$ could not be explained in the total heat budget. This could be considered as being small, but it would lead to a temperature increase of more than 1°C within 20 years. It has also to be compared to the anthropogenic radiative forcing which is estimated to be about $2.3^{W/m^2}$ globally (Stocker et al. 2013). A reason for this could be that energy is not conserved in the sea-ice treatment.

- How does the interactive coupling of a Baltic Sea ocean model affect the regional climate simulation?

The interactive coupling mainly affects the atmosphere above the Baltic Sea surface. The different SSTs directly affect the turbulent heat fluxes between the ocean and the atmosphere and thus the near-surface air temperature. This changes the stability of the atmospheric boundary layer and therefore the vertical momentum transport from the free atmosphere toward the surface. This results in considerably different near-surface wind speeds.

- What is the added value of the coupled model compared to the stand-alone version?

It depends on the specific question and the involved temporal and spatial scales whether the higher cost of the coupled model is justified. The added value is generally confined to the lower atmosphere directly above the sea surface and does not affect much the land part of the Baltic catchment area apart from the coastal areas. For simulations of the past climate, as in this work, only a coupled model can represent some important processes like coastal upwelling acting on short time scales and high spatial gradients, since the spatial and temporal resolution of the observations does not allow to capture those. For climate change studies, where no observations of the sea surface conditions are available and the resolution of GCMs is too coarse to resolve the Baltic Sea adequately, a coupled regional model is necessary to represent the air-sea interactions in this area.

6.2 Outlook

In order to get a more comprehensive understanding of the physical system of the Baltic Sea, the further step is the development of the coupled model towards a regional earth system model. This includes the implementation of a river routing scheme. Before, the problem of the extensive precipitation has to be solved. For this, an in-depth analysis of the whole water cycle in the atmospheric model is necessary to investigate the complex interplay of all relevant processes like evaporation, atmospheric vapor transport etc. This should be done by a holistic approach including process studies using models and observations and model inter-comparisons.

In order to use the coupled model system for climate change studies, it should be improved with respect to the following aspects: The model should be able to simulate the salinity more realistically. In this context, the vertical mixing and thus the turbulence parametrization plays an important role. The questions remains whether the salinity dynamics can be resolved in a model covering the whole Baltic Sea with constant resolution of if other methods as local grid refining are necessary. The simulation of sea ice should also be improved since it is over-estimated in the current model configuration. Also the conservation of energy with respect to sea ice and snow fall should be guaranteed. This could be done by either an improvement of the current parameterization or the implementation of the thermo-dynamic sea ice model from the uncoupled version of BSIOM.

Further studies of the investigated feedbacks in the atmosphere-ocean interactions would be interesting, for example, how the resolved feedback of the upwelling onto the wind affects the upwelling dynamics in the ocean model. The role of the thermocline dynamics for the short-term variability of near-surface winds are another example.

Bibliography

BACC, 2008: *Asessment of Climate Change for the Baltic Sea Basin*. Springer, Berlin.

Bengtsson, L., 2001: Numerical modelling of the energy and water cycle of the Baltic Sea. *Meteorology and Atmospheric Physics*, **77 (1-4)**, 9–17.

Bennartz, R., 1999: On the use of SSM/I measurements in coastal regions. *Journal of Atmospheric and Oceanic Technology*, **16**, 417–431.

Bennartz, R., P. Lorenz, and D. Jacob, 2009: A comparison of the BALTIMOS coupled climate model with atmospheric and sea surface parameters derived from AMSR-E. *Theoretical and Applied Climatology, Special Issue*, 1–9.

Bergström, S. and B. Carlsson, 1994: River runoff to the Baltic Sea 1950 - 1990. *Ambio*, **23 (4-5)**, 280–287.

Berrisford, P., P. Kå llberg, S. Kobayashi, D. Dee, S. Uppala, A. J. Simmons, P. Poli, and H. Sato, 2011: Atmospheric conservation properties in ERA-Interim. *Quarterly Journal of the Royal Meteorological Society*, **137 (659)**, 1381–1399.

Berry, D. I. and E. C. Kent, 2009: A New Air-Sea Interaction Gridded Dataset from ICOADS With Uncertainty Estimates. *Bulletin of the American Meteorological Society*, **90 (5)**, 645–656.

Boé, J., A. Hall, F. Colas, J. C. McWilliams, X. Qu, J. Kurian, and S. B. Kapnick, 2011: What shapes mesoscale wind anomalies in coastal upwelling zones? *Climate Dynamics*, **36 (11-12)**, 2037–2049.

Bumke, K. and L. Hasse, 1989: An analysis scheme for determination of true surface winds at sea from ship synoptic wind and pressure observations. *Boundary-Layer Meteorology*, **47 (1)**, 295–308.

Bumke, K., U. Karger, L. Hasse, and K. Niekamp, 1998: Evaporation over the Baltic Sea as an example of a semi-enclosed sea. *Contributions to atmospheric physics*, **71 (2)**, 249–261.

Bychkova, I. A. and S. V. Viktorov, 1987: Use of satellite data for identification and classification of upwelling in the Baltic Sea. *Oceanology*, **27 (2)**, 158–162.

Bychkova, I. A., S. V. Viktorov, and D. A. Shumakher, 1988: The relationship between large-scale atmospheric circulation and processes involved in the origin of coastal upwelling in the Baltic Sea(O sviazi krupnomasshtabnoi atmosfernoi tsirkuliatsii i protsessov vozniknoveniia pribrezhnogo apvellinga v Baltiiskom). *Meteorologiia i Gidrologiia*, 91–98.

Charnock, H., 1955: Wind stress on a water surface. *Quarterly Journal of the Royal Meteorological Society*, **81 (350)**, 639–639.

Dee, D. P., et al., 2011: The ERA-Interim reanalysis: configuration and performance of the data assimilation system. *Quarterly Journal of the Royal Meteorological Society*, **137 (656)**, 553–597.

Döscher, R., U. Willén, C. Jones, A. Rutgersson, H. E. M. Meier, U. Hansson, and L. P. Graham, 2002: The development of the regional coupled ocean-atmosphere model RCAO. *Boreal environment research*, **7**, 183–192.

Fennel, W. and T. Seifert, 1995: Kelvin wave controlled upwelling in the western Baltic. *Journal of Marine Systems*, **6 (4)**, 289–300.

Fennel, W., T. Seifert, and B. Kayser, 1991: Rossby radii and phase speeds in the Baltic Sea. *Continental Shelf Research*, **11 (1)**, 23–36.

Gidhagen, L., 1987: Coastal upwelling in the Baltic Sea - Satellite and in situ measurements of sea-surface temperatures indicating coastal upwelling. *Estuarine, Coastal and Shelf Science*, **24**, 449–462.

Graham, L., et al., 2008: Projections of future climate change. In: The BACC Author Team (eds.), Assessment of climate change for the Baltic Sea basin, Springer, Berlin, pp. 133-219.

Graham, P., 1999: Modelling runoff to the Baltic Sea. *Ambio*, **28 (4)**, 328–334.

Griffies, S. M., et al., 2009: Coordinated Ocean-ice Reference Experiments (COREs). *Ocean Modelling*, **26 (1-2)**, 1–46.

Gurova, E., A. Lehmann, and A. Ivanov, 2013: Upwelling dynamics in the Baltic Sea studied by a combined SAR/infrared satellite data and circulation model analysis. *Oceanologia*, **55 (3)**, 687–707.

Gustafsson, N., L. Nyberg, and A. Omstedt, 1998: Coupling of a High-Resolution Atmospheric Model and an Ocean Model for the Baltic Sea. *Monthly Weather Review*, **126**, 2822–2846.

Hagedorn, R., 2000: Ein gekoppeltes Atmosphäre-Ozean-Modell für das Ostsee-Einzugsgebiet. Ph.D. thesis, Christian-Albrechts-Universität, Kiel, Germany.

Hagedorn, R., A. Lehmann, and D. Jacob, 2000: A coupled high resolution atmosphere-ocean model for the BALTEX region. *Meteorologische Zeitschrift*, **9 (1)**, 7–20.

Hagemann, S., H. Göttel, D. Jacob, P. Lorenz, and E. Roeckner, 2008: Improved regional scale processes reflected in projected hydrological changes over large European catchments. *Climate Dynamics*, **32 (6)**, 767–781.

Hagemann, S., B. Machenhauer, R. Jones, O. B. Christensen, M. Deque, D. Jacob, and P. L. Vidale, 2004: Evaluation of water and energy budgets in regional climate models applied over Europe. *Climate Dynamics*, **23**, 547–567.

Harder, M., 1996: Dynamik, Rauhigkeit und Alter des Meereises in der Arktis. *Bericht zur Polarforschung, 203, Alfred-Wegener-Institut für Polar- und Meeresforschung, Bremerhaven, Germany.*

Harris, I., P. Jones, T. Osborn, and D. Lister, 2013: Updated high-resolution grids of monthly climatic observations - the CRU TS3.10 Dataset. *International Journal of Climatology*, **34 (3)**, 623–642.

Hela, I., 1946: Coriolis-voiman vaikutuksesta Suomenlahden hydrografisiin oloihin (Coriolis force of the hydrographic conditions in the Gulf of Finland). *Terra*, **58 (2)**, 52–59.

Hela, I., 1976: Vertical velocity of the upwelling in the sea. *Societas Scientarium Fennica, Commentationes Physico-Mathematicae*, **46 (1)**, 9–24.

Hennemuth, B., A. Rutgersson, K. Bumke, M. Clemens, A. Omstedt, D. Jacob, and A.-S. Smedman, 2003: Net precipitation over the Baltic Sea for one year using models and data-based methods. *Tellus A*, **55 (4)**, 352–367.

Hibler, W. D., 1979: A dynamic thermodynamic sea ice model. *Journal of Physical Oceanography*, **9**, 815–846.

Hofmeister, R., J.-M. Beckers, and H. Burchard, 2011: Realistic modelling of the exceptional inflows into the central Baltic Sea in 2003 using terrain-following coordinates. *Ocean Modelling*, **39 (3-4)**, 233–247.

Horstmann, U., 1983: Distribution patterns of temperature and water colour in the Baltic Sea as recorded in satellite images: indicators for phyto- plankton growth. Berichte aus dem Institute für Meereskunde an der Universität Kiel 106. 147 pp. pp.

IBS, 1995: BALTEX Initial Implementation Plan, International BALTEX Secretariat Publication No 2, GKSS-Forschungszentrum, P.O. Box 1160, D-21494 Geesthacht, Germany.

Jacob, D., 2001: A note to the simulation of the annual and inter-annual variability of the water budget over the Baltic Sea drainage basin. *Meteorology and Atmospheric Physics*, **77 (1-4)**, 61–73.

Jacob, D. and R. Podzun, 1997: Sensitivity studies with the regional climate model REMO. *Meteorology and Atmospheric Physics*, **63**, 119–129.

Jacob, D., et al., 2001: A comprehensive model inter-comparison study investigating the water budget during the BALTEX-PIDCAP period. *Meteorology and Atmospheric Physics*, **77 (1)**, 19–43.

Jacob, D., et al., 2007: An inter-comparison of regional climate models for Europe: model performance in present-day climate. *Climatic Change*, **81 (S1)**, 31–52.

Jankowski, A., 2002: Variability of coastal water hydrodynamics in the southern Baltic-hindcast modelling of an upwelling event along the Polish coast. *Oceanologia*, **44 (4)**, 395–418.

Janssen, F., 2002: Statistical analysis of multi-year hydrographic variability in the North Sea and Baltic Sea. Validation and correction of systematic errors in a regional ocean model. Ph.D. thesis, University of Hamburg, Germany.

Janssen, F., C. Schrum, and J. O. Backhaus, 1999: A climatological data set of temperature and salinity for the Baltic Sea and the North Sea. *Deutsche Hydrographische Zeitschrift*, **51 (S9)**, 5–245.

Johannessen, T. W., 1970: The climate of Scandinavia. *World Survey of Climatology*, **5**, 23–79.

Jones, C. G., U. Willén, A. Ullerstig, and U. Hansson, 2004: The Rossby Centre Regional Atmospheric Model Climate Part I: Model Climatology and Performance for the Present Climate over Europe. *Ambio*, **33 (4/5)**, 199–210.

Kaleschke, L., G. Heygster, C. Luepkes, A. Borchert, J. Hartmann, J. Haarpainter, and T. Vihma, 2001: SSM/I sea ice remote sensing for mesoscale ocean-atmosphere interaction analysis : Ice and icebergs. *Canadian Journal of Remote Sensing*, **27 (5)**, 526–537.

Killworth, P., D. Stainforth, D. Webb, and S. Paterson, 1991: The development of a free-surface Bryan-Cox-Semtner ocean model. *Journal of physical oceanography*, **21**, 1333–1348.

Kononen, K. and A. Niemi, 1986: Variation in phytoplankton and hydrography in the outer archipelago. *Finnish Marine Research*, **253**, 35–51.

Krauss, W., 1981: The Erosion of the Thermocline. *Journal of Physical Oceanography*, **11**, 415–433.

Krauss, W. and B. Brügge, 1991: Wind-produced water exchange between the deep basins of the Baltic Sea. *Journal of Physical Oceanography*, **21**, 373–384.

Kronsell, J. and P. Andersson, 2012: Total and regional runoff to the Baltic Sea. Baltic Sea Environment Fact Sheet 2012. Online. http://helcom.fi/baltic-sea-trends/environment-fact-sheets/hydrography/total-and-regional-runoff-to-the-baltic-sea/.

Large, W. and S. Pond, 1981: Open ocean momentum flux measurements in moderate to strong winds. *Journal of Physical Oceanography*, **11 (3)**, 324–336.

Large, W. and S. Yeager, 2009: The global climatology of an interannually varying air-sea flux data set. *Climate Dynamics*, **33 (2-3)**, 341–364.

Large, W. G. and S. Pond, 1982: Sensible and Latent Heat Flux Measurements over the Ocean. *Journal of Physical Oceanography*, **12 (5)**, 464–482.

Launder, B. and D. Spalding, 1972: Mathematical models of turbulence. *Academic Press, London.*

Lehmann, A., 1995: A three-dimensional baroclinic eddy-resolving model of the Baltic Sea. *Tellus A*, **47A**, 1013–1031.

Lehmann, A. and H. Hinrichsen, 2001: The importance of water storage variations for water balance studies of the Baltic Sea. *Physics and Chemistry of the Earth (B)*, **26 (5-6)**, 383–389.

Lehmann, A. and H. H. Hinrichsen, 2000: On the thermohaline variability of the Baltic Sea. *Journal of Marine Systems*, **25**, 333–357.

Lehmann, A., H.-H. Hinrichsen, K. Getzlaff, and K. Myrberg, 2014: Quantifying the heterogeneity of hypoxic and anoxic areas in the Baltic Sea by a simplified coupled hydrodynamic-oxygen consumption model approach. *Journal of Marine Systems*, **134**, 20–28.

Lehmann, A., W. Krauss, and H.-H. Hinrichsen, 2002: Effects of remote and local atmospheric forcing on circulation and upwelling in the Baltic Sea. *Tellus A*, **54 (3)**, 299–316.

Lehmann, A., P. Lorenz, and D. Jacob, 2004: Modelling the exceptional Baltic Sea inflow events in 2002-2003. *Geophysical Research Letters*, **31**, L21308.

Lehmann, A. and K. Myrberg, 2008: Upwelling in the Baltic Sea - A review. *Journal of Marine Systems*, **74**, S3–S12.

Lehmann, A., K. Myrberg, and K. Höflich, 2012: A statistical approach to coastal upwelling in the Baltic Sea based on the analysis of satellite data for 1990-2009. *Oceanologia*, **54 (3)**, 369–393.

Leppäranta, M. and K. Myrberg, 2009: *Physical oceanography of the Baltic Sea.* Springer Berlin, Heidelberg, New York.

Lind, P. and E. Kjellström, 2009: Water budget in the Baltic Sea drainage basin: Evaluation of simulated fluxes in a regional climate model. *Boreal environment research*, **14 (1)**, 56–67.

Lisitzin, E., 1967: Day-to-day variation in sea level along the Finnish coast. *Geophysica*, **9**, 259–275.

Lorenz, P. and D. Jacob, 2009: BALTIMOS – a fully coupled modeling system for the Baltic Sea and its drainage basin. *Theoretical and Applied Climatology, Special Issue*.

Louis, J., 1979: A parametric model of vertical eddy fluxes in the atmosphere. *Boundary-Layer Meteorology*, **17**, 187–202.

Maaß, N. and L. Kaleschke, 2010: Improving passive microwave sea ice concentration algorithms for coastal areas: applications to the Baltic Sea. *Tellus A*, **62 (4)**, 393–410.

Majewski, D., 1991: The Europa-Modell of the Deutscher Wetterdienst. *Seminar proceedings ECMWF*, **2**, 147–193.

Matthäus, W. and H. Franck, 1992: Characteristics of major Baltic inflows - a statistical analysis. *Continental Shelf Research*, **12 (12)**, 1375–1400.

Meier, H. E. M., 2001: On the parameterization of mixing in three-dimensional Baltic Sea models. *Journal of Geophysical Research*, **106 (C12)**, 30,997–31,016.

Meier, H. E. M. and R. Doscher, 2002: Simulated water and heat cycles of the Baltic Sea using a 3D coupled atmosphere-ice-ocean model. *Boreal environment research*, **7 (4)**, 327–334.

Meier, H. E. M., A. Höglund, R. Döscher, H. Andersson, U. Löptien, and E. Kjellström, 2011: Quality assessment of atmospheric surface fields over the Baltic Sea from an ensemble of regional climate model simulations with respect to ocean dynamics. *Oceanologia*, **53 (08)**, 193–227.

Meier, H. E. M. and F. Kauker, 2003: Sensitivity of the Baltic Sea salinity to the freshwater supply. *Climate Research*, **24**, 231–242.

Monin, A. and A. Obukhov, 1954: Basic laws of turbulent mixing in the surface layer of the atmosphere. *Contrib. Geophys. Inst. Acad. Sci., USSR*, **24 (151)**, 163–187.

Myrberg, K. and O. Andrejev, 2003: Main upwelling regions in the Baltic Sea-a statistical analysis based on three-dimensional modelling. *Boreal Environment Research*, **8**, 97–112.

Neumann, G., 1941: Eigenschwingungen der Ostsee. *Archiv der Deutschen Seewarte und des Marineobservatoriums*, **61 (4)**, 59.

Novotny, K., G. Liebsch, A. Lehmann, and R. Dietrich, 2006: Variability of Sea Surface Heights in the Baltic Sea: An Intercomparison of Observations and Model Simulations. *Marine Geodesy*, **29 (2)**, 113–134.

Omstedt, A., L. Meuller, and L. Nyberg, 1997: Interannual , Seasonal and Regional Variations of Precipitation and Evaporation over the Baltic. *Ambio*, **26 (8)**, 484–492.

Omstedt, A. and C. Nohr, 2004: Calculating the water and heat balances of the Baltic Sea using ocean modelling and available meteorological, hydrological and ocean data. *Tellus A*, **56**, 400–414.

Omstedt, A., C. Pettersen, J. Rodhe, and P. Winsor, 2004: Baltic Sea climate: 200 yr of data on air temperature, sea level variation, ice cover, and atmospheric circulation. *Climate Research*, **25**, 205–216.

Omstedt, A. and A. Rutgersson, 2000: Closing the water and heat cycles of the Baltic Sea. *Meteorologische Zeitschrift*, **9 (1)**, 59–66.

Palmén, E. and E. Laurila, 1938: Über die Einwirkung eines Sturmes auf den hydrographischen Zustand im nördlichen Ostseegebiet. *Societas Scientarium Fennica, Commentationes Physico-Mathematicae X (1)*, 1–52.

Parkinson, C. L. and W. M. Washington, 1979: A large-scale numerical model of sea ice. *Journal of Geophysical Research*, **84 (C1)**, 311.

Pirazzini, R., T. Vihma, M. A. Granskog, and B. Cheng, 2006: Surface albedo measurements over sea ice in the Baltic Sea during the spring snowmelt period. *Annals of Glaciology*, **44 (1)**, 7–14.

Raschke, E., et al., 2001: The Baltic Sea Experiment (BALTEX): A European contribution to the investigation of the energy and water cycle over a large drainage basin. *Bulletin of the American Meteorological Society*, **82 (11)**, 2389–2413.

Reuter, M. and J. Fischer, 2009: A comparison of satellite-retrieved and simulated cloud coverage in the Baltic Sea area as part of the BALTIMOS project. *Theoretical and Applied Climatology*, **special is**.

Rodi, W., 1980: Turbulence models and their application in hydraulics - A state-of-the-art review. Tech. rep., Int. Assoc. for Hydraul. Res., 104 pp., Delft, Netherlands.

Roeckner, E., et al., 1996: The atmospheric general circulation model ECHAM-4: Model description and simulation of present-day climate. Tech. Rep. 218, Max Planck Institute for Meteorology.

Roeckner, E., et al., 2003: The Atmospheric General Circulation Model ECHAM5, Part 1: Model description. Tech. Rep. 349, Max Planck Institute for Meteorology.

Rubel, F. and M. Hantel, 2001: BALTEX 1/6-degree daily precipitation climatology 1996-1998. *Meteorology and Atmospheric Physics*, **77**, 155–166.

Rudolph, C. and A. Lehmann, 2006: A model measurements comparison of atmospheric forcing and surface fluxes of the Baltic Sea. *Oceanologia*, **48 (3)**, 333–360.

Rutgersson, A., K. Bumke, M. Clemens, V. Foltescu, R. Lindau, D. Michelson, and A. Omstedt, 2001: Precipitation estimates over the Baltic Sea: Present state of the art. *Nordic Hydrology*, **32**, 285–314.

Samuelsson, M. and A. Stigebrandt, 1996: Main characteristics of the long-term sea level variability in the Baltic sea. *Tellus A*, **48A**, 672–683.

Schrum, C., U. Huebner, D. Jacob, and R. Podzun, 2003: A coupled atmosphere/ice/ocean model for the North Sea and the Baltic Sea. *Climate Dynamics*, **21 (2)**, 131–151.

Semmler, T., 2002: Der Wasser- und Energiehaushalt der arktischen Atmosphaere. Ph.D. thesis, University of Hamburg.

Siegel, H., M. Gerth, and G. Tschersich, 2006: Sea surface temperature development of the Baltic Sea in the period 1990-2004. *Oceanologia*, **48**, 119–131.

Simmons, A. and D. Burridge, 1981: An Energy and Angular-Momentum Conserving Vertical Finite-Difference Scheme and Hybrid Vertical Coordinates. *Monthly Weather Review*, **109 (4)**, 758–766.

Sjöblom, V., 1967: Meriveden kumpuaminen ja Porkkalan niemi (Upwelling of seawater and the cape of Porkkala). *Suomen Kalatalous*, **27**, 1–12.

Spreen, G., L. Kaleschke, and G. Heygster, 2008: Sea ice remote sensing using AMSR-E 89-GHz channels. *Journal of Geophysical Research*, **113 (C2)**, C02S03.

Stigebrandt, A., 1980: Barotropic and baroclinic response of a semi-enclosed basin to barotropic forcing from the sea. In: Freeland HJ, Farmer DM, Levings CD (eds) Fjord oceanography. Plenum, New York. 151–164 pp.

Stigebrandt, A., 2001: Physical Oceanography of the Baltic Sea, Ch. 2. In: A Systems Analysis of the Baltic Sea (eds F. Wulff, L. Rahm and P. Larsson). Springer-Verlag, Berlin.

Stocker, T. F., D. Qin, G. K. Plattner, M. Tignor, S. K. Allen, J. Boschung, and P. M. Midgley, 2013: Climate change 2013: The physical science basis. Intergovernmental Panel on Climate Change, Working Group I Contribution to the IPCC Fifth Assessment Report (AR5)(Cambridge Univ Press, New York).

Stössel, A. and W. Owens, 1992: The Hamburg sea-ice model. DKRZ Techn. Rep. No. 3.

Svansson, A., 1975: Interaction between the coastal zone and the open sea. *Finnish Marine Research*, **39**, 11–28.

Sweet, W., R. Fett, J. Kerling, and P. LaViolette, 1981: Air-Sea Interaction Effects in the Lower Troposphere Across the North Wall of the Gulf Stream. *Monthly Weather Review*, **109**, 1042–1052.

Tian, T., F. Boberg, and O. Christensen, 2013: Resolved complex coastlines and land-sea contrasts in a high-resolution regional climate model: a comparative study using prescribed and modelled SSTs. *Tellus A*, **65**, 1–19.

Vihma, T. and J. Haapala, 2009: Geophysics of sea ice in the Baltic Sea: A review. *Progress In Oceanography*, **80 (3-4)**, 129–148.

Walin, G., 1972a: On the hydrographic response to transient meteorological disturbances. *Tellus*, **24 (3)**, 169–186.

Walin, G., 1972b: Some observations of temperature fluctuations in the coastal region of the Baltic. *Tellus*, **24 (3)**, 187–198.

Wallerius, D., 1932: The heat content of the Baltic Sea water. *Svenska Hydrogr.-Biol. Komm. Fyrskeppsunders.*, 47–62.

Woodruff, S., H. Diaz, J. Elms, and S. Worley, 1998: COADS Release 2 data and metadata enhancements for improvements of marine surface flux fields. *Physics and Chemistry of the Earth*, **23 (5-6)**, 517–526.

Worley, S. J., S. D. Woodruff, R. W. Reynolds, S. J. Lubker, and N. Lott, 2005: ICOADS release 2.1 data and products. *International Journal of Climatology*, **25 (7)**, 823–842.

Yu, L., X. Jin, and R. Weller, 2008: Multidecade Flobal Flux Datasets from the Objectively Analyzed Air-sea Fluxes (OAFlux) Project: Latent and Sensible Heat Fluxes, Ocean Evaporation, and Related Surface Meteorological Variables, OAFlux Project Technical Report (OA-2008-01). Tech. Rep. January, Woods Hole Oceanographic Institution, 1–64 pp.

Yu, L. and R. a. Weller, 2007: Objectively Analyzed Air-Sea Heat Fluxes for the Global Ice-Free Oceans (1981-2005). *Bulletin of the American Meteorological Society*, **88 (4)**, 527–539.

Zapadka, T., B. Woźniak, and J. Dera, 2007: A more accurate formula for calculating the net longwave radiation flux in the Baltic Sea. *Oceanologia*, **49 (4)**, 449–470.

Zhang, Y., W. B. Rossow, A. A. Lacis, V. Oinas, and M. I. Mishchenko, 2004: Calculation of radiative fluxes from the surface to top of atmosphere based on ISCCP and other global data sets: Refinements of the radiative transfer model and the input data. *Journal of Geophysical Research*, **109 (D19105)**.

Zhurbas, V., J. Laanemets, and E. Vahtera, 2008: Modeling of the mesoscale structure of coupled upwelling/downwelling events and the related input of nutrients to the upper mixed layer in the Gulf of Finland, Baltic Sea. *Journal of Geophysical Research*, **113 (C5)**, C05 004.

Zillman, J., 1972: *A study of some aspects of the radiation and heat budgets of the southern hemisphere oceans*. Meteorol. Stud. Rep. 26, Bur. of Meteorol., Dept. of the Interior, Canberra.

Eidesstattliche Erklärung

Hiermit versichere ich, dass ich diese Arbeit selbständig verfasst habe und keine anderen als die angegebenen Quellen und Hilfsmittel benutzt habe.

Thomas Raub

Acknowledgements

I would not have been able to finish this thesis without the support of many people.

First I thank Daniela Jacob for her support during my doctoral studies without losing faith in me during the difficult phases. I also thank Guy Brasseur for the critical comments on my work.

Many thanks go to Andreas Lehmann for the help with BSIOM, the willingness to always discuss my problems with the model and the thesis in Hamburg, Kiel and elsewhere and to allow me to use the high-performance computer in Kiel. I also thank Klaus Getzlaff for all his help in countless scientific discussions in Hamburg, Kiel and on the phone, and the frequent encouragements in the last months. I liked a lot our nice meetings with and without tapas in Kiel, Hamburg and at the conferences.

The REMO group I thank for the discussions of my work and the humorful and inspiring atmosphere.

The SICSS I thank for the pleasant retreats and social events. This work was supported through the Cluster of Excellence 'CliSAP' (EXC177), Universität Hamburg, funded through the German Science Foundation (DFG).

Thanks to my office mates Giovanni, Pankaj, Christine and Kevin for the daily company, the Mensa group(s) for the enjoyable lunch breaks and the Gewaltkicker team for the relieving fights at 15:31.

Thanks to Klaus, Andreas, Kevin, Armelle and Bastian for critical proof reading and to Swantje for the help to prepare the disputation.

Thanks to my parents for their conditionless support all the time.

And finally I thank Johanna for always being there and keeping me alive in the final stage of the thesis.